

Synthesis and Analysis of an Active Independent Front Steering (AIFS) System

Azadeh Farazandeh

A Thesis

In the Department

of

Mechanical and Industrial Engineering

Presented in Partial Fulfillment of the Requirements
for the Degree of
Doctor of Philosophy (Mechanical Engineering) at
Concordia University
Montreal, Quebec, Canada

January 2015

© Azadeh Farazandeh, 2015

CONCORDIA UNIVERSITY

SCHOOL OF GRADUATE STUDIES

This is to certify that the thesis prepared

By: **Azadeh Farazandeh**

Entitled: **Synthesis and Analysis of an Active Independent Front Steering (AIFS) System**

and submitted in partial fulfillment of the requirements for the degree of
DOCTOR OF PHILOSOPHY (Mechanical Engineering)

complies with the regulations of the University and meets the accepted standards with respect to originality and quality.

Signed by the final examining committee:

_____ Chair
Dr. A. Kishk

_____ External Examiner
Dr. Y. He

_____ External to Program
Dr. A. G. Aghdam

_____ Examiner
Dr. R. Sedaghati

_____ Examiner
Dr. H. Hong

_____ Thesis Supervisors
Dr. A. K. W. Ahmed and Dr. S. Rakheja

Approved by

_____ Dr. A. Dolatabadi, Graduate Program Director

Jan 13, 2015

_____ Dr. C. Trueman, Interim Dean
Faculty of Engineering & Computer Science

ABSTRACT

Synthesis and analysis of an active independent front steering (AIFS) system

Azadeh Farazandeh, Ph.D.

Concordia University, 2015

Technological developments in road vehicles over the last two decades have received considerable attention towards pushing the safe performance limits to their ultimate levels. Towards this goal, Active Front Steering (AFS) and Direct Yaw-moment Control (DYC) systems have been widely investigated. AFS systems introduce corrective steering angles to the conventional system in order to realize a target handling response for a given speed and steering input. An AFS system, however, may yield limited performance under severe steering maneuvers involving substantial lateral load shift and saturation of the inside tire-road adhesion. The adhesion available at the outer tire, on the other hand, would remain under-utilized. This dissertation explores effectiveness of an Active Independent Front Steering (AIFS) system that could introduce a corrective measure at each wheel in an independent manner.

The effectiveness of the AIFS system was investigated firstly through simulation of a yaw-plane model of a passenger car. The preliminary simulation results with AIFS system revealed superior potential compared to the AFS particularly in the presence of greater lateral load shift during a high-g maneuver. The proposed concept was thus expected to be far more beneficial for enhancement of handling properties of heavy vehicles, which invariably undergo large lateral load shift due to their high center of mass and roll motion. A nonlinear yaw-plane model of a two-axle single-unit truck, fully and partially loaded with solid and liquid cargo, with limited roll degree-of-freedom (DOF) was thus developed to study the performance potentials of AIFS under

a range of steering maneuvers.

A simple PI controller was synthesized to track the reference yaw rate response of a neutral steer vehicle. The steering corrections, however, were limited such that none of the tires approach saturation. For this purpose, a tire saturation zone was identified considering the normalized cornering stiffness property of the tire. The controller strategy was formulated so as to limit the work-load magnitude at a pre-determined level to ensure sufficient tire-road adhesion reserve to meet the braking demand, when exists.

Simulation results were obtained for a truck model integrating AFS and AIFS systems subjected to a range of steering maneuvers, namely: a J-turn maneuver on uniform as well as split- μ road conditions, and path change and obstacle avoidance maneuvers. The simulation results showed that both AFS and AIFS can effectively track the target yaw rate of the vehicle, while the AIFS helped limit saturation of the inside tire and permitted maximum utilization of the available tire-road adhesion of the outside tire. The results thus suggested that the performance of an AIFS system would be promising under severe maneuvers involving simultaneous braking and steering, since it permitted a desired adhesion reserve at each wheel to meet a braking demand during the steering maneuver. Accordingly, the vehicle model was extended to study the dynamic braking characteristics under braking-in-turn maneuvers. The simulation results revealed the most meritorious feature of the AIFS in enhancing the braking characteristics of the vehicle and reducing the stopping time during such maneuvers. The robustness of the proposed control synthesis was subsequently studied with respect to parameter variations and external disturbance. This investigation also explores designs of fail-safe independently controllable front wheels steering system for implementation of the AIFS concept.

ACKNOWLEDGMENTS

I wish to express my deep gratitude and appreciation to my supervisors, Professor Waiz Ahmed and Professor Subhash Rakheja for their constant guidance, support and encouragement throughout my thesis work. I would also like to thank my committee members for their time, suggestion and insightful comments.

The author wishes to acknowledge the financial, academic and technical support of all faculty and staff of the Concordia University and CONCAVE center for their contributions to this thesis work. My sincere thanks also go to Mrs. Leslie Hosein, graduate program coordinator, for her kindness, friendship and constant support.

I'm also glad to have worked with a wonderful undergraduate student group, team#8, to design the AIFS steering mechanism and the technical staff in EDML group for sharing their knowledge and expertise.

Throughout the past four years, there have been many joyful moments spent with my friends. Thanks a lot to make the lab atmosphere as friendly as possible. Your friendship and support throughout this thesis were invaluable.

Above all, special thanks to my family who provided unconditional love and care in my whole life. I would also like to value the memory of my father who was the first source of encouragement and support in my life. I believe you have been watching me up-close in all moments of my life.

I dedicate my thesis to:

My Father

LIST OF CONTENTS

LIST OF FIGURES	x
LIST OF TABLES	xv
NOMENCLATURE	xvi

CHAPTER 1

LITERATURE REVIEW AND SCOPE OF THE DISSERTATION	1
1.1 Introduction	1
1.2 Review of Relevant Literature	4
<i>1.2.1 Direct yaw-moment control (DYC) system</i>	4
<i>1.2.2 Active front steering (AFS) system</i>	12
<i>1.2.3 Four wheel steering (4WS) system</i>	18
<i>1.2.4 Integrated chassis control systems</i>	22
<i>1.2.5 Vehicle handling models</i>	28
1.3 Active Front Steering Mechanism	30
<i>1.3.1 Steer-by-Wire (SBW) technology for active front steering system</i>	31
<i>1.3.2 Mechanical Mechanisms for AFS</i>	33
1.4 Scope and Objectives	39
1.5 Organization of the Dissertation	41

CHAPTER 2

PERFORMANCE ENHANCEMENT OF ROAD VEHICLES USING ACTIVE INDEPENDENT FRONT STEERING (AIFS)	47
2.1 Introduction	47
2.2 Handling Model	50
2.3 Tire Force and Moment	52
2.4 AIFS Control Strategy	55
2.5 Steering Mechanism	57
2.6 Simulation Analysis	59
<i>2.6.1 Case study1: cornering maneuver</i>	60
<i>2.6.2 Case study 2: sinusoidal maneuver</i>	63

2.6.3	<i>Case study 3: split-μ condition</i>	66
2.6.4	<i>CG height sensitivity analysis</i>	68
2.7	Conclusion	69

CHAPTER 3

PERFORMANCE ANALYSIS OF ACTIVE INDEPENDENT FRONT STEERING (AIFS) FOR COMMERCIAL VEHICLES WITH GREATER LATERAL LOAD SHIFT PROPENSITY		71
3.1	Introduction	71
3.2	Directional Dynamic Model of the Truck	75
3.2.1	<i>Load shift in a partially-filled tank</i>	77
3.3	AIFS Reference Model and Control Strategy	79
3.4	Simulation Results	84
3.4.1	<i>Fully loaded truck</i>	85
3.4.2	<i>Partially filled tank truck</i>	90
3.5	Conclusions	96

CHAPTER 4

AN INDEPENDENTLY CONTROLLABLE ACTIVE STEERING SYSTEM FOR MAXIMIZING HANDLING PERFORMANCE LIMITS OF ROAD VEHICLES		98
4.1	Introduction	98
4.2	Vehicle Model	102
4.3	Control Strategy	104
4.3.1	<i>Controller synthesis</i>	105
4.3.2	<i>AIFS actuator model</i>	107
4.3.3	<i>Tire force saturation</i>	108
4.4	Driver Steering Input	111
4.5	Results and Discussion	113
4.5.1	<i>Ramp-step steering maneuver</i>	113
4.5.2	<i>Single-lane change maneuver</i>	120
4.5.3	<i>Double-lane change maneuver</i>	123
4.6	Conclusion	126

CHAPTER 5

BRAKING AND STEERING PERFORMANCE ANALYSIS OF A ROAD VEHICLE WITH ACTIVE INDEPENDENT FRONT STEERING (AIFS)	128
5.1 Introduction	128
5.2 Vehicle Dynamic Modeling	132
5.3 Controller Synthesis and Method of Analysis	135
5.4 Results and Discussions	140
5.4.1 <i>Effect of road friction</i>	145
5.4.2 <i>Vehicle weight and mass center coordinates</i>	148
5.4.3 <i>Robustness of the AIFS control</i>	150
5.4.4 <i>Disturbance rejection</i>	153
5.5 Conclusion	155

CHAPTER 6

CONCLUSIONS AND RECOMMENDATIONS	156
6.1 Highlights and Major Contributions of the Dissertation Research	156
6.2 Conclusion	159
6.3 Recommendations for Future Studies	161
Appendix A	
AFS MECHANISMS WITH PLANETARY GEAR SYSTEMS	164
Appendix B	
AIFS STEERING MECHANISM PROTOTYPE	171
Appendix C	
VEHICLE PARAMETERS	175
REFERENCES	177

LIST OF FIGURES

Figure 1.1: Cornering force of tires predicted from different tire models [7].	30
Figure 1.2: Designs of steering mechanisms for implementations of AFS control: (a) a steer-by-wire (SBW); and (b) a mechanical planetary gear system [44].	31
Figure 1.3: Steer-by-wire components in an AFS system [107].	32
Figure 1.4: Honda S2000 speed-dependent steering ratio [71].	34
Figure 1.5: Mechanical active steering mechanisms with variable gear ratio actuators: (a) a planetary gear; (b) a differential gear; and (c) a harmonic drive [116].	34
Figure 1.6: A bi-planetary gear with the locking unit in the BMW active steering system [44]. ..	36
Figure 1.7: A differential gear system used for angle superposition of the active steering system [118].	37
Figure 2.1: DOF nonlinear handling model with independent steering angle.	51
Figure 2.2: Tire lateral force zones.	53
Figure 2.3: Inner and the outer tire lateral force in a turning maneuver.	55
Figure 2.4: Independently controllable steering system with two sets of planetary gear systems [117].	58
Figure 2.5: The Simulink model of the vehicle with a PI controller.	59
Figure 2.6: Steering angle input for the J-turn maneuver.	60
Figure 2.7: Lateral acceleration for the J-turn maneuver with AFS controller.	61
Figure 2.8: The yaw rate response for the J-turn maneuver.	61
Figure 2.9: Trajectory of the vehicle in a J-turn maneuver.	62
Figure 2.10: Outer and inner wheel angle with the AFS and AIFS controller.	63
Figure 2.11: Outer and inner wheel side- slip angle.	63
Figure 2.12: Steering angle input for the sinusoidal maneuver.	64
Figure 2.13: Yaw rate response for the sinusoidal maneuver.	64
Figure 2.14: Trajectory of the vehicle in the sinusoidal maneuver.	65

Figure 2.15: Outer and inner wheel angle with the AFS and AIFS controller.	65
Figure 2.16: Outer and inner wheel side-slip angle with AFS and AIFS.	66
Figure 2.17: Lateral acceleration of the vehicle in the sinusoidal maneuver.....	66
Figure 2.18: Yaw rate response for the split- μ maneuver.....	67
Figure 2.19: Vehicle trajectory generated by the AFS and AIFS controllers.	67
Figure 2.20: Outer and inner wheel angle with the AFS and AIFS controller.	68
Figure 2.21: Outer and inner wheel side-slip angle with the AFS and AIFS controller.....	68
Figure 2.22: Lateral acceleration for the split- μ maneuver with AFS controller.	68
Figure 2.23: Height sensitivity analysis for yaw rate response with AFS and AIFS.....	69
Figure 3.1: Three-DOF directional dynamic model of a two axle truck: (a) roll-plane; and (b) yaw-plane.....	76
Figure 3.2: Partially filled tank truck model.....	78
Figure 3.3: Comparisons of (a) yaw rate; and (b) steer angle responses of the model employing AFS control based upon idealized and modified time-delayed reference yaw rate.....	82
Figure 3.4: Normalized cornering stiffness and identification of saturation zone of a truck tire. 84	
Figure 3.5: Steer angle corresponding to a J-turn maneuver.	85
Figure 3.6: Comparisons of responses of the fully loaded truck with AFS and AIFS control with those of the reference model (Ref) and model without active steering control (NC): (a) lateral acceleration; (b) yaw rate; and (c) path trajectory.	86
Figure 3.7: Comparison of work-loads of steered wheels of the vehicle model with AFS and AIFS control.....	87
Figure 3.8: Comparison of steered wheels angle developed with AFS and AIFS control.	88
Figure 3.9: Normal load on each wheel of the vehicle model with Active Steering Control.....	89
Figure 3.10: Variations in (a) lateral position of the liquid cargo CG; and (b) sprung mass roll angle responses of the 50%-filled liquid and equivalent rigid cargo vehicles.....	91
Figure 3.11: Comparison of the inner and outer wheel loads of the 50%-filled liquid and equivalent rigid cargo vehicles: (a) front axle wheels; and (b) rear-axle wheels.	92

Figure 3.12: Comparison of yaw rate responses of 50%-filled liquid and equivalent rigid cargo vehicles with the reference model response.....	92
Figure 3.13: Comparisons of directional response of the 50%-filled liquid cargo truck without active steering (NC), and with AFS and AIFS control: (a) yaw rate; and (b) path trajectory.	93
Figure 3.14: Comparisons of work-loads of the steered wheels of the 50%-filled liquid cargo truck with AFS and AIFS control.	93
Figure 3.15: Comparisons of steered wheels angles of the vehicle with AFS and AIFS control. 95	
Figure 3.16: Variations in normal loads of tires of the 50%-filled vehicle with active steering control.	95
Figure 4.1: Three-DOF directional dynamic model of a two axle truck: (a) roll-plane and; (b) yaw-plane.....	103
Figure 4.2: Schematic of the control structure.....	105
Figure 4.3: Normalized cornering stiffness and identification of the saturation zone of a truck tire [140].....	110
Figure 4.4: The structure of the AIFS control synthesis integrating tire-road adhesion saturation limits.	110
Figure 4.5: Ramp-step steer input.....	111
Figure 4.6: Driver path preview model coupled with the linear vehicle model.	112
Figure 4.7: (a) Desired path trajectory; and (b) steer angle corresponding to a single-lane change maneuver derived from the ideal driver model (83 km/h).....	112
Figure 4.8: (a) Desired trajectory; and (b) steer angle corresponding to an obstacle avoidance maneuver derived from the linear vehicle model coupled with the ideal driver model.	113
Figure 4.9: Comparisons of yaw rate and path trajectory of the truck model with conventional AFS and AIFS control and without control (NC) with those of the reference model (Ref): (a) yaw rate; and (b) path trajectory under uniform and split- μ road conditions at 57 km/h.....	114
Figure 4.10: Front inner and outer wheel angle of the model on a (a) uniform; and (b) split- μ road condition with conventional AFS and AIFS control (57 km/h).....	115
Figure 4.11: Front inner and outer wheels work-load of the model on a (a) uniform; and (b) split- μ road condition with conventional AFS and AIFS control (57 km/h).	116

Figure 4.12: Front inner and outer wheels slip angle of the model on a (a) uniform; and (b) split- μ road condition with conventional AFS and AIFS control (57 km/h).	116
Figure 4.13: Comparisons of the inner and outer wheels (a) steering angles; and (b) work-loads of the model with AIFS control at 52 km/h and 57 km/h on a uniform road.	119
Figure 4.14: Comparisons of (a) yaw rate; and (b) path trajectory responses of the vehicle model without active steering (NC), and with conventional AFS and AIFS control (Lane-change maneuver at 83 km/h).	120
Figure 4.15: Variations in work-loads of the (a) left-; and (b) right-steered wheels; and (c) the corresponding steer angles developed with conventional AFS and AIFS (Lane-change maneuver at 83 km/h, uniform road).	121
Figure 4.16: Variations in work-loads of the (a) left-; and (b) right-steered wheels; and (c) the corresponding steer angles developed with conventional AFS and AIFS (Lane-change maneuver at 83 km/h, split- μ road).	122
Figure 4.17: (a) Yaw rate; and (b) path trajectory responses of the vehicle model without active steering (NC), and with conventional AFS and AIFS (double lane-change at 83 km/h).	123
Figure 4.18: Work-loads of the (a) left; (b) right steered wheels; and (c) the corresponding steer angles developed with conventional AFS and AIFS (double lane-change maneuver at 83 km/h, uniform road).	124
Figure 4.19: Work-loads of the (a) left; (b) right steered wheels; and (c) the corresponding steer angles developed with conventional AFS and AIFS (double lane-change maneuver at 83 km/h, split- μ road).	125
Figure 5.1: Full vehicle model for braking and turning maneuver.	132
Figure 5.2: (a) Tire slip angle; and (b) rotational dynamics of the wheel.	135
Figure 5.3: Schematic of the AIFS control structure.	137
Figure 5.4: Simulink diagrams illustrating: (a) the full vehicle model; (b) AIFS controller block; and (c) the brake system model.	138
Figure 5.5: (a) Steer angle; and (b) braking torque during the braking in a turn maneuver.	139
Figure 5.6: Comparisons of longitudinal slip ratios of the inside tires of the vehicle with AFS and AIFS control ($Tb=5580$ Nm; $\mu=0.78$ at 57 km/h).	140
Figure 5.7: Comparisons of directional responses of the vehicle with conventional AFS and AIFS control and without steering control: (a) path trajectory; (b) yaw rate; (c) longitudinal velocity; and (d) longitudinal and lateral accelerations ($V=57$ km/h, $\mu=0.78$).	142

Figure 5.8: Inner and outer wheels (a) steer angle; and (b) work-load responses of the vehicle models with conventional AFS and AIFS control ($V=57$ km/h, $\mu=0.78$).....	144
Figure 5.9: Comparisons of (a) tire slip angle; and (b) longitudinal slip ratio responses of the vehicle model with conventional AFS and AIFS control ($V=57$ km/h, $\mu=0.78$).....	144
Figure 5.10: Comparisons of maximum brake torque and stopping time of the vehicle model with conventional AFS and AIFS systems for a range of speeds and adhesion coefficients.	146
Figure 5.11: Comparisons of (a) side-slip angle; and (b) path trajectory of the vehicle model without active steering (NC), conventional AFS and AIFS control on a low friction road ($\mu = 0.5$; $V=52$ km/h).....	147
Figure 5.12: Comparisons of (a) steered wheel angles; and (b) inner tire work-load developed with AIFS for different loading conditions ($Tb=6945$, $V =57$ km/h and $\mu =0.78$).....	148
Figure 5.13: (a) Unity-feedback plant and controller functions; and (b) closed-loop system integrating the AIFS controller and actuator model.	151
Figure 5.14: The robust stability criterion showing magnitudes of the perturbation function with maximum and minimum tire cornering stiffness.	152
Figure 5.15: Comparisons of the lateral path deviations of the vehicle models with AIFS and without a steering control (NC) under a 8 kN side force disturbance: (a) $V= 80$ km/h; and (b) $V= 120$ km/h.	153
Figure 5.16: Comparison of vehicle path deviations of the vehicle models with AIFS and without a steering control (NC) under braking on a split- μ surface ($V= 100$ km/h; $Tb=6$ kNm.	154
Figure A.1: Relation between the steering wheel angle and the front wheels angle in: (a) conventional; and (b) active steering system [154].	165
Figure A.2: Configuration I of planetary gear system [155].	166
Figure A.3: Configuration II of planetary gear system [156].	167
Figure A.4: Configuration III of planetary gear system [154].	168
Figure B.1: 3D-layout of proposed AIFS mechanism.	172
Figure B.2: First prototype of the AIFS mechanism.....	172
Figure B.3: Designed AIFS prototype installed on a project vehicle structure.	172
Figure B.4: Modified connection between the tie rods and racks using threaded rods	174

LIST OF TABLES

Table 1.1: Summary of reported studies on DYC controller for enhancing the dynamic responses of road vehicles.	11
Table 1.2: Summary of reported studies on AFS controller for enhancing the dynamic responses of road vehicles.	19
Table 1.3: Summary of reported studies on 4WS controller for enhancing the dynamic responses of road vehicles.	22
Table 1.4: Relative merits and limitations of the AFS, DYC, and integrated AFS and DYC systems.	28
Table 1.5: Comparison of application of SBW and mechanical steering system.	38
Table 3.1: Comparisons of tire work-loads and steady-state steering responses of the fully loaded truck with AFS and AIFS control.	90
Table 3.2: Comparisons of tire work-loads and steady-state steering responses of the 50%-filled tank truck with AFS and AIFS control.	96
Table 4.1: Steady-state directional responses of the truck with conventional AFS and AIFS control on a uniform and split- μ surfaces.	117
Table 4.2: Variations in steady-state angles and workloads of the inside and outside wheels with increasing forward speed of the vehicle model with AFS and AIFS subject to a steady-turning maneuver on a uniform and a split- μ road surface.	117
Table 5.1: Comparisons of the braking characteristics of the vehicle with conventional AFS, AIFS and without steering control (NC) on two different road surfaces ($\delta st = 0.07$ rad).	141
Table 5.2: Critical slip ratio and braking distribution for different road adhesion coefficients ($\delta st = 0.07$ rad)	145
Table 5.3: Effect of variations in CG height and longitudinal coordinate on the stopping time and brake torque of the vehicle with AFS and AIFS control ($\delta st = 0.07$ rad, $\mu = 0.78$).	150
Table A.1: Summary of the planetary gear configurations and resulting pinion angle.	169
Table C.1: Simulation parameters for a step van vehicle.	175
Table C.2: Simulation parameters for fully loaded two-axle truck.	175

NOMENCLATURE

SYMBOL	DESCRIPTION
ACT-SUS	Active Suspension
ABC	Active Brake Control
ABS	Anti-lock Brake System
AIFS	Active Independent Front Steering
AFS	Active Front Steering
ARC	Active Roll Control
ARS	Active Rear Steering
CCV	Control Configured Vehicle
CG	Center of Gravity
DAS	Driver Assist Systems
DBC	Differential Braking Control
DYC	Direct Yaw-moment Control
ECU	Electronic Control Unit
EPS	Electronic Power Steering
ERC	Emergency Roll Control
ESC	Electronic Stability Control
ESP	Electronic Stability Program
HILS	Hardware-In-the-Loop-Simulation
INS	Inertial Navigation System
KKT	Karush-Kuhn-Tucker
LCV	Long Combination Vehicle
LQR	Linear-Quadratic Regulator
MPC	Model Predictive Control
NC	No Control
PI	Proportional Integral
PID	Proportional Integral Derivative

PMSM	Permanent Magnet Synchronous Motor
QFT	Quantitative Feedback Theory
RMM	Robust Model Matching
RMS	Root Mean Square
RWA	Rearward Amplification
RWS	Rear Wheel Steering
SBW	Steer-By-Wire
SM	Sliding Mode
SOSM	Second Order Sliding Mode
SUV	Sport Utility Vehicles
TCS	Traction Control System
TTR	Time-To-Rollover
VDC	Vehicle Dynamics Control
VGR	Variable Gear Ratio
VSC	Vehicle Stability Control
VSR	Variable Steering Ratio
VTD	Variable Torque Distribution
4WS	Four Wheel Steering
4WIS	4-Wheel Independent Steering
A_W	Vehicle side area
a_x	Vehicle longitudinal acceleration
a_y	Vehicle lateral acceleration
a_{yc}	Lateral acceleration at liquid load CG
b	Distance of CG from front axle
c	Distance of CG from rear axle
C_W	Aerodynamic side force coefficient
$C_{\phi F}$	Front suspension roll damping
$C_{\phi R}$	Rear suspension roll damping

e_w	Distance between geometric center of side body and CG
F_{Xij}	Tire longitudinal force, (i =front and rear, j =right and left)
F_{Yij}	Tire lateral force, (i =front and rear, j =right and left)
F_{Zij}	Tire normal force, (i =front and rear, j =right and left)
F_W	Wind force
h_c	Liquid CG height from roll center
h_{cg}	Total mass CG height from the ground
h_{cgs}	Sprung mass CG height from the ground
h_{Froll}	Front roll center height from ground
h_{Rroll}	Rear roll center height from ground
h_s	Sprung mass CG height from the roll center
h'_s	Chassis CG height from roll center
h_{uF}	Height of front unsprung mass CG from ground
h_{uR}	Height of rear unsprung mass CG from ground
I_w	Wheel moment of inertia
I_{xs}	Total sprung mass moment of inertia about x-axis
I_{xsc}	Chassis and load mass moment of inertia about x-axis
I_{xzs}	Total sprung mass moment of inertia about xz-axis
I_{xzsc}	Chassis and load mass moment of inertia about xz-axis
I_{zs}	Total sprung mass moment of inertia about z-axis
I_{zsc}	Chassis and load mass moment of inertia about z-axis
I_{zu}	Total unsprung mass moment of inertia about z-axis
K_p	Proportional gain
K_I	Integral gain
K_D	Derivative gain
K_{ins}	Instantaneous cornering stiffness
K_{int}	Initial cornering stiffness
k_{bF}	Front wheel brake torque distribution factor
k_{bR}	Rear wheel brake torque distribution factor
k_{bRj}^*	Rear wheel lock-up gain

K_{FO}	Nominal front tire cornering stiffness
K_{RO}	Nominal rear tire cornering stiffness
$K_{\phi F}$	Front suspension roll stiffness
$K_{\phi R}$	Rear suspension roll stiffness
L	Wheelbase
m	Total vehicle mass
m_c	Load mass
m'_s	Chassis mass without load
m_{sF}	Front sprung mass
m_{sR}	Rear sprung mass
m_{uF}	Front unsprung mass
m_{uR}	Rear unsprung mass
M_{ij}	Tire self-aligning moment
r	Yaw rate
r_{ref}	Reference yaw rate
r_{ref}^*	Refined reference yaw rate
R_w	Wheel radius
T_{bij}	Braking torque
T_{dij}	Driving torque
T_F	Half front track
T_R	Half rear track
V	Vehicle speed
V_x	Longitudinal velocity
V_y	Lateral velocity
W_F	Front axle weight
W_R	Rear axle weight
W_T	Tire work-load
α_{ij}	Tire slip angle
α^*	Saturated tire slip angle
β	Vehicle side-slip angle

γ	Liquid free surface gradient
δ_C	Steering correction command
δ_I	Inner wheel angle
δ_l	Left wheel angle
δ_l^*	Limiting steering value of inner wheel
δ_O	Outer wheel angle
δ_r	Right wheel angle
δ_{st}	Average wheel steering angle
θ	Yaw angle
λ_{ij}	Longitudinal slip ratio
λ^*	Limited longitudinal slip ratio
μ	Tire-road friction coefficient
μ_r	Tire-road friction coefficient at right wheel
μ_l	Tire-road friction coefficient at left wheel
τ	Time constant
ϕ	Roll angle
ω	Frequency of the system
Ω_{ij}	Wheel angular velocity

CHAPTER 1

LITERATURE REVIEW AND SCOPE OF THE DISSERTATION

1.1 Introduction

The steering system of a road vehicle facilitates the execution of the human driver's command to the vehicle, which subsequently determines the resulting handling and stability performances. The increasing demands for active safety systems in road vehicles have evolved into an array of automated driver-assist or driver-independent steering systems. The active front steering (AFS) system is one example of such developments, which can substantially enhance the handling dynamics functions of a road vehicle, with greater safety limits and ease of operation by the driver [1,2]. The steering mechanism in conventional road vehicles is generally designed to closely follow the Ackerman ratio for the inner and outer wheels steer angles at low speeds. The presence of slip angles developed at the tires at high speeds, however, tends to substantially alter the path following ability of the vehicle to a given steering input. This phenomenon attributed to the compliance of the pneumatic tires, also known as the vehicle understeer characteristic, can be effectively compensated through active control of wheels as a function of the forward speed and the maneuver demands.

A number of concepts in active front steering (AFS), capable of providing continuous and situation-dependent variations in the steering ratio, have evolved during the past two decades for realizing improved low-speed maneuverability and high-speed stability performance of the vehicle. An AFS system alters the inner and the outer wheels angles simultaneously in order to realize a pre-determined target response depending on the forward speed and steering input. The

AFS designs, however, do not consider the tire saturation limits associated with the available road adhesion. Owing to the nonlinear cornering characteristics of pneumatic tires, a wheel may approach lateral force saturation under a high lateral acceleration maneuver and thereby limit its ability to generate the required lateral force. The AFS system may thus exhibit a distinct limitation in providing the target response or controllability under high-g maneuvers that lead to significant lateral load shift as in the case of commercial vehicles with high center of mass.

Vehicle stability control (VSC) systems such as direct yaw-moment controllers (DYC) are known to be more effective than the AFS under high lateral acceleration maneuvers, since these generate the required yaw moment via differential braking [3,4]. A DYC system alone, however, yields limited performance in tracking a target vehicle response to steering inputs, apart from longer stopping distance during an emergency braking maneuver and reduced tire life [5,6]. Furthermore, it may cause a directional instability in an emergency braking maneuver on a split- μ road condition, where the road adhesion limits of the left and right side could be substantially different [1]. A number of studies have explored the coordinated control of AFS and DYC to realize enhanced vehicle control performance under a wide range of operating conditions. The integrated AFS and DYC control, however, is considered to be far more complex involving relatively large number of tracking or estimated parameters [7-9].

Alternatively, the performance potentials of an AFS could be greatly enhanced through independent control of the inner and outer wheels' steer angles with appropriate considerations of the tires saturation. This would permit optimal utilization of the available adhesion of both the wheels to meet the cornering demand of the vehicle, particularly under the large magnitude lateral load transfers caused by high-acceleration maneuvers. Such a concept, referred to as

Active Independent Front Steering (AIFS) system in this dissertation, would likely lead to enhanced handling and stability over a wide range of operating conditions, including the operation under split- μ road conditions. Furthermore, the AIFS system can also be integrated with DYC to achieve improved yaw stability limits of the vehicle. The AIFS control could also allow for improved distribution of available road adhesion in realizing desired fore-aft and lateral tire forces under simultaneous braking and steering maneuvers.

The implementation of AIFS, however, would necessitate the design of a practical mechanism to achieve independent variations in the inside and outside wheels angles, which forms the major challenge in realizing the AIFS concept. The reported studies on adaptive steering systems generally propose the use of “Steer-by-Wire” (SBW) together with a mechanical backup system [10-12]. A few mechanical active steering systems have also evolved to achieve variable steering ratio (VSR), and thereby assist the driver’s steering effort [13-15]. Such systems, however, do not permit independent steering control of the inner and outer wheels.

The proposed dissertation research investigates the concept of an AIFS control strategy for realizing enhanced handling performance limits of road vehicles under a range of operating conditions. A controller synthesis is formulated so as to utilize the available adhesion limits of both the steered wheels prior to their saturation. The performance potentials of the AIFS are investigated through formulation and simulations of a nonlinear handling model of a road vehicle considering independent steering of the inner and outer wheels. The effectiveness of the AIFS control is particularly explored for high center of mass vehicles involving large longitudinal and lateral load shifts, and operation on uniform as well as split- μ road conditions. A fail-safe

mechanical steering mechanism is subsequently described for implementation of the proposed AIFS concept.

1.2 Review of Relevant Literature

Technological developments in road vehicles over the last two decades have been directed towards realizing enhanced safety performance limits, while limiting the control demands on the drivers. This is primarily achieved by overcoming various conflicting parametric requirements through the use of adaptive elements and controllers. Prime examples of these developments include the active suspensions (ACT-SUS) [16], active roll control (ARC) [17], variable gear ratio steering (VGR) [15] with an active front steering system (AFS), electronic power steering (EPS) [18], direct yaw-moment control (DYC) utilizing the anti-lock-braking systems (ABS) [19] and the traction control systems (TCS) [19].

Since the focus of the current research is active steering system, an extensive review of literature has been carried out on topics related to active steering, together with handling and direction control performance of road vehicles. The studies on chassis control systems such as direct yaw-moment control (DYC), active front steering (AFS), four wheel steering (4WS) as well as integrated AFS/4WS and DYC are considered to be the most relevant topics. The review is carried out in order to develop the scope of the dissertation research towards advancements in active steering system. The reported studies on various chassis control systems, together with their relative merits and limitations, are summarized in the following sub-sections.

1.2.1 Direct yaw-moment control (DYC) system

Concepts in direct yaw-moment control (DYC) systems have mostly evolved during the past

two decades as effective methods to enhance vehicle directional stability in emergency situations, where the vehicle experiences a high lateral acceleration [3,20-22]. Under such driving conditions, the tire forces reach the saturation region, leading to rapid increase in the vehicle side-slip angle, which limits the steered wheels ability to generate the required yaw moment for ensuring adequate directional control and stability. A DYC control strategy imposes the desired yaw moment by distributing differential longitudinal forces between the left and right wheels as well as by controlling the engine throttle. Stability control systems employing such a control strategy have been denoted in widely different terms such as: DYC (Direct Yaw-moment Control) [3], VDC (Vehicle Dynamic Control) [4], ESC (Electronic Stability Control) [23], ESP (Electronic Stability Program) [24], VTD (Variable Torque Distribution) [25] and DBC (Differential Braking Control) [26]. These strategies generally utilize anti-lock braking system (ABS) [27] technology along with different sensors, hardware and controllers.

The yaw rate and side-slip angle are the two key response parameters that not only describe but also serve as essential quantities for controller designs for realizing enhanced handling and stability performance of the vehicle [24]. The reported studies have invariably shown that a DYC control system could effectively generate the required yaw moment by tracking either the yaw rate [21,28] or the vehicle side-slip angle [22,29]. A number of studies have also proposed yaw moment control through control of both the parameters simultaneously. The majority of these use the linear quadratic regulator (LQR) theory in conjunction with different weightings for the yaw rate and the side-slip angle [4,6,30]. It is also known that, tracking of the side-slip angle is far more challenging than the yaw rate [6,22].

Several attempts have been made to explore DYC systems with different control approaches

so as to enhance the handling, control and stability of the vehicle. The preliminary discussions and analyses of the DYC concepts emerged in 1993 [3]. This study integrated the dynamics of a seven-degrees-of-freedom (DOF) vehicle model with a DYC system in the nonlinear region, where the tires approached saturation limits during high speed turning maneuvers. The study proposed the “ β -method”, suggesting that the vehicle side-slip angle would serve as the key indicator of the vehicle stability and dynamics in different states of motion including the nonlinear and transient motions. This technique was utilized to generate the required yaw moment with transversal distribution of traction and braking forces between the left- and the right- rear wheels. Through simulation results, it was shown that the proposed controller could yield transient directional responses close to the steady-state cornering responses, and thereby improves the vehicle maneuverability limits.

Subsequently, Van Zanten et al. [4] developed the DYC system hardware including the steering wheel angle and yaw rate, lateral acceleration and wheel speed sensors as well as hydraulic and the electronic control unit. This DYC system was introduced as the Vehicle Dynamic Control (VDC) system, and was evaluated on the test track under different driving conditions. A cascade control was synthesized consisting of inner loop for wheel slip control and outer feedback loop for tracking the desired yaw moment by adjusting the steering angle, engine torque and the wheel brake pressures. The stability of the vehicle equipped with VDC system was evaluated through experiments and simulations under rapid lane change, slalom and J-turn maneuvers at different speeds. It was shown that the proposed VDC system could achieve the enhanced handling performance and stability limits under severe operating and road conditions. A VDC system based on the vehicle side-slip control was also developed by Bosch [24], which

was referred to as electronic stability program (ESP). The ESP system generated the required yaw moment by controlling the vehicle side-slip through individual wheel slip control. The Bosch study also reported the five years long experience with the ESP system, suggesting notable reductions in fatalities in severe accidents with vehicles employing the ESP.

The significance of DYC system as an active safety control in road vehicles was also emphasized by Abe [22] through relative performance analyses of DYC and other available active safety control systems. Similar to the study reported in [3], the stability limits of a vehicle were investigated in the vicinity of the tire nonlinear region (tire force saturation zone) using a simple two-DOF vehicle model including the yaw rate and the side-slip angle. Through solution of the characteristic equation of the system, it was shown that a reduction in the rear tire cornering stiffness caused by a large vehicle side-slip angle, low tire-road friction coefficient or large load transfer between the front and rear axles during braking could lead to lateral instability of the nonlinear vehicle model. A sliding mode (SM) control method was subsequently synthesized to track the side-slip angle using the DYC system. It was concluded that a DYC could provide most effective control of the directional instability in the presence of a high lateral acceleration compared to the four wheel steering systems. Similarly, Hamzah [31] examined the directional stability of a DYC system using the sliding mode control methodology. It was shown that the discontinuous control action of the sliding control could cause high frequency chatter and thereby rapid mechanical wear and passenger discomfort. Alternatively, a second order sliding mode (SOSM) control was proposed to generate continuous control action. Although, both the SM and SOSM could effectively track the desired responses with similar accuracy, the SM control technique caused greater reduction in the vehicle speed due to higher braking

pressures applied to the wheels, which is not desirable particularly during high-speed lane-change maneuvers.

The DYC has been widely studied during the past decade, focusing on its potential merits and limitations. For instance, a recent study proposed a DYC synthesis with minimal usage of the external yaw moment considering a simple two-DOF linear yaw-plane model of the vehicle [6]. The controller synthesis was realized to minimize the external yaw moment so as to reduce the undesirable effects of braking-base yaw moment control, namely the reduction in the vehicle speed and the tire wear. It was shown that limiting the external yaw moment would yield relatively higher path tracking errors, and that the DYC control based on side-slip angle tracking can provide enhanced lateral stability compared to that based on the yaw rate response, particularly for the low adhesion roads or high lateral acceleration turning maneuvers.

Tamaddoni et al. [32] investigated the stability of a vehicle with the DYC considering driver as an additional controller. The study employed a close-loop steering using a driver model in conjunction with the game theory. The steering input of the driver and the corrective yaw moment input from the DYC were considered as two players in the controller synthesis. Using the Nash optimal strategy, the driver was considered to provide the steering control, while the DYC ensured optimal performance and robustness of the coupled driver-vehicle system. The study employed a nonlinear vehicle model in the CarSim platform [33] and concluded that increasing the driver preview time could effectively enhance the vehicle stability and reduce the driver's effort.

The vast majority of the studies have generally focused on DYC with an objective to enhance the directional stability limit of the vehicle, a few studies have suggested improved

vehicle rollover immunity during high speed turning maneuvers. For example, Chen et al. [34] studied the roll dynamics of a sport utility vehicle (SUV) with a DYC controller using a three-DOF yaw-roll model of the vehicle. The model was verified against the fourteen-DOF vehicle model in the Trucksim platform. The time-to-rollover (TTR) metric was used to detect the onset of a rollover and for activation of the DYC controller. The study showed that the braking force applied by DYC on the steered wheels, reduced the longitudinal velocity, yaw rate and the tire lateral force, which resulted in lower lateral acceleration. The rollover prevention DYC control was synthesized based on the lateral acceleration feedback and its effectiveness was demonstrated through both the simulator- and the test track results under a wide range of operating conditions. The proposed controller, however, could not effectively assure the rollover immunity under extreme maneuvers. Alternatively Hopkins et al. [35] proposed a DYC control together with an emergency roll control (ERC) system to achieve improved lateral and roll stability of a linear two-DOF yaw-plane vehicle model. The simulation results depicted that the DYC control could reduce the vehicle roll by limiting the lateral acceleration, while the ERC control could enhance the roll threshold limit of the vehicle.

Although DYC control could yield definite handling performance gains particularly during high lateral acceleration maneuvers, a number of studies have also demonstrated its limited performance during different maneuvers. For instance, an emergency braking on a split- μ surface condition may lead to low magnitude yaw rate due to asymmetric longitudinal forces developed at the steered wheels [1,5,36,37]. Furthermore, a vehicle equipped with DYC system may not be able to effectively reject the yaw moment generated by the wind force on a split- μ surface depending on the directions of the moment due to disturbance caused by asymmetric wheel

forces. The DYC may also adversely affect the braking performance of the vehicle since it emphasizes the yaw stability over braking [5].

The reduction in the forward speed is perhaps the most important limitations of a DYC, which generates the desired moment through application of braking. Such a speed reduction would be highly undesirable during rapid path change or obstacle avoidance maneuvers [38]. Activation of the DYC is thus known to cause noticeable vehicle deceleration, noise and pedal pulsation, which are generally perceived as annoyance by the driver. The design of a DYC thus involves a trade-off between vehicle stability and driver comfort [5,39]. The DYC also accelerates tire wear due to frequent braking applications [6]. Furthermore, the DYC system can generate only limited corrective moment due to relatively smaller track width and actuation through selective braking. Alternatively, an active steering system can provide the required moment more effectively since the wheelbase is significantly larger than the track width [1].

It has been suggested that a vehicle equipped with a DYC system based on tracking of the side-slip angle could yield higher stability limits. The direct measurement of side-slip angles, however, is more complex. A number of studies have thus proposed slip angle estimation methods from directly measured responses of the vehicle such as yaw rate, longitudinal velocity and lateral acceleration [40,41]. Ryu et al. [42] also proposed a side-slip estimation scheme based on GPS and INS (inertial navigation system) measurements, which are considered to be expensive for implementation in production vehicles. The major contributions and conclusions of the reviewed studies with DYC systems are summarized in Table 1.1.

Table 1.1: Summary of reported studies on DYC controller for enhancing the dynamic responses of road vehicles.

Author	Vehicle model	Tracked parameter	Control method	Results
Shibahata et al. (1993)	7-DOF	side-slip angle	β -method	Firstly introduced DYC system; and Improved transient directional responses of vehicle maneuverability.
Van Zanten et al. (1995, 2000)	3-DOF	side-slip angle and yaw rate	wheel slip control (ABS) and state-space feedback controller (LQ optimal method)	Development of the DYC system hardware; and Test track evaluation under different driving conditions.
Abe (1999)	2-DOF	side-slip angle	sliding mode	Comparison of DYC with 4WS in high-g maneuvers.
Chen et al. (2001)	14-DOF vehicle model in TruckSim platform	lateral acceleration and roll angle	proportional gain feedback	Improved rollover immunity during high speed turning maneuvers.
Mirzaei (2010)	2-DOF	side-slip angle and yaw rate	LQ optimal method	Reduced adverse effect of external yaw moment with braking-base controller.
Hopkins et al. (2010)	2-DOF	lateral acceleration and yaw rate	Lyapunov stability criteria	Improved lateral and roll stability with integrated DYC and ERC controllers under extreme maneuvers.
Tamaddoni et al. (2011)	comprehensive vehicle model in CarSim platform	lateral deviation, lateral velocity, yaw angle and yaw rate	game theory using Nash optimal strategy	Robust DYC system design integrated with driver model.
Hamzah et al. (2012)	2-DOF	side-slip angle and yaw rate	conventional sliding mode and second order sliding mode	Reduced high frequency chattering; and improved passenger comfort with second order sliding mode compared to conventional sliding mode controller.

1.2.2 *Active front steering (AFS) system*

Active front steering systems (AFS) have been designed to vary steer angles in an active manner to realize a target directional response. The steer angles of both the inner and outer wheels are altered simultaneously, while maintaining nearly Ackerman geometry [43]. The concept of AFS was first explored by Kasselmann and Keranen [2] of Bendix as early as 1969. The proposed system was referred to as “Adaptive Steering” with objective to achieve improved vehicle stability under disturbances caused by wind gusts and rough road conditions. The control strategy was synthesized using the yaw rate responses compared to a desired model response in order to calculate the corrective steering angle. Both the computer simulations and road tests results suggested that proposed steering system could provide enhanced handling performance, while minimizing the driver corrective actions in presence of external disturbances. Despite the proven performance and the technical feasibility of the proposed adaptive steering, the implementations were realized only during the last decade, most likely due to the high cost. First implementation of the concept thus was reported as recently as 2003, when ZF Lenksysteme GmbH [44] developed and introduced AFS in the market.

Accordingly, a number of studies have explored the effectiveness of the AFS under cross-wind disturbances that strongly affect the directional stability and control performance of the vehicle [45-47]. Oraby et al. [45] studied the lateral stability of a three-DOF yaw-plane model of a car with the AFS system under side force disturbances when overtaking a truck. The study employed the optimal control theory based on the LQR method and concluded that the proposed AFS control system could not only augment the handling performance and stability of the vehicle by decreasing the lateral path deviation, but also could reduce the steering effort of the

driver. Accordingly, the steering assistance feature of the AFS has been extensively evaluated through simulation and experimental results [13,48-51]. Oraby et al. [52] compared the AFS performance with that of a four wheel steering (4WS) vehicle under random side wind disturbances during high speed straight line maneuvers. The results suggested that the AFS controller could significantly augment the lateral stability of the vehicle through considerable reduction in the side-slip angle compare to the 4WS vehicle. The frequency response of the steering wheel angle was further used to demonstrate the significant reduction in the steering effort by the driver. The proposed AFS system, however, resulted in higher roll motion of the vehicle due to the additional steering angle.

Owing to strong dependence of the vehicle behavior on a large number of design and operating parameters, the robustness of the AFS control has been emphasized in a number of studies. The reported studies have investigated the AFS sensitivity to various certain or uncertain parameters such as speed, mass, CG location, tire cornering stiffness and tire-road adhesion. Tagawa et al. [51] proposed an active front steering system based on robust model matching (RMM) control algorithm to study the nonlinear dynamics of the vehicle generated by the tire forces. The study employed a very simple single-track bicycle model of the vehicle and two different controllers aimed at reference model tracking to realize the yaw rate frequency response and robustness compensator using a second order low-pass filter function. The effectiveness of the proposed controller was demonstrated during a lane change maneuver for a range of road surface friction and forward speeds. It was shown that the method could yield enhanced vehicle handling performance with reduced drivers' steering effort. Ackerman [53] proposed an alternate approach in designing a robust active front steering control strategy by decoupling the lateral and

yaw motions of a simplified single-track vehicle model. Decoupling was achieved through negative yaw rate feedback, and it was concluded that the decoupling control technique could effectively reduce the influence of a yaw disturbance on both the yaw rate and the side-slip angle, which subsequently resulted in enhanced handling and stability of the vehicle. The concept was subsequently validated through road tests [54].

Alternatively, Fukao et al. [46] proposed an adaptive nonlinear control strategy to enhance robustness of the AFS system under different steering and driving conditions using a three-DOF nonlinear single track vehicle model. Model reference adaptive nonlinear control strategy was formulated so as to track a desired model consisting of linear integration of the yaw rate and the lateral acceleration. The stability of the proposed controller was assured through a Lyapunov candidate function. The simulation results revealed substantial yaw disturbance rejection originating from the side wind gusts or high speed turning on low friction surfaces. Zhang et al. [55] investigated the effects of the vehicle parameters' variations on the handling performance of the AFS system using quantitative feedback theory (QFT) in the frequency domain. Unlike the aforementioned studies, a comprehensive vehicle model developed in ADAMS/Car platform was employed and combined with Matlab/Simulink for the purpose of control application. Uncertainty in the parameters and the robustness of the proposed controller synthesis was illustrated through a parameter sensitivity analysis. The results of aforementioned studies however revealed the performance limits of the AFS, where the steered wheels approached saturation.

The analysis of safety of the AFS components has also been the focus of many studies. Chen et al. [49] designed an active steering system comprising two actuators: an AFS actuator

intended to achieve improved stability and handling performance of the vehicle and an electric power steering actuator (EPS) with purpose of providing the assisting torque. The AFS control strategy involved a feed-forward control to determine the front wheel angle according to the desired variable steer ratio (VSR) as a function of the speed, and a feedback control of the yaw rate and side-slip angle to achieve stable performance. The results obtained through hardware-in-the-loop-simulations (HILS) suggested that the proposed AFS control could yield enhanced handling performance and stability of the vehicle during severe maneuvers such as lane change on a wet road and braking on a split- μ road condition. The EPS system could help reduce the reaction steering torque and thus reduced driver effort. Reinelt et al. [50] investigated the safety dynamics of the open- and close-loop AFS system considering the dynamics of various subsystems such as the steering rack, electric motor, planetary gear system, steering column and the hand steering wheel. These studies, however, did not address the concerns related to saturation of inner wheel during an extreme maneuver when the control is realized by an AFS.

Since the stability is of primary concern for the vehicles with high loads and high center of gravity, the applications of AFS have also explored for commercial vehicles. From the review of studies reporting the performance potentials of AFS applied to commercial vehicles, it is apparent that the AFS control strategy has been mostly explored with an objective to reduce the rollover hazard in an emergency maneuver [56-59]. Ackerman et al. [60], however, reported that although the AFS controller could enhance the vehicle rollover threshold, it may lead to a lateral instability during an evasive maneuver. An AFS system alone may thus provide enhanced vehicle rollover immunity at the expense of poor handling performance through relatively greater

path deviations. Integration of DYC together with active steering was thus proposed in order to limit the path deviations.

Odenthal et al. [56] investigated the application of AFS system for rollover avoidance of a single-unit commercial vehicle. A controller synthesis comprising three feedback loops involving continuous steering control, emergency steering control and emergency braking control was analyzed considering a simple three-DOF constant velocity vehicle model. The first feedback controller generated the additional steering angle through the velocity gain scheduled feedback of roll rate and roll acceleration to improve the roll damping of the vehicle over a wide range of vehicle speed. The nonlinear emergency steering control was designed to correct the steering angle when the sprung mass lateral acceleration exceeded a predefined threshold value. This controller thus assigned the rollover avoidance priority over lane-keeping since a tripped vehicle would not be steerable during an emergency high-lateral acceleration maneuver. Integrating the emergency braking feedback controller, however, could help reduce the path deviation caused by the emergency steering control system.

The directional response characteristics of tucks with AFS have also been reported in a few studies. Kharrazi et al. [61], in a recent study, investigated applications of active steering of the towed unit axles, dolly and semitrailer of a long combination vehicle (LCV) in view of the lateral dynamic performance of the vehicle combination. The main objective of the active steering controller was to reduce the time delay between the driver steering input and the lateral forces generating at the towed units particularly under high speed maneuvers. The desired steer angle of the towed unit axles was realized using a combination of the feed-forward and feedback controller, using a linear single-track model of a truck-dolly-semitrailer. The feed-forward

controller was designed to increase the response rate by compensating for the time lag as a function of the vehicle speed and the steering input frequency estimated from a reference model. The feedback controller was synthesized to minimize the error between the desired and actual yaw rate of the towed axles. The simulation results under a series of single and double-lane change maneuvers showed considerable damping of the yaw velocity, rearward amplification (RWA), lateral acceleration and off-tracking responses of the towed units when compared to those without the controller.

In another study, Junjovich et al. [62] studied the handling responses of an articulated heavy vehicle incorporating active steering of the individual tri-axle trailer. The steering control strategy was developed to enhance path following of the rear trailer, where the path was defined by the fifth wheel coordinates, together with minimization of the trailer axle tire forces. The test track results revealed improved performance in terms of reduced entrance tail swing, trailer off-tracking, peak lateral force, exit settling distance and tire scrubbing.

McCann et al. [63] studied the application of an AFS system to an articulated tractor-semitrailer combination with an objective to prevent jackknife instabilities during severe driving maneuvers considering the effects of driver's perception to vehicle responses. Yu [64] investigated the yaw stability of a bus equipped with an AFS system, where the required steer angle was estimated through a PI controller synthesized to minimize the yaw rate tracking error. The validity of the proposed controller was demonstrated through experiments under different steering maneuvers on various road conditions. The results suggested the significant role of the AFS as an automatic driver-assistance system in enhancing the maneuverability and stability of the vehicle during high-speed maneuvers coupled with external disturbances such as side-wind

gust. The study also showed similar results from the PI controller and the H_∞ loop shaping technique with vehicle operation on high friction coefficient surfaces, while the stability of both the controllers could not be ensured on low friction surfaces. Furthermore the AFS has been considered as an effective safety option in articulated steering vehicles used in the construction and forestry sectors such as scrapers, loaders and forestry skidders [65].

The reported studies invariably suggest that an AFS system can assist the driver in realizing desired vehicle handling effort by introducing a corrective steering angle and thereby a moment to suppress the yaw instability that may be caused by disturbances, such as variation in tire-road friction and side wind gust. The effectiveness of an AFS system under high lateral acceleration maneuvers leading to potential tire force saturation, however, is evident only when it is coupled with a DYC system. The vast majority of the studies neglect to examine the inherent potential for inner wheel to approach saturation when control is realized by AFS alone during an extreme maneuver. Table 1.2 summarizes the key reported studies in AFS system together with the control logic, vehicle model and the important findings.

1.2.3 Four wheel steering (4WS) system

Considerable efforts have been also made towards four wheel steering (4WS) or active rear steering (ARS) systems [66-68]. The 4WS was the first generation of chassis control systems developed for enhancing the dynamic performance of vehicles. Sano et al. [69] employed a three-DOF nonlinear vehicle model to evaluate dynamic responses of a speed-dependent 4WS vehicle. The rear wheels angle was actively controlled with opposite steering of the front wheels for realizing improved maneuvering of the vehicle at low speeds. Both the front and rear wheels were steered in the same direction at higher speeds for realizing enhanced lateral stability.

Table 1.2: Summary of reported studies on AFS controller for enhancing the dynamic responses of road vehicles.

Author	Vehicle model	Tracked parameter	Controller method	Results
Tagawa et al. (1996)	2-DOF	yaw rate	robust model matching	Firstly investigated AFS system; and designed robust system to variation of road-tire friction coefficient and vehicle forward speed.
Ackerman (1997)	2-DOF	yaw rate	feedback of integrated yaw rate to front wheel steering	Robust controller with decoupled lateral and yaw motions; and improved yaw rate disturbance generated by braking on split- μ road surface.
Odenthal et al. (1999)	3-DOF	roll angle, roll rate, lateral acceleration	gain scheduled feedback control	Attenuated rollover hazard and improved lateral stability.
Fukao et al. (2001)	3-DOF	yaw rate and lateral acceleration	model reference adaptive nonlinear controller	Reduced yaw disturbance originating from the side wind gusts and high speed turning on low friction road surfaces.
McCann et al. (2004)	tractor and trailer- each 3-DOF	yaw rate	optimal feedback controller	Attenuated jackknife instabilities of articulated tractor-semitrailer.
Oraby et al. (2004, 2007)	3-DOF	state model variables	LQR optimal theory	Reduced side wind force excitation and driver effort.
Yu (2007)	3-DOF	yaw rate	PI/sliding mode controller	Improved yaw stability of a bus in existence of the external disturbances.
Zhang et al. (2008)	comprehensive vehicle model in ADAMS/Car platform	yaw rate	quantitative feedback theory	Robust controller with respect to speed, mass, CG location, tires cornering stiffness and tire-road adhesion.
Chen et al. (2008)	2-DOF	yaw rate and lateral acceleration	feedforward and feedback control (LQR method)	Safety analysis of the AFS components; and design of variable steer ratio (VSR) based on vehicle velocity.
Kharrazi et al. (2012)	three rigid bodies- each 2-DOF	yaw rate	model-based feedforward and feedback controller	Improved directional and roll stability of the long combination vehicle with towed unit axles.

Shibahata et al. [66] investigated the handling performance of a similar 4WS vehicle under different maneuvers through simulations and experiments. In experimental vehicle, the rear suspension was modified to adopt the rear steering mechanism. The study concluded that it was necessary to familiarize the driver with the opposite-phase rear wheel steering response at low speeds since the rear end of the vehicle could considerably project outward. It was further shown that the 4WS could provide improved stability at higher speeds by reducing the side-slip angle, while the yaw rate response gain of the 4WS vehicle would be lower compared to the conventional front steering vehicle. Subsequently, it was suggested to utilize independent controllers for low-speed and high-speed driving conditions.

In the aforementioned studies, the 4WS controller was synthesized to steer the rear wheels in proportion to the front wheels. This proportional gain was obtained as a function of the vehicle speed and ensured close to the neutral steer condition. Although this control strategy could provide improved handling performance, it may lead to a directional instability under high-lateral acceleration maneuvers on low-friction surfaces, primary due to lack of consideration of the side-slip angle in the controller design. A number of subsequent studies thus suggested the integration of the yaw rate and side-slip angle control [68] or combination of front wheel steer angle and yaw rate control [22,70] in order to improve the stability limits under severe maneuvers.

Owing to the presence of uncertain or perturbed vehicle parameters the robustness of the 4WS controllers has also been emphasized in a few studies. For example, Hirano [68] studied the robustness of an active rear steering (ARS) system with respect to variations in the road condition and vehicle speed. A reference model-following controller was synthesized based on

the yaw rate and the side-slip angle responses of the vehicle, and the frequency-dependent feedback gains were evaluated using the μ -synthesis control method. The study also proposed a velocity-dependent observer for estimating the required control parameters and to attenuate the sensors' noise. The results suggested greater robustness of the proposed ARS control under different driving conditions.

Lee et al. [70] proposed an energy efficient 4-wheel independent steering (4WIS) system to improve the high-speed cornering stability limits of the vehicle with independently steered right- and left- rear wheels. Considering that the vehicle response is more strongly affected by the outer wheels with higher normal load compared to the inner wheels, the proposed 4WIS control actuator was designed to steer the rear outside wheel while the rear inside wheel was kept in neutral position. Simulation results obtained under high-speed J-turn and double lane-change maneuvers, suggested that the proposed 4WIS could provide handling performance similar to the 4WS system. The 4WIS system however, provided rapid actuation with lower power requirement compared to the conventional 4WS systems.

The implementation of 4WS in heavy commercial is considered to be impractical due to high energy demand for steering of dual rear wheels with high inertia [64]. Such systems, however, have been applied to farm trucks and intercity buses, which may require high maneuverability within limited spaces [64]. The studies reporting the performance characteristics of vehicles with 4WS are further summarized in Table 1.3.

Table 1.3: Summary of reported studies on 4WS controller for enhancing the dynamic responses of road vehicles.

Author	Vehicle model	Tracked parameter	Controller method	Results
Sano et al. (1986)	3-DOF	vehicle speed	proportional gain controller	Firstly introduced 4WS system with active steering of the rear wheels proportional to front wheels based on the vehicle speed.
Shibahata et al. (1986)	2-DOF	yaw rate and lateral acceleration	decoupling the lateral and yaw rate transfer functions	Practical limitation analysis of the 4WS under different maneuvers.
Hirano (1997)	2-DOF	integration of the yaw rate and side-slip angle	model-following feedback controller	4WS analysis with respect to road condition and vehicle speed variation.
Lee et al. (1999)	comprehensive vehicle model in ADAMS/Car platform	integration of the front steer angle and yaw rate	proportional gain controller	Proposed new 4WIS system to improve both control responsiveness and power consumption of the actuators.

1.2.4 Integrated chassis control systems

It has been widely suggested that DYC control coupled with either 4WS or AFS could yield near optimal handling as well as enhanced directional stability performance of road vehicles. Coordinated control of various chassis control systems has thus been emphasized to achieve safety performance beyond the limits of the individual systems. The chassis control system of Mercedes F400-Carving is one example of the advanced integrated control for achieving enhanced directional stability and driving comfort with a combination of 4WS and DYC systems [71]. Several coordinated control methodologies are continuing to evolve for integrating chassis center systems to achieve optimal or near optimal vehicle performance.

Selby et al. [9] investigated a coordinate approach for AFS and controllers coupled with a four-DOF vehicle model with longitudinal and lateral motions. The AFS controller was synthesized to improve the lateral dynamics of the vehicle under low to mid-levels of lateral acceleration maneuvers and to reduce the undesired effects of DYC such as speed reduction and shortening the tire life. The DYC system based on a simple proportional controller was integrated to achieve high lateral stability under high acceleration maneuvers. The study suggested that it would be essential to limit the rate of the yaw moment at the instant of switching between the controllers to ensure vehicle stability. The results showed that optimal actions of each controller under specific operating conditions could lead to enhanced handling and stability limits of the vehicle.

A number of control algorithms have been proposed for coordinated control of AFS/4WS and DYC systems by tracking the yaw rate and side-slip angle responses of a reference vehicle model. These include the fuzzy controller [72,73], H_∞ control method [74,75], optimal LQR method [76,77], sliding mode control [38,78], gain-scheduled control [79,80], model-matching control [81,82] and model predictive control (MPC) methods [83,84]. These studies have generally focused on distribution of forces among the tires to attain nearly optimal directional responses of the vehicle.

In a recent study, Nagai [81], investigated the performance of an integrated AFS and DYC system during a combined steering and braking maneuver, where the required yaw moment was generated through an optimal distribution of the longitudinal and lateral force among the tires. The model-matching control structure was formulated to track the desired yaw rate and side-slip angle by applying a corrective steering angle and additional yaw moment through the braking

system. A feedforward compensator was used to realize the corrective steer angle, together with a feedback compensator to minimize the tracking errors. The results revealed robust responses under slippery road conditions and severe braking-in-turn maneuver, in addition to external disturbance rejection. The study, however, employed both AFS and DYC systems simultaneously, while the limitations of the individual control systems were not considered.

Different supervisory control approaches have also been explored for allocating the control needs to the steering and brake-base control systems [5,9,85]. Bedner et al. [5] employed a supervisory control structure, consisting of a reference model, a state estimator and a feedback control to achieve the optimal performance of an integrated 4WS system with the brake-based DYC system. In contrast to the controller proposed by Nagai [81], which employed feedback from both the steer angle and yaw moment, the yaw moment served as a common feedback for both the systems to prevent the probable conflict between the steering and braking controllers. It was further suggested that the yaw moment generated by each controller should be in the same direction with defined magnitude and phase relationship. In the study, the corrective yaw moment was developed considering limitations and capabilities of the individual system, and variations in temperature and voltage. The experimental results revealed that the 4WS was relatively less intrusive to driver commands compared to the DYC system. Furthermore, the steering-based control could greatly affect the system bandwidth with changes in the temperature and operating voltage. The results also suggested significant improvements in terms of vehicle stability, driver comfort and longitudinal dynamics, which could be achieved by relatively less brake actuation while giving priority to the 4WS activation.

In another recent study, Yim et al. [38] investigated an integrated AFS and DYC system considering the physical limitation of the tires and the steering mechanism such as maximum steer angle. An optimization problem was formulated to calculate the yaw moment distribution between the AFS and DYC, which was solved using Karush-Kuhn-Tucker (KKT) optimality condition subject to limit constraint on the AFS steer angle. The proposed integrated controller imposed greater braking force by DYC to compensate for the limited yaw moment by the constrained AFS. A relatively larger reduction in vehicle speed was thus obtained compared to the integrated controller without the steering limits.

A number of studies have also studied the coordinated controller robustness in the presence of unmodeled dynamics, parameter perturbation and external disturbances. Yang et al. [77] investigated the robustness of an integrated AFS and DYC control based on the optimal guaranteed cost theory. In contrast to the conventional LQR controller, the model incorporated the time-varying uncertainties of the system parameters such as variations in the tire forces with varying road surface friction. The simulation results revealed superior performance of the proposed controller in stabilizing the vehicle during high-speed lane-change maneuvers on an icy road. The proposed controller, however, involved considerable greater control effort compared with the conventional LQR controller, which may lead to actuator saturation.

Wang et al. [86] studied the performance of a vehicle with a combination of 4WS and DYC control under an evasive maneuver, where the tires approach the nonlinear zone. An adaptive controller was proposed considering variations in the road conditions using a parameter identification method. The study linearized the vehicle model, while the variations in the parameters, mainly the tire-road friction, were continuously monitored. Similar to the earlier

reported studies [5,9], the 4WS control system was employed when the tire lateral force was in linear region, while the DYC system was activated only when the tire force approached the saturation zone. The simulation results revealed enhanced vehicle and reduced driver steering effort with controller adapting to varying driving conditions. In another recent study, Ding et al. [7] synthesized an adaptive control algorithm for integrated AFS and DYC using direct Lyapunov method. The adaptive controller considered variations in the tire cornering stiffness to ensure robustness of the controller. A single-point preview driver model was also used with the integrated AFS and DYC control systems to study vehicle responses to steering inputs in a closed-loop manner. Simulation results suggested the effectiveness of the proposed controller in enhancing the stability during evasive maneuvers on a low friction road surface.

A few studies have also investigated the coordination of the individual chassis control systems in commercial vehicles [78,87], where the roll stability needs to be prioritized since it mostly occurs earlier than a lateral instability. Zhao et al. [78], applied the AFS control together with a DYC control to realize improved yaw response and lateral stability of a truck-trailer combination. The AFS control was prioritized for generating the required yaw moment considering lateral force saturation of the tires. A mapping function was proposed to calculate the desired tire slip angle and subsequently the required steer angle as a function of the instantaneous normal load. The simulation results obtained, under high-speed lane change maneuvers, showed greater effectiveness of the combined AFS and DYC control in limiting the trailer lateral swing and enhancing the jackknife stability limit of the combination. Furthermore, the AFS could effectively eliminate the undesired reduction in the vehicle speed caused by the

DYC system. The generation of the required yaw moment during low to medium acceleration level was limited only to the AFS control.

Studies reporting either individual or integrated AFS and DYC system generally suggest that DYC is vital for enhancing the vehicle handling stability during emergency-type evasive or high-speed lane change maneuvers. In such emergency-type steering maneuvers, the contributions of steering corrections to the yaw moment are small due to the resulting large tire slip angles. The effectiveness of a DYC system tends to diminish in some driving situations such as emergency braking on a split- μ road surface. In the absence of the AFS, the conventional ABS employed in the DYC control will not allow the tires on the high- μ side to generate maximum braking forces. As a result, the available tire-road adhesion is not effectively utilized to minimize the vehicle stopping distance. The AFS, on the other hand, could introduce additional steering of the wheels to supplement the yaw moment and maximize the braking forces. Table 1.4 summarizes the relative merits and limits of the AFS, DYC and integrated AFS/DYC systems.

The developments and implementations of the integrated AFS and DYC control system pose substantial challenges associated with accurate estimations of the vehicle state. Some of the vehicle states could be measured directly using relatively low cost sensors such as the wheel speed sensor, accelerometers, engine speed sensor and yaw rate gyroscope. Considerable challenges, however, continue to exist for accurate estimates or measurements of the tire cornering stiffness, side-slip angle and tire-road friction coefficient [42,88,89].

Table 1.4: Relative merits and limitations of the AFS, DYC, and integrated AFS and DYC systems.

Active Control Systems	AFS	DYC	AFS+DYC
Emergency braking on a split- μ condition	good	poor	good
Rapid lane-change maneuver	good	poor	good
Side-wind gust	good	poor	good
Driver's comfort/sensation	good	poor	good
Yaw moment magnitude	good	poor	good
Hardware requirements	poor	good	poor
Tire saturation limitation	poor	good	good
Complexity and cost	poor	good	poor

1.2.5 *Vehicle handling models*

The reported studies of active chassis control systems have employed widely different vehicle models ranging from a linear 2-DOF bicycle model to comprehensive models in the CarSim or ADAMS platforms. The majority of the studies have employed simple vehicle models to evaluate relative performance potentials of different controls. The linear 2-DOF single-track model of the vehicle has been most widely employed to realize the controller synthesis based on the lateral and yaw velocity states [90-92]. This simple model also permits reasonably good understanding of the vehicle handling properties. The difference between the outer and the inner wheel angles, however, is neglected in the single-track model. Moreover, this model does not permit the analysis of the contributions due to variations in many vehicle parameters such as vehicle track, vehicle roll and lateral load shift during handling maneuvers. The single-track model also does not permit the yaw moment generation through distributed brake pressures applied to the left- and right-wheels [93,94]. Alternatively, a few studies have employed a 3-

DOF four-wheel yaw-plane model including the longitudinal, lateral and yaw motions of the vehicle [95-97].

Thorough and reliable analysis of AFS and DYC, however, requires a more comprehensive vehicle model to accurately describe the tire force distributions and saturation. A number of studies have employed an eight-DOF vehicle model to describe vehicle motions along the longitudinal, lateral, yaw and roll directions as well as each wheel rotational motion considering nonlinear tire forces [6,76,77,81,98,99]. Analyses of the active chassis control systems under maneuvers involving combinations of steering and severe braking or acceleration further require an adequate suspension model and thereby additional vertical DOF of the sprung and unsprung masses apart from the body pitch. The majority of the studies, however, assume negligible effects of variations in roll axis inclination, tire inclination, self-alignment moment and roll steer compliance which can lead to additional steering angle. Some of the recent studies have employed more comprehensive vehicle models available in the Car/TruckSim and ADAMS, which describe the component characteristics more accurately [32,34,55,100].

For analysis of active chassis control systems, it is important to utilize a proven tire model since the controllers are invariably designed to control the forces developed by the tires. Earlier studies had generally used linear tire models and thus could not be considered valid under severe directional maneuvers that may cause tire saturation. It is recognized that the tire model should be sufficiently simple to permit on-board efficient computing but it must describe the essential features such as tire force saturation and effects of vertical and traction/braking forces accurately.

A number of well-known theoretical tire models, namely, “Brush tire model” [93] and “Dugoff tire model” [101] as well as empirical tire model such as “Magic Formula” [102] have

evolved for applications in vehicle models. Many studies reporting handling potential of AFS have used the nonlinear Dugoff tire model [49,72]. The vast majority of the studies [76,102-104], however, employed the widely-proven Magic Formula tire model developed by Pacejka and Bakker [102]. This model is known to provide reasonably accurate predictions of tire forces and moment over a wide range of operating conditions including large tire slip angle and longitudinal slip ratios. Ding et al. [7] proposed an alternative combined-slip tire model, which estimates the pure lateral and longitudinal forces using the Magic formula and the Dugoff model, respectively. The combined-slip vector, which is a function of both the tire slip angle and longitudinal slip ratio, is used to determine tire forces under combined steering and braking. It was also suggested that the lateral force developed by different tire models such as Magic formula, Dugoff and “Rational Function” models is different specifically at sever handling maneuver, where the tire slip angle is relatively large as shown in Fig. 1.1.

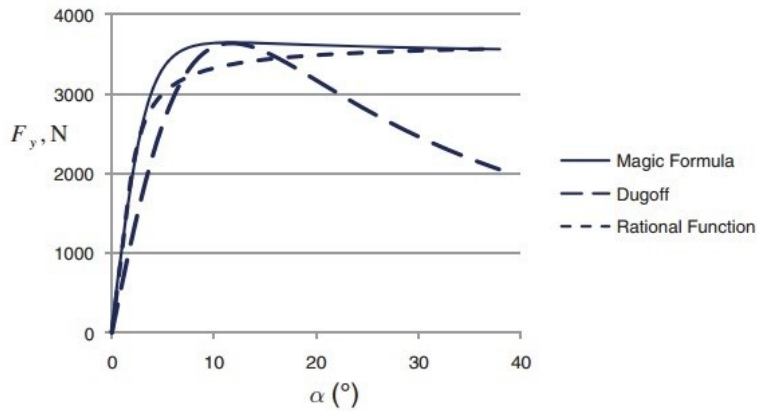


Figure 1.1: Cornering force of tires predicted from different tire models [7].

1.3 Active Front Steering Mechanism

The hardware requirements of a DYC system are relatively simple since it relies on differential braking or brake pressure modulations. Implementations of AFS, RWS and 4WS

controls, however, require design of reliable steering mechanisms and actuators. Considerable efforts have thus been directed towards design of steering mechanisms and actuators that can be used to apply corrective steer angles as per the active control strategies. The steering mechanisms developed for implementations of the AFS controls could be grouped in two categories: steer-by-wire (SBW) and mechanical active steering mechanism (Fig. 1.2). In view of the present dissertation research on active steering, a brief review of the reported designs for AFS systems are presented in the following.



Figure 1.2: Designs of steering mechanisms for implementations of AFS control: (a) a steer-by-wire (SBW); and (b) a mechanical planetary gear system [44].

1.3.1 Steer-by-Wire (SBW) technology for active front steering system

With developments in digital control theory and hardware, as well as compact electric drives, a number of revolutionary designs in light-weight and compact steering systems have been reported. The concepts in steer-by-wire (SBW) evolved from the “Fly-by-Wire” technologies in the aircraft sector [105]. The SBW systems are designed to achieve improved vehicle handling by active control while reduce the driver effort [106]. In the steer-by-wire design, mechanical steering mechanism is replaced by a control unit consisting of actuators, sensors and a controller as shown in Fig. 1.3. The SBW system as shown is divided into the steering wheel motor control and the front wheel motor control. The purpose of the steering

wheel motor is to generate the reactive torque on the steering wheel that reflects the road force. It generally allows lower steering wheel effort at low speeds and increases the effort required at high speeds to improve the driver steering feel. The signals obtaining from the steering angle sensor and a torque sensor are transmitted to the electronic control unit (ECU) in order to calculate the reactive torque in the steering wheel. The purpose of the front wheel motor control is to steer the front road wheels so as to improve vehicle maneuverability and stability. The ECU determines the front wheel motor and subsequently the road wheels positions based on the signals receive from the steering angle sensor, accelerometer or yaw rate gyroscope [107-110].

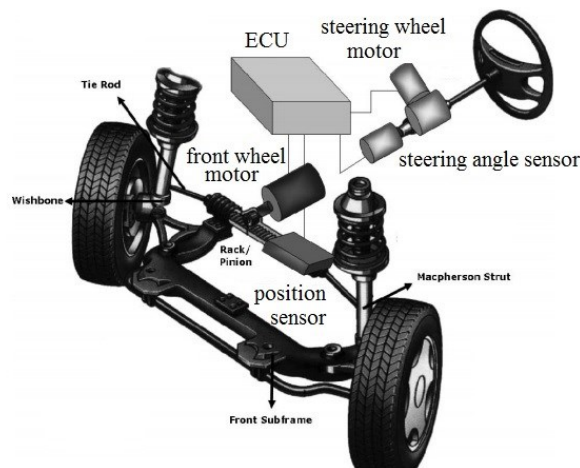


Figure 1.3: Steer-by-wire components in an AFS system [107].

Despite the potential for flexible steering control applications including independent control, the safety of the SBW has always been a concern for implementation in road vehicles [111,112]. Feick et al. [112] investigated the effects of possible faults in the SBW system such as sensor-, actuator- and computer-faults. The results suggested that in order to safely implement a SBW in road vehicles, the designed system should be insensitive to at least one fault in each subsystem components simultaneously. Although the absence of the steering column in such system can

isolate the driver from the road vibrations, the loss of the driver's steering feel is an important concern. In order to provide sense of the road irregularities to the driver, it is suggested that the reaction torque produced by the steering wheel motor be realized by feedback of either the steering wheel angle signal [12] or the external force applied to the rack from the road [110]. Steering wheel angle feedback method, however, does not provide a driver with real feel of the tire and road conditions [12,110,113].

It may therefore be concluded that although SBW could provide significant potential for a controlled system such as AIFS, it has not yet been considered as a failed-safe system for road vehicles unless it is integrated with a mechanical backup system. Furthermore, it is considered as an expensive and complex system which requires many redundant elements in order to assure the safety of the vehicle.

1.3.2 Mechanical Mechanisms for AFS

Although, a vast majority of active steering systems presented in literature is based on the steer-by-wire, the systems using this technology cannot be considered reliable for application to road vehicles [111]. Review of literature indicates that the first mechanical AFS system was introduced as an option in BMW 5 series [114] with ZF Lenksysteme GmbH [44]. This steering system enabled automatic steering interventions without loss of the mechanical connection between the steering wheel and road wheels [13]. The mechanism was designed to enhance the maneuverability of the vehicle by realizing a variable steer ratio (VSR)/variable gear ratio (VGR) based on the vehicle speed [13,115]. For example, at low speeds such as parking, the steering angle is often large, thus for avoiding a large effort of steering by driver and increasing the vehicle agility, it would be helpful if a low steering ratio is used. Similarly, at high speeds

when stability and safety are important factors, a high steering ratio would be appropriate. The variation of steering gear ratio with speed adapted for Honda S2000 in comparison to convention system is shown in Fig. 1.4 [71].

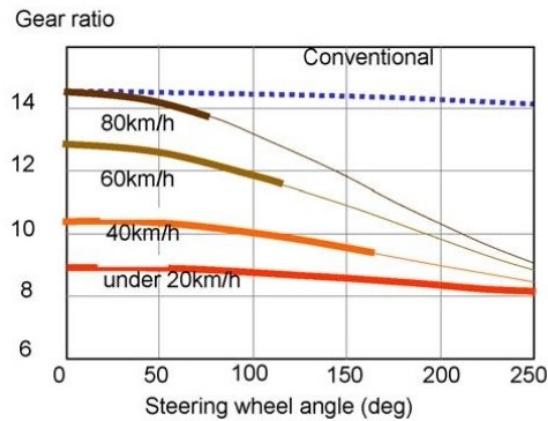


Figure 1.4: Honda S2000 speed-dependent steering ratio [71].

There are few mechanical mechanisms with variable gear ratio (VGR) which have been applied in the AFS systems such as: bi-planetary or planetary gear, differential planetary gear and harmonic drive mechanisms [116]. Fig. 1.5 shows these mechanical VGR mechanisms where the additional input to the steer angle is realized by introducing the second input to the system. Each system in this figure is briefly explained in the following sections.

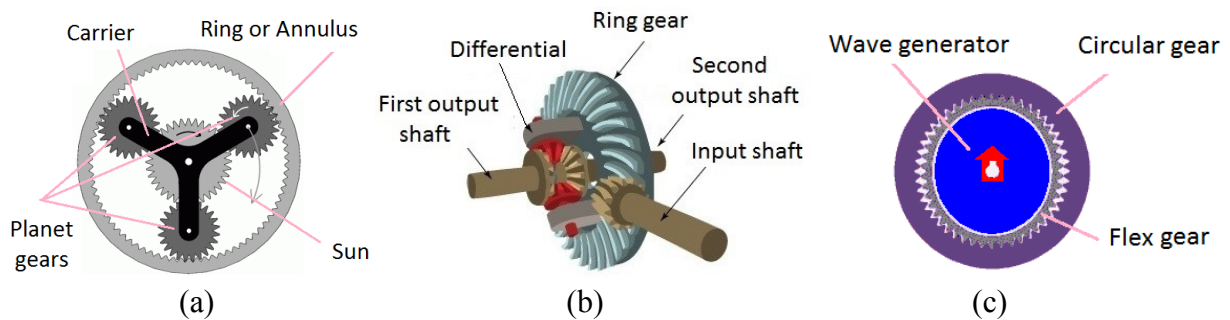


Figure 1.5: Mechanical active steering mechanisms with variable gear ratio actuators: (a) a planetary gear; (b) a differential gear; and (c) a harmonic drive [116].

Planetary gear system

The well-known planetary gear system with two-DOF as shown in Fig. 1.5(a) consists of a sun gear, a set of planet gears, a ring or an annulus and a planet carrier. This system is able to produce varying gear ratio depending on which gears are used for the multiple inputs, which gear as the output and which one is kept fixed. For example, assuming that the sun and the ring are the two independent input variables one from the driver and the other from the control motor, the output to the wheel angle can be provided by the angular motion of the carrier. The resulting planet carrier velocity due to two independent inputs from the sun gear and the controlled annulus can be expressed as:

$$\omega_c = \frac{\omega_s Z_s \mp \omega_a Z_a}{Z_s + Z_a} \quad (1.1)$$

where ω_c , ω_s and ω_a are the angular velocities of the planet carrier, sun and annulus, respectively, while Z_s and Z_a refer to sizes of the sun and the annulus gears, respectively. The kinematic syntheses of the steering mechanism consisting planetary gear systems with potentials for application to AIFS concept are described in details in the Appendix A.

The ZF active steering system of BMW shown in Fig. 1.6 uses the concept of planetary gear superposition to provide active control of the steering ratio. This system utilizes conventional rack-and-pinion steering, while a bi-planetary gear set with additional input provided by an electric motor based on vehicle speed along with the driver input generates the overall gear ratio for the steering system. As shown in the figure, the system is also equipped with an electromagnetic locking unit that locks the motor when alteration of steering ratio is not required or there is an error in the system. In case of an error, the locked motor prevents any additional

input beside the driver's command making the system a conventional one with a constant steer ratio and always remains fully steerable [44]. This fail-safe mechanism for VSR is extended in [117] by incorporating a pair of planetary gear systems in an innovative manner that can be utilized for realizing the concept of AIFS investigated in this dissertation.

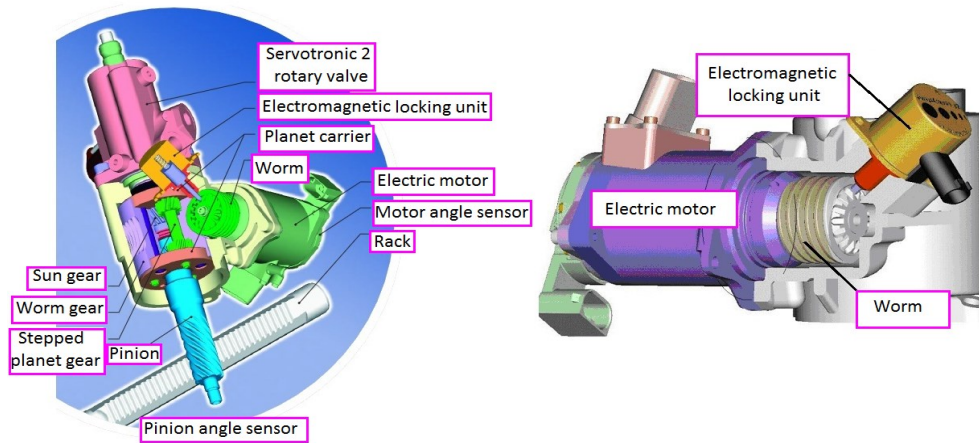


Figure 1.6: A bi-planetary gear with the locking unit in the BMW active steering system [44].

Differential gear system

Similar to planetary gear mechanism, the differential system mechanism used for vehicle drive train has also been used for angle superposition of the active steering system [118,119]. A differential gear system basically consists of three connected shafts: one as the input drive which is divided into two useable outputs as shown in Fig. 1.7. The differential mechanism could easily be adapted for the active steering application by allowing two inputs and one output. Figure 1.7 presents a small size vehicle differential gear system used to integrate two inputs, driver steering angle and electric motor steering command, with the single output which was fed into the steering system. While it is suggested to coaxially position the driver's input and the steering output of the differential, it is also important to choose an appropriate input and output shafts based on the gear ratios and the torque requirement from the controlled motor [7].

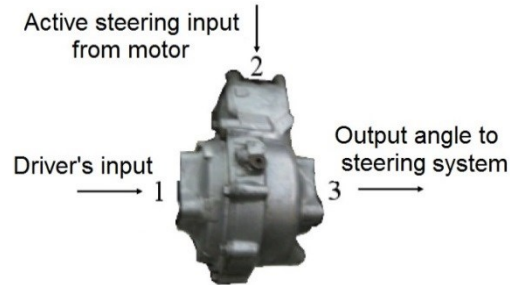


Figure 1.7: A differential gear system used for angle superposition of the active steering system [118].

Harmonic drive actuator

Harmonic drive system or strain wave gearing has been successfully used in robotics and aerospace industry. Every harmonic drive mechanism consists of three main parts as illustrated in Fig. 1.5(c): wave generator, flexible gear and a rigid circular gear. The generator and the flex gear both are positioned inside the rigid circular gear which has internal teeth. When the ellipse-shaped generator is rotated, the flex gear adopts the shape of the rotating generator. The flex gear, with outside positioned teeth, is thus coupled with the circular gear along the major axis of the generator ellipse. In design of the harmonic drive parts, the flex gear is designed with less teeth than the circular gear. This mechanism is capable of achieving up to 320:1 output/input torque ratio. The various combinations of the main elements of a harmonic drive system could provide different functionality. [120].

In 2009, Audi employed the harmonic drive technology as a new active steering system called “Dynamic Steering”[14]. Its functionality is similar to a planetary gear mechanism but in a smaller and much lighter package. In this active steering system, the electric motor turns the wave generator while the flexible gear is connected to the steering input shaft. At the vertical axes of the ellipse-shaped generator, the flexible gear is meshed with inside teeth of the circular

gear which acts on the steering output shaft. The superposition of the generator and the flexible gear movement thus could effectively alter the steering ratio.

Based on the review of the literature on the available active steering mechanisms, it may be concluded that while the SBW technology has greatest flexibilities in structure design and application potentials for the AIFS system, it has not yet been considered as a failed-safe system to be employed in the road vehicles without any mechanical backup systems [112]. Some of positive and negative aspects of SBW in comparison to those of mechanical steering systems discussed are summarized in Table 1.5.

Since a feasible system for active steering in vehicle application must be fail-safe, one of the mechanical systems discussed must be extended to design a mechanism capable of generating independent control of the steered wheels required in an AIFS system. Among all the mechanical systems reviewed and discussed in this section, the most readily applicable system for the concept of AIFS is the mechanism based on tandem planetary gears presented in [117].

Table 1.5: Comparison of application of SBW and mechanical steering system.

Features	SBW	Mechanical steering system
Structure design flexibility	good	Poor
NVH isolation	good	poor
Frontal crash safety	good	poor
Accurate response time	good	good
Steering ratio flexibility	good	good
Cost of the system's parts	poor	good
Driver road feeling	poor	good
Safety and fault tolerance	poor	good

1.4 Scope and Objectives

From the review of reported studies, it is evident that both AFS and DYC chassis control systems yield enhanced handling performance of the road vehicles together with driver comfort. The AFS systems, in particular, are most beneficial in improving safety dynamics of the road vehicles. The AFS, however, yields limited benefits under more severe directional maneuvers involving high lateral accelerations. The performance of AFS is limited particularly for commercial vehicles, which encounter high magnitude lateral load transfers, where the tires may approach situation. The limitation of AFS is further aggravated in situations requiring emergency braking, the wheels provide very little adhesion reserve to achieve desired braking distance under higher steering maneuvers.

The aforementioned limitations of current AFS designs could be circumvented by integrating a DYC system with the AFS. The DYC system provides the additional moment through selective braking and thereby could enhance the vehicle handling and stability, mainly during the high lateral acceleration emergency-type of maneuvers. The DYC control, however, exhibits its own drawbacks and has adverse effects on vehicle stability during braking on a split- μ road condition, tire life and undesired reduction in the vehicle speed, which is not perceived very well by the drivers during rapid path change maneuvers. Combined AFS and DYC control systems, however, have been recommended as an alternative solution to the AFS limitations. The integration of AFS and DYC systems, and their control aims to address a wider range of operations, which could overcome most of the dynamic compromises. The integrated AFS and DYC control, however, would result in a significantly complex control system along with estimation and tracking of various parameters. A stand-alone AIFS system offers attractive

potential to overcome the limitations of the AFS without the additional DYC control. The primary objective of this dissertation research is thus formulated to investigate the concept of an AIFS for realizing not only the enhanced handling performance during high-g maneuvers but also to ensure sufficient adhesion reserve to permit braking during such maneuvers by operating the tires away from the saturation zone.

The specific objectives of this dissertation research are as follows:

1. Formulate an appropriate handling dynamic model of a road vehicle comprising right- and left- wheels with independent steering angles and a nonlinear tire model for predicting tire forces under severe maneuvers, and possible impending cornering force saturation as well as the interaction between the longitudinal and the lateral forces in combined braking and steering maneuvers.
2. Develop a handling model of a high center of mass cargo truck to simulate vehicle behavior under high magnitude lateral load shift such as that encountered in a partly-filled tank truck.
3. Determine the tire force saturation limits using a performance parameter in terms of the “tire work-load” in order to identify the steering limits of the saturated wheel and adhesion reserve for each steered tire.
4. Synthesize a controller design for the proposed AIFS concept to track the steering response of an idealized reference model in conjunction with dynamic characteristics of the steering actuator considering the tire saturation limits and investigate the robustness of the controller to model parameter perturbations and external disturbances.
5. Investigate the performance potential of the proposed AIFS control in terms of variable handling and directional control measures under a wide range of steering maneuvers such as

J-turn, path change, obstacle avoidance and braking-in-turn maneuvers on uniform as well as split- μ road conditions.

6. Compare the performance characteristics of AIFS with those of the conventional AFS and to highlight the performance benefits of the AIFS.
7. Review the designs of different steering mechanisms to achieve independent steering of the inner and outer wheels.

1.5 Organization of the Dissertation

This dissertation research has been written according to the manuscript-based format described in “Thesis Preparation and Thesis Examination Regulation” booklet of the School of graduate Studies of Concordia University. This dissertation is organized in 6 chapters including the review of the relevant literature (chapter 1). Chapter 2 to 5 presents the articles that have been either published or submitted for publication in the journals. The major contributions and conclusions of the study are summarized in chapter 6 together with recommendations for additional further studies.

Chapter 2 presents the following article:

Farazandeh, A., Ahmed, A., and Rakheja, S., “Performance Enhancement of Road Vehicles Using Active Independent Front Steering (AIFS),” *SAE International Journal of Passenger Cars- Mechanical Systems*, 5, 1273-1284, 2012.

This paper presents the concept of AIFS together with its preliminary analysis when applied to passenger cars. A yaw-plane model of a road vehicle was formulated considering independent steering of the right- and the left-wheels including the longitudinal, lateral and yaw motions of

the vehicle, nonlinear cornering properties of the tires, and the load shift along the longitudinal and lateral axes. A simple PI controller was synthesized to provide a corrective steering action to achieve a target yaw rate response corresponding to a neutral-steer vehicle. The gains for the controller in this case were established by trial and error. The resulting corrective action was distributed over the inner and outer-wheels with manually-tuned distribution gains based on the saturation limits of the tires. Unity values of gains were chosen for low speed cornering maneuvers, where the steer angle was modified by the AIFS strategy, while maintaining pro-Ackerman geometry similar to an AFS system. Simulation results were obtained for pure cornering maneuvers in the absence of braking or acceleration. The handling performance characteristics of the vehicle model integrating the AIFS controller were investigated considering three different cases of operating conditions: high-friction steady-turning maneuver idealized by a ramp-step steer input, J-turn maneuver, a lane-change type of steer input idealized by a sinusoidal input, and a steady-turning input on a split-friction road surface. The resulting responses of the model were also compared with those obtained with the AFS controller and the reference model. The results of the sensitivity analysis suggested greater effectiveness of the AIFS control compared to the AFS control for high center of gravity (CG) vehicles under high-speed turning maneuvers. In this preliminary study, the tire forces were limited to pre-saturation levels in order to compare the performance characteristics of the AIFS with that of the AFS.

One of the major challenges in realizing the concept of AIFS would be a fail-safe mechanism design for independent steering control. A design concept of a mechanical fail-safe steering mechanism based on two sets of planetary gear system that can be readily adapted for

the implementation of AIFS is also presented in this paper. The first prototype of the mechanism built to examine the functionality of the mechanism is presented in Appendix B.

Chapter 3 presents the following article:

Farazandeh, A., Ahmed, A. and Rakheja, S., “Performance Analysis of Active Independent Front Steering (AIFS) for Commercial Vehicles with Greater Lateral Load Shift Propensity,” *SAE International Journal of Commercial Vehicles*, 6, 288-300, 2013.

Based on the results achieved in the first article and sensitivity analysis with respect to the CG height of the vehicle, this paper emphasizes the performance characteristics of an AIFS for applications in commercial vehicles with high CG and lateral load transfers. For this purpose, a two-axle tank truck was considered as the candidate vehicle. A nonlinear yaw-plane model of the tank truck integrating roll dynamics of the sprung mass was developed to study the directional performance potential of the AIFS. In addition, the load shift associated with liquid cargo motion in the roll plane of a cylindrical tank was evaluated using the quasi-static approach and incorporated in the vehicle model in terms of resultant lateral force and roll moment attributed to quasi-static cargo shift. The AIFS control strategy based on a yaw rate reference model was modified considering delays associated with the tire lag and steering response of the truck. A performance parameter in terms of the “tire work-load” was thus defined in order to limit the steering of the inner wheel with relatively lower normal load, prior to approaching the saturation zone. A limiting value of the inner tire work-load was subsequently identified on the basis of the normalized cornering stiffness of the tire. For a given normal load on a tire, the normalized cornering stiffness was referred to as “instantaneous saturated slip angle” of the inner tire, which was used to obtain the limiting value of the steer angle. This approach permits independent

control of each wheel so as to enhance handling performance limit through maximum utilization of the available tire-road adhesion prior to approaching the saturation limit. For heavy vehicles, the controller in chapter 2 was extended by incorporating a first-order time lag function to compensate for high inertia and lag in tire response. Simulation results were obtained for both the full and partial load conditions of the truck under a steady-turning maneuver at different forward speeds to demonstrate the effectiveness of the AIFS system for applications in rigid as well as partly-filled liquid cargo trucks.

Chapter 4 presents the following article:

Azadeh Farazandeh, A.K.W. Ahmed and S. Rakheja, “An independently controllable active steering system for maximizing handling performance limits of road vehicles,” *Proceedings of the IMechE, Part D: Journal of Automobile Engineering*. (Accepted for publication in October 2014)

Results achieved through previous two articles suggested the effectiveness of the proposed AIFS system for vehicles with higher C.G and greater lateral load shifts such as cargo trucks compared to the conventional AFS system during high-speed cornering maneuvers. The potential performance of the proposed AIFS system was furthermore evaluated over a wide range of steering maneuvers involving uniform as well as split- μ road conditions.

The paper proposes a more refined controller synthesis together with the steering actuator dynamics and a closed-loop driver path-following algorithm. The nonlinear equations of motion for the vehicle model were linearized for the purpose of developing the control algorithm based on the lateral, yaw and roll responses. The transfer function of the vehicle model was thus

obtained relating yaw rate and the steer angle. Since the corrective steering command from the controller is generally constrained by the bandwidth of the steering actuator, the characteristic of the steering actuator was also modeled as a second-order dynamic system and integrated to the vehicle model. Subsequently, the PI controller gains were tuned by comparing the characteristics equation of the resultant closed-loop function with the optimum equation based on the minimum ITAE (Integral of Time-weighted Absolute Error) performance index. The effectiveness of the proposed AIFS control was evaluated under various pre-defined steering inputs. These included: (i) a ramp-step steer input to simulate a steady-cornering maneuver; (ii) a lane-change maneuver; and (iii) an obstacle avoidance maneuver. The steer angles corresponding to the path change maneuvers were generated considering the standardized path coordinates for the given speed. A linear vehicle model coupled with an ideal driver model, described by a PID function, was used to derive the required steering inputs, which were applied to the nonlinear vehicle model with AIFS in an open loop manner.

Chapter 5 presents the following submitted article:

Azadeh Farazandeh, A.K.W. Ahmed and S. Rakheja, “Braking and Steering Performance Analysis of a Road Vehicle with Active Independent Front Steering (AIFS)”, (*Submitted for review, International Journal of Heavy Vehicle Systems, October 2014*)

This paper highlights the potential benefits of the AIFS control in permitting sufficient adhesion reserve for braking demands during a high-speed steering maneuver. The dynamic responses of the vehicle integrating AIFS control are investigated to study the braking efficiency as well as stability of the vehicle during braking-in-turn maneuvers. The vehicle model presented in the earlier articles was extended to include the braking dynamics by introducing additional

essential DOFs. The simulation results were obtained under a wide range of braking-in-turn maneuvers on different road conditions such as dry, wet, snow-covered and split- μ roads. The paper also presented sensitivity analysis to illustrate the influences of variations in selected vehicle design parameters on the performance characteristics of the AIFS control. These included the vehicle weight and CG coordinates. The robustness of the synthesized controller was investigated considering variations in vehicle model parameters such as cornering stiffness of tires, and external disturbances originating from the side wind force or driving on roads with asymmetric friction between the left and right tires. The simulation results showed promising features of the AIFS under combined high- g cornering and hard-braking maneuvers. It was shown that the AIFS control helps limiting the saturation of the inside tire by reducing its steer angle and subsequently providing sufficient reserve in the event of a braking demand. It was concluded that the AIFS control would prevent locking of the inner tire and subsequently reduce the stopping time in such maneuvers, when compared to the AFS control.

The highlights of the dissertation research together with the major conclusion and recommendation for future works are presented in chapter 6. The planetary gear mechanism that can be adapted for the design of AIFS system is synthesized in detail and is presented in Appendix A. The first prototype of the mechanism built to examine the functionality of the system is presented in Appendix B. The simulation parameters used for the investigations in this research are summarized in the Appendix C.

CHAPTER 2

PERFORMANCE ENHANCEMENT OF ROAD VEHICLES USING ACTIVE INDEPENDENT FRONT STEERING (AIFS)

2.1 Introduction

The steering system design plays a vital role in determining the handling and stability performance of the road vehicles. During a directional maneuver, depending on the speed and nature of maneuver, the cornering force may be limited when one of the wheels approaches the adhesion limit before the others, which may affect the handling performance in an adverse manner. Active chassis controls such as anti-lock brake systems (ABS) and vehicle stability control (VSC) systems have thus drawn substantial efforts for enhancement of safety dynamic performance of road vehicles. Considerable efforts have been made towards steering- and yaw moment-based VSC systems such as active front steering (AFS) and direct yaw moment control (DYC) that are designed to meet the cornering demand for enhanced vehicle handling and stability performance [4,121].

The steering mechanism in conventional road vehicles is generally designed to closely follow the Ackerman steering ratio involving different steer angles of the inner and outer wheels at low speeds. At high speeds, the dynamics of a vehicle and the side-slip angles developed at the tires cause the vehicle to follow a different path at different speeds for an identical steering input. This phenomenon due to the compliance of the pneumatic tire is known as understeer characteristic, which can be neutralized by actively controlling or modifying the steer angles of the steered wheels depending on the forward speed and the maneuver demands. This permits to

enhance the lateral force developed by the tire to meet the cornering demands. Various concepts in active front steering (AFS) capable of providing continuous and situation-dependent variations in the steering ratio have thus been investigated to achieve improved low-speed maneuverability and high-speed stability performance. The concept of AFS was firstly introduced by Kasselman and Keranen in 1969 [2]. Substantial further efforts have been made over the past two decades on different concepts and control strategies for the AFS system [51,122]. The AFS system, however, alters the steer angles of both the inner and the outer wheels simultaneously in order to realize a pre-determined target depending on the forward speed and steering input, while the saturation limits associated with road adhesion are not considered. Owing to the nonlinear characteristics of pneumatic tires, a wheel may approach lateral force saturation under a high lateral acceleration maneuver and thereby limit its ability to generate the required lateral force. The AFS system may thus exhibit a very distinct limitation in providing the target response or controllability under high-g maneuvers that lead to significant lateral load shift between the inner and the outer wheels.

The yaw moment-based VSC systems (DYC), on the other hand, have been proven to be more effective than the AFS under high lateral acceleration maneuvers, since these generate the required yaw moment via differential braking [3,32]. A DYC system alone, however, yields limited performance in tracking a target vehicle response to steering inputs. Furthermore, it may cause a directional instability in an emergency braking maneuver on a split- μ condition, where the road adhesion limits of the left and right side could be substantially different. A number of studies have reported different limitations of the DYC systems, which include relatively longer stopping distance during emergency braking [5], reduced tire life due to more frequent braking,

and over-ruled feeling of the driver by the additional corrective yaw moment [6]. Considering that the DYC and AFS systems could yield enhanced performance under different ranges of operating conditions, many studies have focused on coordinated control of AFS and DYC [8,9]. Although the integration of AFS and DYC systems has provided definite performance gains over a broad range of operating conditions, it results in a more complex control system involving various tracking or estimated parameters.

The performance potential of an AFS system could be considerably enhanced by introducing independent variations in the inner and outer wheels steering. This would permit the optimal utilization of the available adhesion of the both wheels to meet the cornering demand under high-acceleration maneuvers. Such a concept, referred to as Active Independent Front Steering (AIFS) system in this paper, would likely lead to enhanced handling and stability performance in the presence of split- μ conditions. Furthermore, the AIFS system can also be integrated with DYC for further enhancement of yaw stability performance since AIFS can also generate yaw moment by introducing differential lateral forces of the steered wheels. The implementation of AIFS, however, would necessitate the design of a practical mechanism capable of providing the desired steering ratio, which is perhaps one of the major challenges in realizing this concept. The reported studies on adaptive steering systems generally propose the use of “Steer-by-Wire” [10,11], which has been widely investigated for the purpose of active front steering. The implementations of steer-by-wire technology in production cars, however, have been attempted together with a mechanical backup system. The mechanical active steering systems comprising a planetary gear system, harmonic drive system and variable ratio racks have been employed by BMW, Audi and Mercedes, respectively [13-15]. These are generally designed with an objective

to realize variable steering ratio (VSR), and thus aid the driver's steering effort by actively altering the steering ratio between the steering angle and the wheels' steer angles.

This paper investigates the concept of AIFS and a control strategy for a vehicle with an understeer characteristic to examine its effectiveness in enhancing the handling performance limit when compared to that realized by the AFS system. A control strategy is formulated and explored so as to utilize the maximum capability of both the steered wheels in order to augment the handling performance limit. For this purpose, the performance limit is defined as the maximum speed or curvature that can be negotiated in an adaptive manner to satisfy the ideal or target (yaw rate and trajectory) responses for a given road adhesion. A nonlinear handling model of a vehicle considering independent steering of the inner and outer wheels, and the lateral /longitudinal load shifts is employed to study the performance potentials of AIFS. The analyses are performed under ramp-step and sinusoidal steering inputs, and both uniform and split- μ conditions. A simple controller synthesis based upon PI control is applied to assess potential performance gains of the AIFS concept. Furthermore, since the concept of AIFS is based on load shift between the inner and outer wheels, this study also examines the sensitivity of the height of the center of gravity for the vehicle equipped with both AFS and AIFS systems. The simulation results demonstrate that AIFS performance is as good as those obtained by AFS system in non-critical handling maneuver. However, the effectiveness of AIFS in comparison to the AFS is significant when maneuvers performed are at the limits. A design concept of a mechanical fail-safe steering mechanism, reported in [117], is also explored for realizing the AIFS function.

2.2 Handling Model

A yaw-plane model of a road vehicle is formulated considering independent steering of the

right- and the left-wheels to study the handling performance potentials of the AIFS system. The model, illustrated in Fig. 2.1, includes the longitudinal, lateral and yaw motions of the vehicle, nonlinear cornering properties of the tire and the load shift along the longitudinal axis. In the figure, δ_r and δ_l refer to two independent steering inputs to the right- and left-wheels, respectively. The relations between the steering wheel input (δ_{st}) and the right- and left-wheel angles, according to Ackerman geometry, can be expressed as:

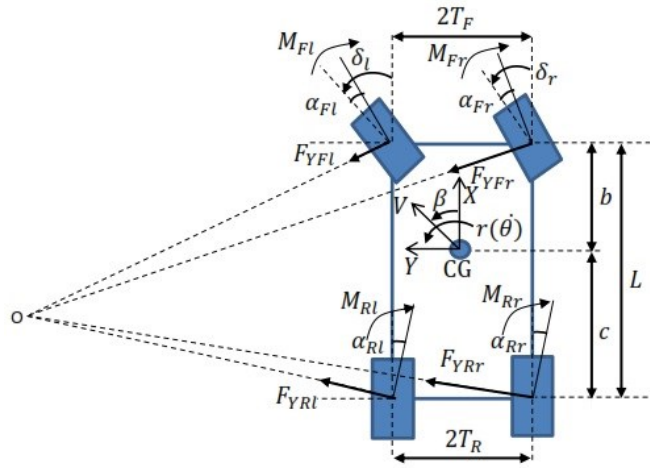


Figure 2.1: DOF nonlinear handling model with independent steering angle.

$$\delta_r = \tan^{-1} \left[\frac{\sin(\delta_{st})}{\cos(\delta_{st}) + \frac{T_F \sin(\delta_{st})}{L}} \right] \quad (2.1)$$

$$\delta_l = \tan^{-1} \left[\frac{\sin(\delta_{st})}{\cos(\delta_{st}) - \frac{T_F \sin(\delta_{st})}{L}} \right] \quad (2.2)$$

where T_F and T_R are half tire track width of the front and rear axle, respectively, L is the wheelbase and δ_{st} refers steering command of the driver reflected at the wheels considering parallel steering. The studies reporting handling models generally consider lateral force normal to the fore-aft tire axis as opposed to the direction of travel, assuming considerably lower side-

slip angles compared to the steer angles [93]. The tires may undergo substantial side-slip during sever handling maneuvers, which would not only alter the effective yaw moment but also the coordinates of the instantaneous center of rotation. It is thus important to consider slip angles of tires in deriving the effective forces and the yaw moment. The equations of longitudinal, lateral and yaw motions of the vehicle model, derived in the absence of braking or acceleration force, are given below:

$$ma_x = -F_{YFr} \sin(\delta_r - \alpha_{Fr}) - F_{YFl} \sin(\delta_l - \alpha_{Fl}) + F_{YRr} \sin(\alpha_{Rr}) + F_{YRl} \sin(\alpha_{Rl}) \quad (2.3)$$

$$ma_y = F_{YFr} \cos(\delta_r - \alpha_{Fr}) + F_{YFl} \cos(\delta_l - \alpha_{Fl}) + F_{YRr} \cos(\alpha_{Rr}) + F_{YRl} \cos(\alpha_{Rl}) \quad (2.4)$$

$$I_{zz} \dot{\Omega} = - \sum_{i=F}^R \sum_{j=r}^l M_{ij} + F_{YFr} \{bc \cos(\delta_r - \alpha_{Fr}) - T_F \sin(\delta_r - \alpha_{Fr})\} + \dots \quad (2.5)$$

$$+ F_{YFl} \{bc \cos(\delta_l - \alpha_{Fl}) + T_F \sin(\delta_l - \alpha_{Fl})\} + F_{YRr} \{-c \cos(\alpha_{Rr}) + T_R \sin(\alpha_{Rr})\} - \dots$$

$$- F_{YRl} \{c \cos(\alpha_{Rl}) + T_R \sin(\alpha_{Rl})\}$$

In the above equations α_{Fj} and α_{Rj} are the slip angles of tires on the front and rear axles, where the second subscript ($j = r, l$) refers to right- and left- wheels, respectively. For a given forward velocity, the path trajectory of the vehicle in the global coordinate system is obtained from the instantaneous yaw angle of the vehicle, such that:

$$X = \int_0^t V \cos\theta dt, \quad Y = \int_0^t V \sin\theta dt \quad (2.6)$$

where V and θ are the vehicle speed and the yaw angle of the vehicle, respectively.

2.3 Tire Force and Moment

In this study, the ‘‘Magic Formula’’ tire model [94] has been utilized to derive lateral force F_{Yij} ($i = F, R; j = r, l$) developed at the tire-road interface and the aligning moment, where

subscripts F and R refer to front and rear tires, and r and l denote the right and left wheels, respectively. The tire lateral force can be characterized in two distinct ranges of side-slip angles, as it is evident in the cornering force properties of tires shown in Fig. 2.2. The tire force generally lies in the nearly linear region under typical vehicle maneuvers. Under extreme maneuvers or slippery road conditions, the tire force occurs in the nonlinear or the saturation region, which is vital in this study considering that one of the requirements for the proposed AIFS system is to prevent the tire from approaching the saturation. As shown in the figure, the changes in the tire lateral force and consequently the yaw rate with change in the steering angle tend to diminish at the end of the saturation zone.

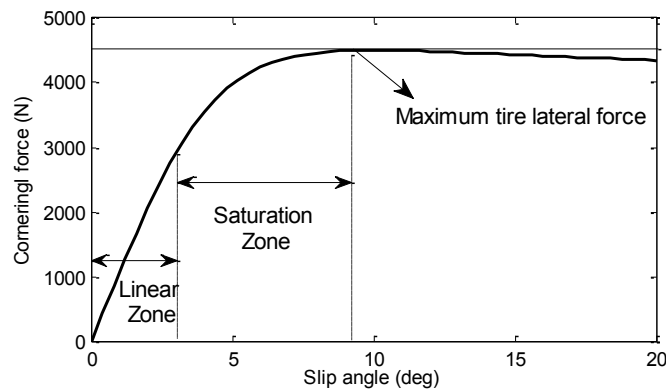


Figure 2.2: Tire lateral force zones.

Tire normal load is the other major factor that influences the cornering behavior of the tires. In a severe turning maneuver, the normal load shift between the outer and inner wheels plays a greater role. Furthermore, the relation between the normal load and the lateral force is nonlinear, which leads to a reduction in the total cornering force developed during a turning maneuver and greater side-slip angle in order to meet the lateral force demand [94]. Neglecting the load shift attributed to vehicle roll in the context of the yaw-plane model considered in the study, the

normal loads on each wheel $F_{Zij}(i = F, R; j = r, l)$ can be expressed as functions of the longitudinal (a_x) and lateral (a_y) accelerations in the following manner:

$$F_{ZF_r} = \frac{W_F}{2} - \frac{ma_x h_{cg}}{2L} + \frac{ma_y h_{cg} c}{2T_F L} \quad (2.7)$$

$$F_{ZF_l} = \frac{W_F}{2} - \frac{ma_x h_{cg}}{2L} - \frac{ma_y h_{cg} c}{2T_F L} \quad (2.8)$$

$$F_{ZR_r} = \frac{W_R}{2} + \frac{ma_x h_{cg}}{2L} + \frac{ma_y h_{cg} b}{2T_R L} \quad (2.9)$$

$$F_{ZR_l} = \frac{W_R}{2} + \frac{ma_x h_{cg}}{2L} - \frac{ma_y h_{cg} b}{2T_R L} \quad (2.10)$$

The side-slip angles of the tires are expressed as functions of the forward and lateral velocity and yaw rate of the vehicle, as follows:

$$\alpha_{F_r} = \delta_r - \tan^{-1} \left[\frac{b\Omega + V_y}{V_x + T_F \Omega} \right] \quad (2.11)$$

$$\alpha_{F_l} = \delta_l - \tan^{-1} \left[\frac{b\Omega + V_y}{V_x - T_F \Omega} \right] \quad (2.12)$$

$$\alpha_{R_r} = \tan^{-1} \left[\frac{c\Omega - V_y}{V_x + T_R \Omega} \right] \quad (2.13)$$

$$\alpha_{R_l} = \tan^{-1} \left[\frac{c\Omega - V_y}{V_x - T_R \Omega} \right] \quad (2.14)$$

The tire lateral force and self-aligning moment are subsequently obtained from the Magic Formula Tire model as functions of the tire normal force and slip angle:

$$Y(X) = D \sin \{ C \tan^{-1} [BX - E (BX - \tan^{-1} (BX))] \} \quad (2.15)$$

where $Y(X)$ presents the cornering force or the self-aligning moment, X is tire slip angle; C is the shape factor and B, D and E are coefficients dependent upon the normal load.

2.4 AIFS Control Strategy

A control strategy for AIFS is synthesized considering the two distinct regions of the tire cornering properties. Under relatively low lateral acceleration maneuvers, the tire is expected to operate in its linear range. The steering control strategy in this region is identical to that of the AFS system, where a corrective angle is applied equally to both the front wheels in order to track the desired yaw rate target. In this case, the wheels approximately follow the Ackerman geometry, where $\delta_l > \delta_r$ for the left turn maneuver illustrated in Fig. 2.1. Greater load transfer and centrifugal force encountered during a high lateral acceleration maneuver, however, could cause saturation of the inner wheel, while the available adhesion of the outer wheel being under-utilized, as illustrated by points 'A' and 'B' in Fig. 2.3. This tendency would limit the performance of the AFS controller as one of the wheels approach or exceed the saturation regime.

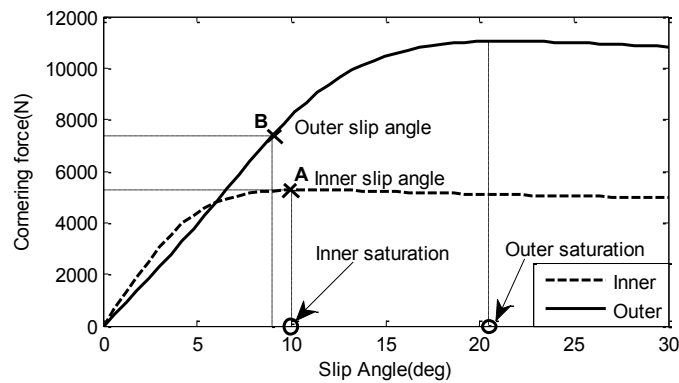


Figure 2.3: Inner and the outer tire lateral force in a turning maneuver.

Subsequently, the AIFS controller is synthesized to ensure maximum utilization of the available adhesion limits of both the wheels in a high lateral acceleration maneuver. Unlike the AFS controller, the proposed control strategy considers independent steering corrections applied

to the right- and left- wheels, which can be realized through design of an independent steering system. The proposed design, presented in the subsequent sections, permits distribution of the corrective action between the inner and the outer wheels with different gains depending upon the operating conditions namely the speed, road adhesion and instantaneous steering wheel angle. For an understeer vehicle, the controller thus results in relatively greater steering of the outer wheel than the inner wheel so as to utilize the available adhesion limit of the outer wheel more efficiently, while limiting the inner wheel to operate slightly below its saturation limit. In this case, depending on the maneuver, the outer wheel steer angle may exceed that of the inner wheel, thereby forcing the steering system towards anti-Ackerman geometry.

A simple PI controller is synthesized in this preliminary investigation of performance potential of the proposed AIFS concept. The controller is designed to provide a corrective steering action to achieve a target yaw rate. The target or reference yaw rate corresponds to a neutral steer condition, which is established from the forward velocity and instantaneous driver steering command, such that:

$$\Omega_{ref} = \frac{V\delta_{st}}{L} \quad (2.16)$$

The desired steer angle correction from the PI controller is estimated from the instantaneous yaw rate error, such that:

$$\delta_c = K_p\Delta\delta_{st} + K_i \int \Delta\delta_{st} \quad (2.17)$$

where K_p and K_i are proportional and integral gains, respectively, δ_c is the steering correction to be distributed over the inner and outer wheels, and $\Delta\delta_{st}$ is input to the controller, which is directly related to the yaw rate error, $\Delta\Omega = \Omega_{ref} - \Omega_{act}$, such that:

$$\Delta\delta_{st} = K_{st}\Delta\Omega \quad (2.18)$$

The gain K_{st} defines the linear relation between the reference yaw rate and the steering angle, denoted as the steering factor, and is obtained from Eq. (2.16), as:

$$K_{st} = \frac{\delta_{st}}{\Omega_{ref}} = \frac{L}{V} \quad (2.19)$$

While the controller gains in this study have been identified through repeated simulations, the resulting corrective action is distributed over the inner and outer-wheels through the steering mechanism, such that:

$$\delta_I = \delta_{st} + \rho_I\delta_C \quad (2.20)$$

$$\delta_O = \delta_{st} + \rho_O\delta_C \quad (2.21)$$

The ρ_I and ρ_O are the distribution gains, which assume identical value of 1, when operating in the linear regime. The unity values of the gains would also be applicable for the AFS controller, whether it operates in the linear or non-linear regime. In case of the proposed AIFS controller, ρ_O is always greater than ρ_I for an understeer vehicle.

2.5 Steering Mechanism

Various steer-by-wire systems proposed in the literature could be readily applied for implementation of the AIFS control strategy. A few studies, however, have expressed concerns related to reliability of the steer-by-wire systems [123,124]. In this study, a fail-safe mechanical steering system is explored to permit independent control of the steering angle at each wheel of the vehicle. This innovative design detailed in [117] is presented in Fig. 2.4, which consists of two set of planetary gear trains. Each set of planetary gear system includes a sun gear, three or four planet gears, an annulus or a ring gear and a planet carrier. The steering column drives the

sun gears of both the planetary gear sets. The planet carriers play the role of pinions as in a conventional rack and pinion system. It can be seen that the proposed design reverts to a conventional steering system, when the annulus is locked. Each gear set is also equipped with a DC servo motor that serves as the control actuator. Each electric motor applies the corrective angles by turning the annuluses, thereby providing a variable steering ratio through simultaneous turning of the annulus and the steering wheel. The resulting planet carrier velocity due to two independent inputs from the sun gear and the controlled annulus can be expressed as:

$$\omega_c = \frac{\omega_s Z_s \mp \omega_a Z_a}{Z_s + Z_a} \quad (2.23)$$

where ω_c , ω_s and ω_a are the planet carrier, sun and annulus velocities, respectively, and Z_s and Z_a refer to sizes of the sun and the annulus gears, respectively. In the above relation, it should be noted that the annulus may also apply a correction opposing the steer angle input depending on the driving situation.

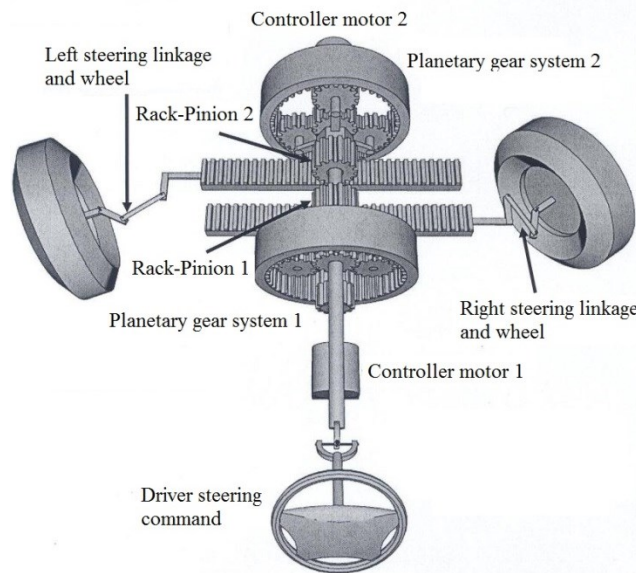


Figure 2.4: Independently controllable steering system with two sets of planetary gear systems [117].

2.6 Simulation Analysis

The effectiveness and potential performance gains of the proposed AIFS concept are investigated through simulations of the yaw-plane model integrating the proposed controller synthesis. The resulting closed-loop simulation model, shown in Fig. 2.5, solved using Matlab/Simulink. The vehicle parameters representing a step van used in this investigation are summarized in Table C.1 (Appendix C) and are similar to those reported in [125]. The handling performance characteristics of the vehicle model integrating AIFS controller are obtained considering three different cases of operating conditions: high-friction steady-turning maneuver idealized by a ramp-step steer input; a lane-change type of steer input idealized by a 0.16 Hz sinusoidal input, and a split-friction steady-turning input. The resulting responses of the model are also compared with those obtained with the AFS controller and the reference model.

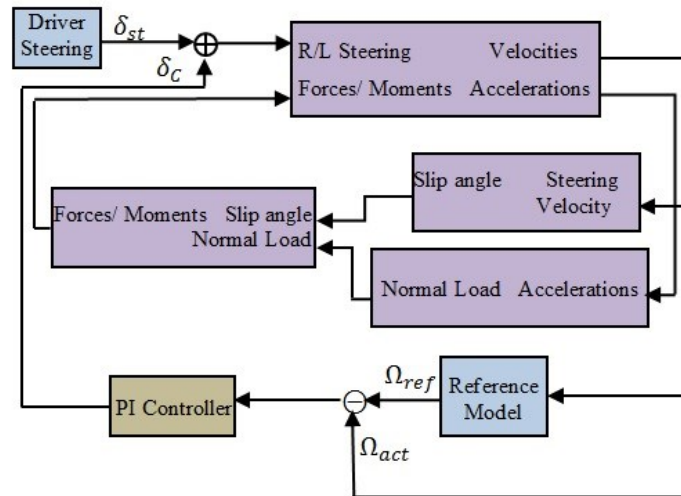


Figure 2.5: The Simulink model of the vehicle with a PI controller.

As discussed earlier, AIFS is essentially an AFS at low speeds and both can realize the target response until one of the tires in the AFS system approaches its saturation limit. The AIFS

system with independent control of wheel angles has the potential to provide target handling beyond the limits of AFS system. For selected steering commands, results are presented in this paper only for speeds where the advantages of AIFS over the AFS can be easily demonstrated.

2.6.1 Case study1: cornering maneuver

The cornering maneuver for the reference vehicle is evaluated by simulating vehicle responses to a J-turn steering input as illustrated in Fig. 2.6. The average steering input at the wheel rises in 2 second to 2.29 degree in sinusoidal wave shape and stays constant at 2.29 degree for the entire simulation leading to a circular trajectory for the vehicle motion. The input for the right-wheel designated as the outer and the left-wheel designated as the inner are established based on Ackerman geometry and given by Eq. (2.1) and Eq. (2.2), respectively. The results have been obtained on a dry road surface for a forward velocity of 20.5 m/s. The resulting lateral acceleration of the vehicle presented in Fig. 2.7 demonstrates the severity of the turning maneuver for the medium heavy vehicle selected for the case study.

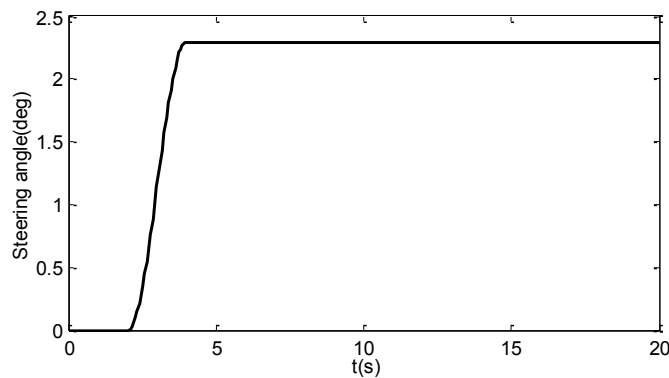


Figure 2.6: Steering angle input for the J-turn maneuver.

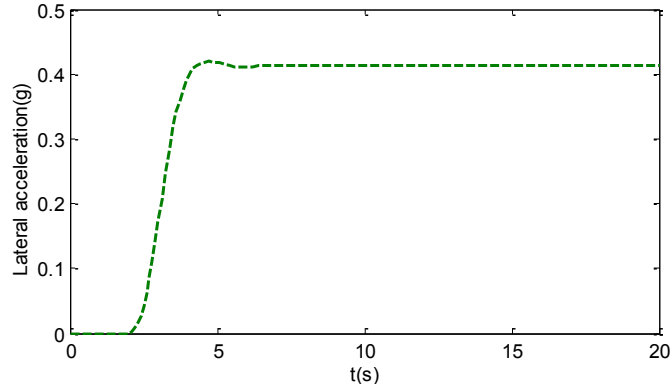


Figure 2.7: Lateral acceleration for the J-turn maneuver with AFS controller.

The ideal or target radius of curvature and the yaw rate are established from the simplified vehicle model with same parameters except the C.G location is modified to obtain neutral steer characteristic. The results for yaw rate and vehicle trajectory obtained for both AFS and AIFS simulation are compared with the reference response as shown in Fig. 2.8 and Fig. 2.9. The results show that the AFS with same corrective angle added to both wheels cannot generate the target response as the one of the wheels reach saturation. On the other hand, the AIFS as shown is capable of producing the target response without any of the wheels reaching saturation.

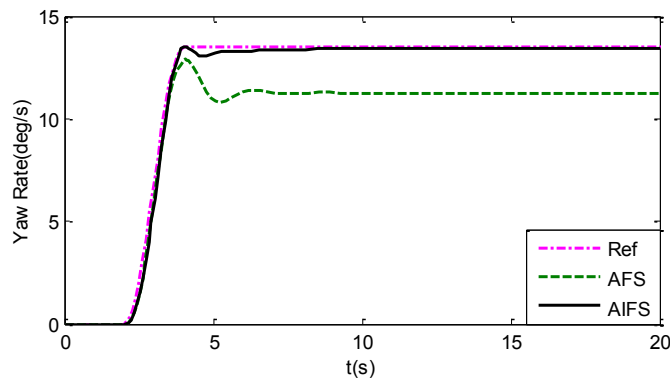


Figure 2.8: The yaw rate response for the J-turn maneuver.

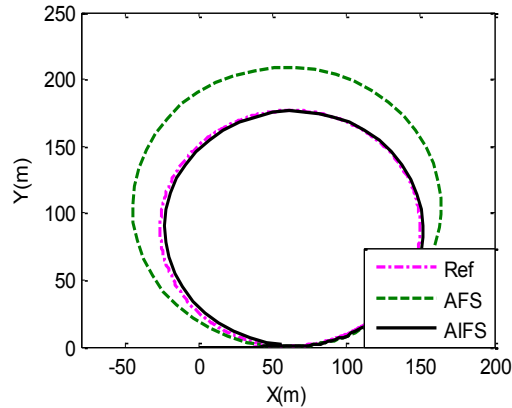


Figure 2.9: Trajectory of the vehicle in a J-turn maneuver.

The required steer angles at the inner and outer wheels generated by the controller in attempts to provide the target response to the J-turn input of 2.29 degrees are shown in Fig. 2.10. In all cases the steer angles at the wheels are increased until one of the tire reaches saturation level. The results show that the AFS controller increased the steer angles at both wheels in attempts to provide the target, while the AIFS increased the angle at the outer wheel significantly more than the inner to ensure that neither of the tires reached saturation while successfully provide the target response. The corresponding slip angles at each of front wheels for the same maneuver are shown in Fig. 2.11. The figure also identifies the limit of slip angle that can be reached at each wheel prior to saturation for the tire properties used and dynamic vertical load generated due to the maneuver. The results clearly show the superiority of the AIFS system and the control strategy to utilize the available road adhesion in generating the best possible performance. It is further noted that the AIFS did not reach the saturation even for this severe maneuver performed. The results, however, show that the steer angle needed at the outer wheel and the slip angle are quite large for AIFS as it tries to provide target. As discussed earlier this

trend is expected since the tires capability to generate lateral force diminishes for high values of slip angle.

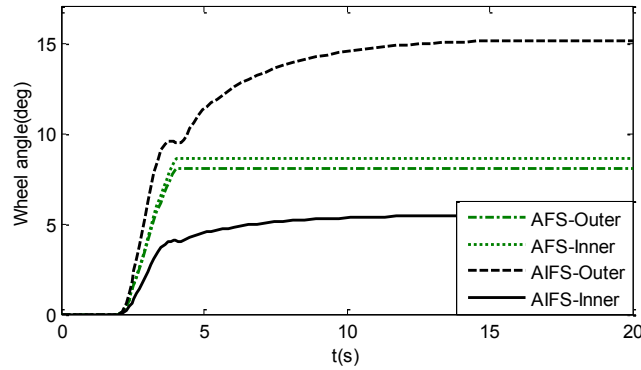


Figure 2.10: Outer and inner wheel angle with the AFS and AIFS controller.

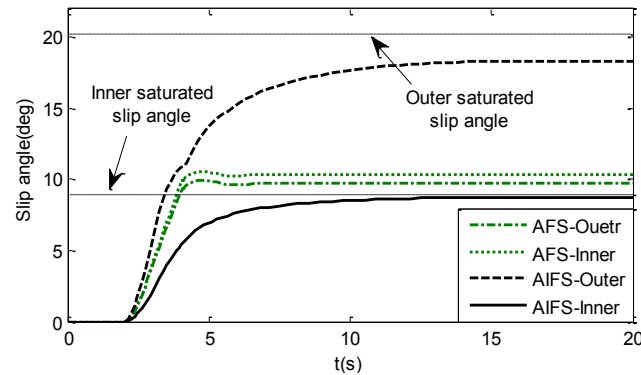


Figure 2.11: Outer and inner wheel side- slip angle.

2.6.2 Case study 2: sinusoidal maneuver

Simulation results are next generated for the vehicle with AFS and AIFS systems under a sinusoidal steering input. For this the average steer angle at the wheels with peak angle of 2.29 degrees and period of 6.28 seconds is used as presented in Fig. 2.12. The simulations were performed with a forward velocity of 23.6 m/s on a dry road. In this case, the outer or the inner wheel for each half cycle is not the same. In other words, if in the first half cycle the outer wheel is the right one, in the second half cycle the outer is the left wheel of the vehicle. Thus, this

would require further step for the controller to first identify the inner and outer wheels and then add the corrective angle to the appropriate wheel. The vehicle's response in terms of yaw rate as a function of time for the AFS and AIFS systems is shown in Fig. 2.13. The reference yaw rate response here is the one realized by a neutral steer vehicle. The magnitude of steer angle and velocity used are comparable to those used for J-turn above leading to a severe maneuver. As the results show, the AIFS system with the control strategy is very effective in realizing the target response, whereas the AFS fails to be close to the target as the tire reaches saturation limit. The corresponding trajectories for the two systems shown in Fig. 2.14 also demonstrate the superior performance of the AIFS system. It is expected that the limitation of AFS will be more prominent if higher frequency sinusoidal input is used.

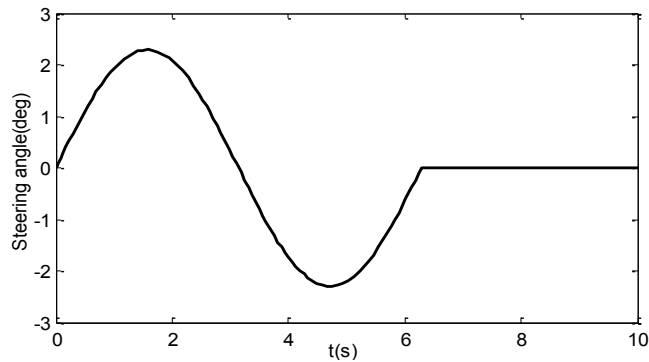


Figure 2.12: Steering angle input for the sinusoidal maneuver.

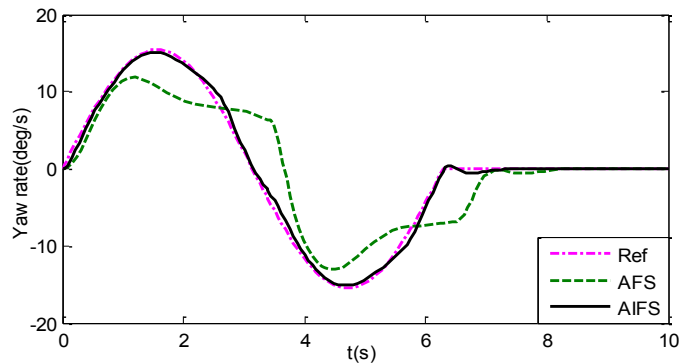


Figure 2.13: Yaw rate response for the sinusoidal maneuver.

The steer angles generated for the inner and outer wheels by the controllers of AFS and AIFS systems to realize the above responses are shown in Fig. 2.15. The corresponding side slip angles at each of the steered wheels are also shown in Fig. 2.16. These results demonstrate the manner in which the steer angles are modified over each half cycle of the input. Figure 2.16 further showing saturation limits for positive slip angles indicate that both AFS and AIFS reach the saturation limit in realizing the simulated responses. The AIFS, however, reaches the saturation level for a fraction of a second and similar to previous results, large angles are needed at the outer wheel in order to realize the target in a severe maneuver. The lateral acceleration of the vehicle under the sinusoidal maneuver is shown in Fig. 2.17. It is evident that the peak lateral acceleration reached for this maneuver is more severe than the one for J-turn presented earlier.

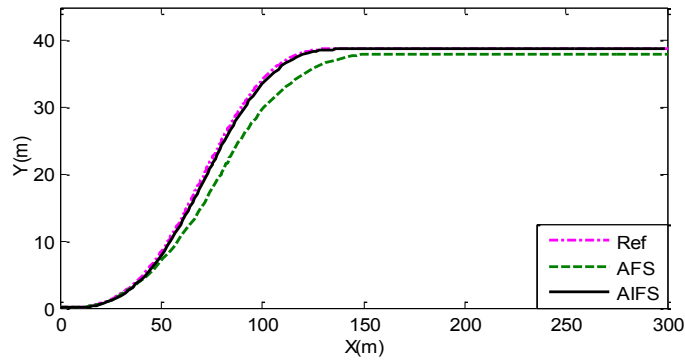


Figure 2.14: Trajectory of the vehicle in the sinusoidal maneuver.

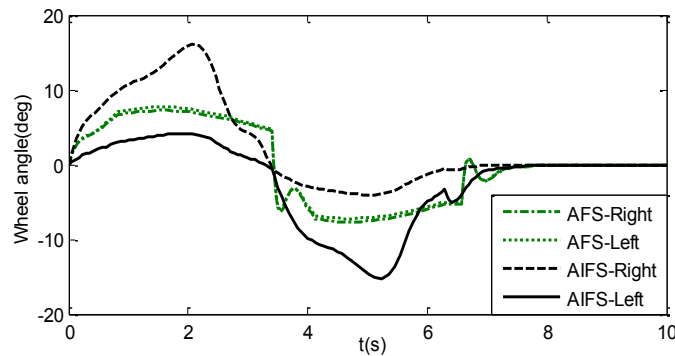


Figure 2.15: Outer and inner wheel angle with the AFS and AIFS controller.

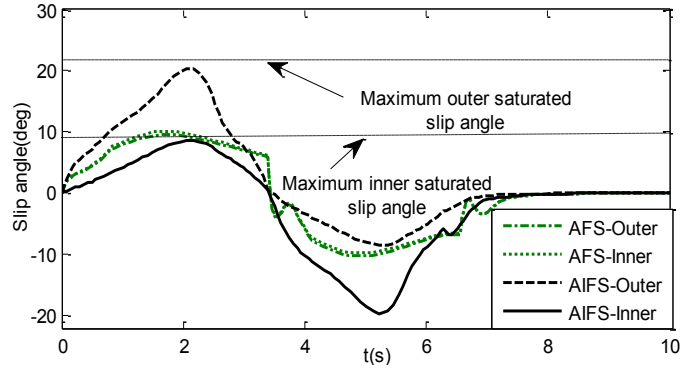


Figure 2.16: Outer and inner wheel side-slip angle with AFS and AIFS.

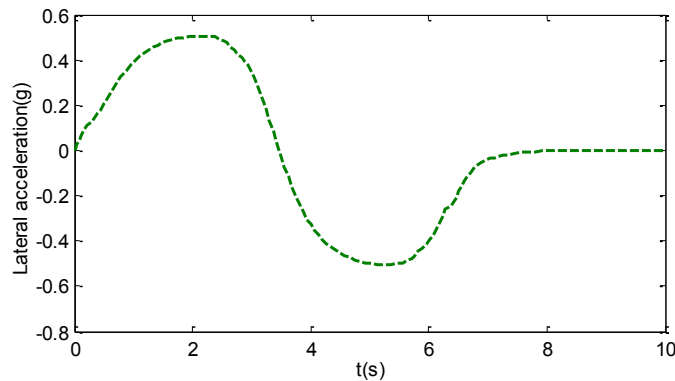


Figure 2.17: Lateral acceleration of the vehicle in the sinusoidal maneuver.

2.6.3 Case study 3: split- μ condition

Split- μ describes a condition for the road where the coefficient of friction is not same for each of the tire-road interface. It is expected that for such road condition, a system with capability for independent control of wheel steer angle should provide a superior performance. To examine this, a set of simulations were finally performed using the vehicle equipped with AFS and AIFS systems for the split- μ road conditions ($\mu_R = 1$, $\mu_L = 0.2$). The steering input used for this simulation is same as that used for J-turn maneuver, while the forward velocity is set at 18 m/s. The results in terms of yaw rate time history is presented in Fig. 2.18 and Fig. 2.19 shows the corresponding trajectory of vehicle motion. These results again demonstrate the effectiveness of AIFS and the inability of AFS to realize the target. It should be pointed out that

the severity of the maneuver considered for split- μ is significantly lower than that used earlier for uniform road condition. The inner and outer steer angles generated by the AFS and AIFS in order to generate these responses are shown in Fig. 2.20. As the result shows, the steering angle needed here for the outer wheel of AIFS was significantly less than that for earlier maneuver. The corresponding side slip angles at each wheel of both systems shown in Fig. 2.21 indicate that while AFS tire has reached saturation, the AIFS tire is capable of producing much more cornering force if required. The lateral acceleration of the vehicle is demonstrated in Fig. 2.22.

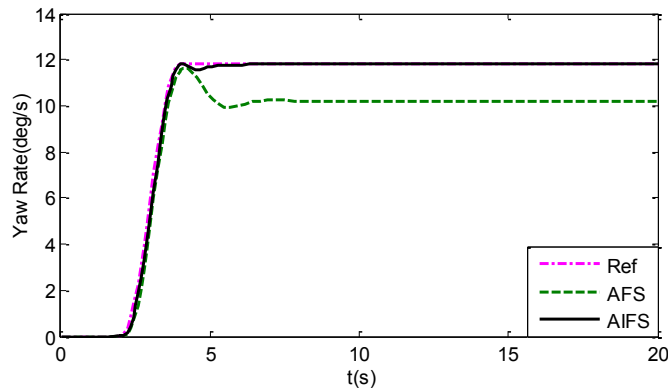


Figure 2.18: Yaw rate response for the split- μ maneuver.

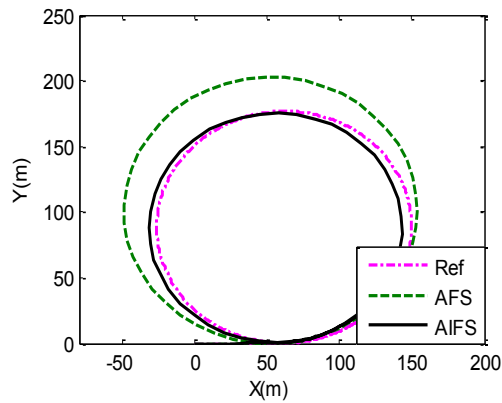


Figure 2.19: Vehicle trajectory generated by the AFS and AIFS controllers.

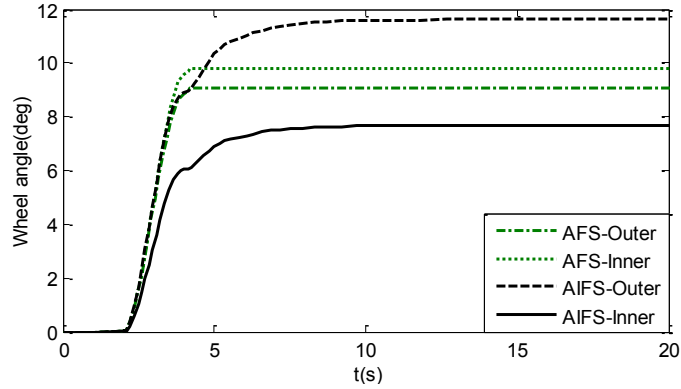


Figure 2.20: Outer and inner wheel angle with the AFS and AIFS controller.

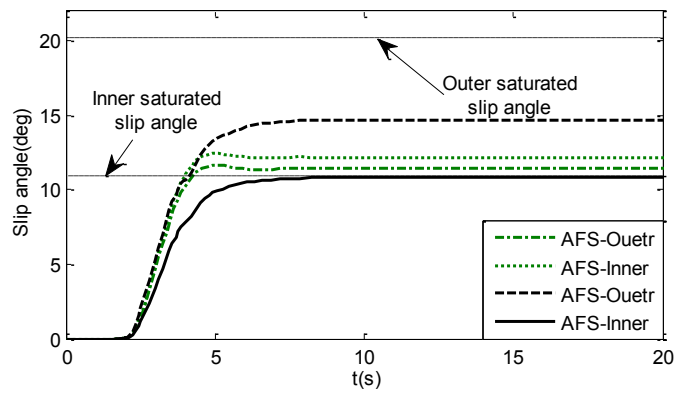


Figure 2.21: Outer and inner wheel side-slip angle with the AFS and AIFS controller.

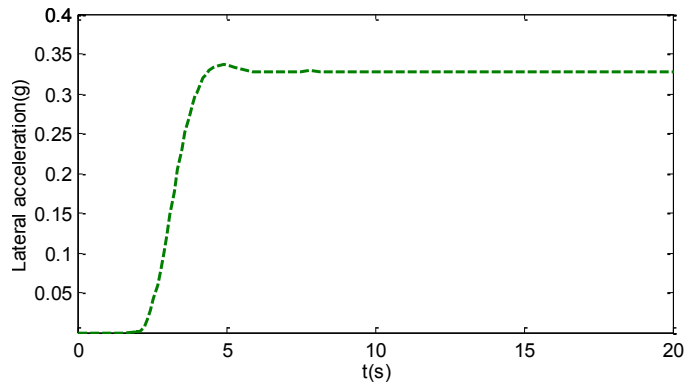


Figure 2.22: Lateral acceleration for the split- μ maneuver with AFS controller.

2.6.4 CG height sensitivity analysis

The effectiveness of AIFS over the AFS system strongly relies on the magnitude of load shift during a maneuver. The magnitude of this load shift on the other hand is largely dependent

on the height of the center of gravity (CG). It is thus an interesting parameter to examine for sensitivity to the effectiveness of AIFS system. A set of results are therefore obtained using the baseline parameters for the vehicle while the height of CG is varied from 0.5 m to 1.2 m. The yaw rate response to J-turn maneuver has been established similar to the first set of results in this paper. Figure 2.23 summarizes the results for the range of CG height considered. The results show that for low cg heights, AFS is equally as effective as the AIFS in realizing a target response. However, as the CG height is increased, AIFS is the only active steering system that can provide effective result.

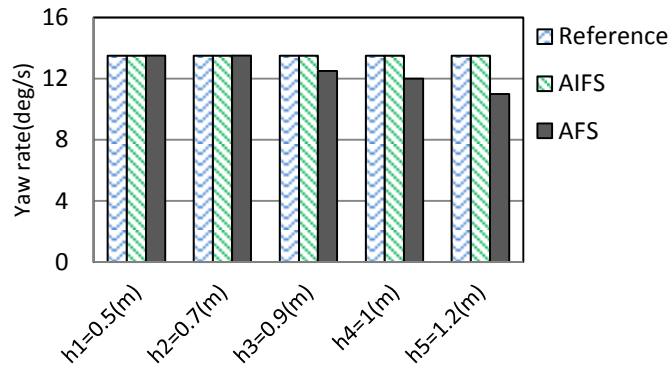


Figure 2.23: Height sensitivity analysis for yaw rate response with AFS and AIFS.

2.7 Conclusion

The simulations results revealed that the proposed Active Independent Front Steering (AIFS) system and the control strategy yields enhanced handling performance under a range of severe road maneuvers and surface conditions, when compared to the AFS. The AIFS system yields performance gains identical to those of the AFS under typical vehicle maneuvers but provides superior tracking of the target responses under more severe maneuvers that cause the tires to either approach the lateral force saturation such as high-g directional maneuvers or

barking/steering on split- μ road conditions. The results show that the proposed AIFS system modifies the steer angle with speed at low speeds, while retaining Ackerman geometry, as in the case of the AFS system. Unlike the AFS, the proposed AIFS system utilizes the maximum available tire-road adhesion to meet the cornering demand in a severe maneuver through unequal distribution of the desired steer correction over the inside and outside wheels. As the inner tire approaches its saturation limit during a high- g maneuver, the AIFS system controller tends to enhance the cornering force by generating greater steer angle of the outer tire, effectively introducing anti-Ackerman geometry. The proposed AIFS system exhibits superior potential compared to the AFS particularly in the presence of greater lateral load shift during a high- g maneuver. The proposed concept is thus expected to be far more beneficial for enhancement of handling properties of heavy vehicles, which invariably undergo large lateral load shift due to their high center of mass and roll motion. The study also proposed the design of an independently controllable front wheels steering system for implementation of the AIFS. Based on the results to date, the proposed design offers a potentially fail-safe mechanism for implementation of the AIFS system. The present study, however, is limited to a simple PI control synthesis to investigate the performance potentials of the AIFS concept, while the vehicle considered is understeer. It is desirable to seek alternate adaptive control algorithms so as to improve the tracking performance of the AIFS and robustness of the controller.

CHAPTER 3

PERFORMANCE ANALYSIS OF ACTIVE INDEPENDENT FRONT STEERING (AIFS) FOR COMMERCIAL VEHICLES WITH GREATER LATERAL LOAD SHIFT PROPENSITY

3.1 Introduction

Active Front Steering Systems (AFS) have been designed to vary steer angles in an active manner to realize a target directional response [122]. The steer angles of both the inner and outer wheels, however, are altered simultaneously, while maintaining Ackerman geometry [93]. Furthermore, the ability of a tire to generate a lateral force is not adequately considered in the AFS synthesis. Alternatively, an Active Independent Front Steering (AIFS) concept that can realize steer angle corrections of the right- and left-steered wheels in an independent manner has been shown to outperform the conventional Active Front Steering (AFS) system in the context of handling performance of automobiles [126]. The AIFS concept permits maximum utilization of the tire-road adhesion available at each wheel/road contact without approaching cornering force saturation to realize the target response. In doing so, the AIFS can maximize the performance limit of a road vehicle not only on a homogeneous surface but also on a split- μ road condition. The lateral load transfers encountered during a steering maneuver could lead to loss of cornering ability of the steered wheels and thereby limited handling performance under high speed maneuvers. The control strategy of AIFS system is based on compensation of the tire cornering force loss attributed to lateral load transfer across the steered wheels apart from utilization of the

available tire-road adhesion so as to achieve improved handling performance, particularly under more severe high-g steering maneuvers.

The results obtained through parametric sensitivity analysis of the AIFS concept suggested greater effectiveness of AIFS for vehicles with higher mass center and thus greater load transfer [126]. The AIFS is thus expected to yield better performance for commercial vehicles with their inherent high center of mass and roll motions that lead to large lateral load shifts. This phenomenon is more pronounced in liquid cargo vehicles particularly under partial fill conditions, where the lateral load transfers could be far more significant under steering and braking maneuvers [127]. The main focus of the present study is thus to examine the effectiveness of an AIFS in enhancing the handling performance of tank trucks with full and partial loads. It is well known that partially filled tank trucks exhibit substantially lower directional stability and control limits compared to rigid cargo trucks, which is primarily attributed to their high mass center and excessive cargo movement under steering maneuvers [128]. Such vehicles are thus more frequently involved in road accidents [129]. The implications of accidents involving such vehicles could be catastrophic, particularly when hazardous materials are involved. Numerous studies have illustrated the adverse influences of the liquid cargo movement within tank trucks on their directional stability and rollover propensity, which are further dependent upon the tank cross-section and the fill volume [130-132]. A partial fill condition yields lower center of mass (CG) height, and therefore superior stability limit and handling performance may be expected. The additional roll moment caused by cargo movement, however, may not only counter the gain due to lower CG height but also lead to lower directional control performance of the vehicle. This trend is evident from the reported studies on wider

cross-section tanks such as oval and modified oval tank vehicles [130]. For cylindrical cross-section tank, it has been shown that the additional roll moment due to cargo movement nearly nullifies the low CG gain in the context of rollover threshold limit. The cylindrical tank trucks thus exhibit lower sensitivity of the rollover threshold to variations in the fill height, when cargo load is constant as observed in general purpose tank truck fleets transporting products of varying weight density [132]. The handling performance of partly-filled tank trucks, which exhibit excessive load transfers irrespective of the tank cross-section, may be enhanced through AIFS.

From the review of studies reporting the performance potentials of AFS, it is apparent that AFS control strategy has been mostly explored with an objective to reduce the rollover hazard in an emergency maneuver [57]. However, the results suggest that enhancing the vehicle rollover threshold may lead to lateral instability during an evasive maneuver. An AFS system may thus provide enhanced vehicle rollover immunity at the expense of poor handling performance through relatively greater path deviation [60]. Some studies have proposed integration of Direct Yaw-moment Control (DYC) together with Active Steering in order to compensate for the path deviations [56]. Such an approach would lead to significant system and control complexities. Furthermore, it has been reported that systems with DYC frequently lead to a level of disturbance and annoyance to the driver [5,6]. The application of AFS control to an articulated tractor-semitrailer combination has also been studied for prevention of jackknife instabilities during severe driving maneuvers [63].

The AIFS control that can apply differential steering to right- and left-steered wheels in an independent manner with appropriate considerations of instantaneous load transfer and possible cornering force saturation of the tires offers considerable advantages for enhanced handling

performance over a wider speed range. The potential handling performance gains of an AIFS have been illustrated for a passenger car [126]. The study also showed far greater performance potentials of an AIFS for high CG vehicles subject to high-g maneuvers, the situations involving greater load transfers. For passenger cars with only moderate load shift across the steered wheels, the performance gain was realized by primarily increasing the steer angle of the outer wheel with larger normal load, while the controller strategy was based on predetermined slip angle limit for tire saturation. Alternatively, an improved control strategy may be realized through online monitoring of impending tire force saturation in terms of tire work-load. A control strategy that attempts to equalize tire work-loads of inner and outer wheels would not only permit maximum possible cornering force but also retain sufficient road adhesion for developing essential longitudinal forces.

In this study, the performance characteristics of an AIFS are investigated for applications in commercial vehicles with high CG and lateral load transfers. A two-axle tank truck is considered as a case example. A nonlinear yaw-plane model of the tank truck integrating roll dynamics of the sprung mass is developed to study the directional performance potential of the AIFS. The load shift associated with liquid cargo motion in the roll plane of a cylindrical tank is evaluated using the quasi-static approach and incorporated in the vehicle model in terms of resultant lateral force and roll moment attributed to quasi-static cargo shift. The AIFS strategy based on a yaw rate reference model is synthesized considering delays associated with tire lag and steering response. The controller strategy permits independent control of each wheel so as enhance handling performance limit through maximum utilization of the available tire-road adhesion prior to approaching the saturation limit. Simulation results are obtained for both the full and

partial load conditions under a steady-turning maneuver at different forward speeds to demonstrate the effectiveness of an AIFS system for applications in rigid as well as partly-filled liquid cargo trucks.

3.2 Directional Dynamic Model of the Truck

A simple yaw-plane model of a two-axle truck with roll-DOF is formulated, as shown in Fig. 3.1. The model comprises right- and left- wheels with independent steering angles in order to study the performance potentials of the AIFS. The model also considers nonlinear tire model in order to predict tire forces under severe maneuvers and possible impending cornering force saturation. The model with independent steering of the right- and left-wheels is formulated considering roll motion of the sprung mass, as well as lateral and yaw motions of the vehicle, as shown in Figs. 3.1(a) and 3.1(b), respectively. In the figure, ‘RC’ refers to roll center of the sprung mass and ϕ denotes the sprung mass roll angle. The equations of motions obtained considering large steer angles are summarized below:

$$mV(\dot{\beta} + r) - m_s h_s \ddot{\phi} = F_{YFr} \cos \delta_r + F_{YFl} \cos \delta_l + 2(F_{YRr} + F_{YRl}) \quad (3.1)$$

$$(I_{xs} + m_s h_s^2) \ddot{\phi} - I_{xzs} \dot{r} - m_s h_s V(\dot{\beta} + r) = (m_s g h_s - K_{\phi F} - K_{\phi R}) \phi - (C_{\phi F} + C_{\phi R}) \dot{\phi} \quad (3.2)$$

$$(I_{zs} + I_{zu}) \dot{r} - I_{xzs} \ddot{\phi} = - \sum_{i=F}^R \sum_{j=r}^l M_{ij} + F_{YFr} (b \cos \delta_r - T_F \sin \delta_r) + \dots \\ F_{YFl} (b \cos \delta_l + T_F \sin \delta_l) - 2c(F_{YRr} + F_{YRl}) \quad (3.3)$$

where V, r and β are the speed, yaw rate and side-slip angle of the vehicle, respectively. The distances of the front and rear axle from the CG are denoted by b and c . I_{xs} , I_{xzs} and I_{zs} are sprung mass moments of inertia about the x, xz and z axis at the mass center, respectively, and I_{zu} is the moment of inertia of the unsprung mass. $K_{\phi i}$ and $C_{\phi i}$ ($i = F, R$) are the total front-

and rear-axle suspension roll stiffness and roll damping, respectively.

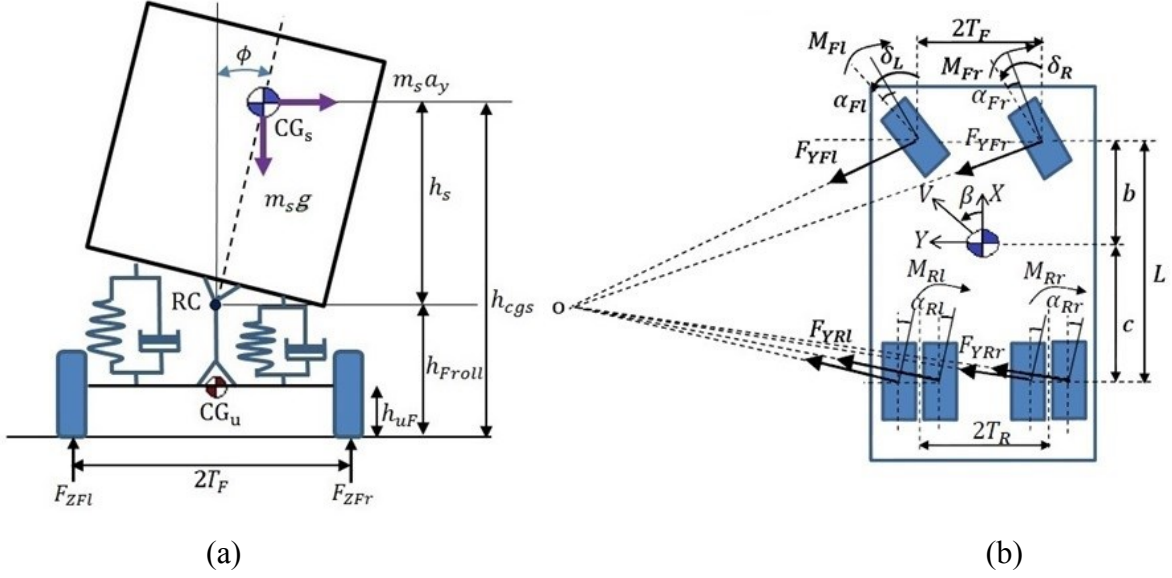


Figure 3.1: Three-DOF directional dynamic model of a two axle truck: (a) roll-plane; and (b) yaw-plane.

In the above equations, tire lateral force F_{Yij} and self-aligning moment M_{ij} ($i = F, R; j = r, l$) are derived using the Magic Formula [102] considering the normal load F_{Zij} and slip angle α_{ij} of each wheel, where subscripts F and R refer to front- and rear-tires, and r and l denote the right- and left-wheels, respectively. The normal load on each wheel can be derived as a function of the longitudinal (a_x) and lateral (a_y) accelerations as well as the suspension roll stiffness ($K_{\phi i}$) and damping ($C_{\phi i}$), in the following manner:

$$\begin{aligned}
 F_{ZFr} = & \frac{W_F}{2} - \frac{a_x}{2L} (m_s h_{cgs} + m_{uF} h_{uF} + m_{uR} h_{uR}) + \dots \\
 & \frac{a_y}{2T_F} (m_{sF} h_{Froll} + m_{uF} h_{uF}) + \frac{1}{2T_F} (K_{\phi F} \phi + C_{\phi F} \dot{\phi})
 \end{aligned} \tag{3.4}$$

$$F_{ZF_l} = \frac{W_F}{2} - \frac{a_x}{2L} (m_s h_{cgs} + m_{uF} h_{uF} + m_{uR} h_{uR}) - \dots \quad (3.5)$$

$$\frac{a_y}{2T_F} (m_{sF} h_{Froll} + m_{uF} h_{uF}) - \frac{1}{2T_F} (K_{\phi F} \phi + C_{\phi F} \dot{\phi})$$

$$F_{ZR_r} = \frac{W_R}{4} + \frac{a_x}{4L} (m_s h_{cgs} + m_{uF} h_{uF} + m_{uR} h_{uR}) + \dots \quad (3.6)$$

$$\frac{a_y}{4T_R} (m_{sR} h_{Rroll} + m_{uR} h_{uR}) + \frac{1}{4T_R} (K_{\phi R} \phi + C_{\phi R} \dot{\phi})$$

$$F_{ZR_l} = \frac{W_R}{4} + \frac{a_x}{4L} (m_s h_{cgs} + m_{uF} h_{uF} + m_{uR} h_{uR}) - \dots \quad (3.7)$$

$$\frac{a_y}{4T_R} (m_{sR} h_{Rroll} + m_{uR} h_{uR}) - \frac{1}{4T_R} (K_{\phi R} \phi + C_{\phi R} \dot{\phi})$$

where T_F and T_R are the half tire track widths of the front and rear axles, respectively, L is the wheelbase, m_{si} and m_{ui} ($i = F, R$) refer to the front and rear sprung and unsprung masses, respectively, and m_s is the total sprung mass.

3.2.1 Load shift in a partially-filled tank

Equations (3.1) to (3.7) describe the steering dynamic responses of the vehicle with only rigid cargo. The vehicle however is subjected to additional lateral load shift, lateral force and the roll moment due to lateral movement of liquid cargo within the partly-filled tank. Figure 3.2 illustrates the roll plane of the vehicle equipped with a partly-filled cylindrical tank. The center of mass of the liquid cargo experiences a lateral shift (y_c) due to roll motion of the sprung mass and the maneuver-induced lateral acceleration a_{y_c} . The magnitude of y_c depends on the tank geometry, fill height and liquid free surface gradient (γ). Assuming quasi-static motion and inviscid fluid cargo, the liquid free surface gradient is related to a_{y_c} and ϕ , such that [130]:

$$\gamma = \frac{a_{y_c} + \phi}{1 - a_{y_c} \phi} \quad (3.8)$$

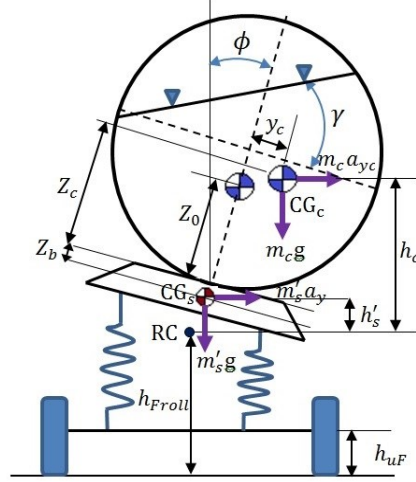


Figure 3.2: Partially filled tank truck model.

For a cylindrical tank of radius R , the lateral (y_c) and vertical (Z_c) movements of the liquid cargo mass center can thus be expressed as [130]:

$$y_c = (R - Z_0) \sin \gamma \quad (3.9)$$

$$Z_c = (R + Z_b) - (R - Z_0) \cos \gamma \quad (3.10)$$

where Z_0 is static CG height of the liquid cargo, which depends on the fill level. Z_b is tank base height from the chassis CG, as shown in Fig. 3.2. Assuming relatively small sprung mass roll angle compared to the lateral acceleration encountered during a steering maneuver yields, $\gamma \approx a_{yc}$. Furthermore, assuming $\sin \gamma \approx \gamma$ yields:

$$y_c = (R - Z_0) a_{yc} \quad (3.11)$$

The lateral acceleration at the cargo mass center may be expressed in terms of the vehicle forward speed, vehicle side-slip angle, roll acceleration and the yaw rate, as:

$$a_{yc} = V(\dot{\beta} + r) - h_c \ddot{\phi} \quad (3.12)$$

From Fig. 3.2, it is evident that lateral movement of the cargo imposes an additional roll moment (OM) about the roll center, as:

$$OM = m_c g y_c \quad (3.13)$$

Substituting for y_c from Eqns (3.11) and (3.12) yields following expression for OM :

$$OM = m_c(R - Z_0)(V(\dot{\beta} + r) - h_c \ddot{\phi}) \quad (3.14)$$

Subsequently, considering independent steering of the right- and the left-wheels, the equations of motion for the partly-filled tank truck model incorporating forces and moments due to cargo motion are formulated as:

$$mV(\dot{\beta} + r) - (m'_s h'_s + m_c h_c) \ddot{\phi} = F_{YFr} \cos \delta_r + F_{YFl} \cos \delta_l + 2(F_{YRr} + F_{YRl}) \quad (3.15)$$

$$I_{xsc} \ddot{\phi} - I_{xzsc} \dot{r} - (m'_s h'_s + m_c(h_c + R - Z_0))V(\dot{\beta} + r) + m_c h_c(R - Z_0) \ddot{\phi} = \\ = ((m'_s h'_s + m_c h_c)g - K_{\phi F} - K_{\phi R})\phi - (C_{\phi F} + C_{\phi R})\dot{\phi} \quad (3.16)$$

$$(I_{zsc} + I_{zu})\dot{r} - I_{zxsc} \ddot{\phi} = - \sum_{i=F}^R \sum_{j=r}^l M_{ij} + F_{YFr}(bc \cos \delta_r - T_F \sin \delta_r) + \\ F_{YFl}(bc \cos \delta_l + T_F \sin \delta_l) - 2c(F_{YRr} + F_{YRl}) \quad (3.17)$$

where m'_s is the mass due to chassis and the tare tank, and m_c is mass of the liquid cargo. I_{xsc} , I_{xzsc} and I_{zsc} are the mass moments of inertia of the chassis and the cargo mass about the x , xz and z axis, respectively, at the roll center. I_{zu} is mass moment of inertia of the unsprung mass.

3.3 AIFS Reference Model and Control Strategy

The AIFS control structure has been formulated to track the steering response of an idealized reference model based upon maximum utilization of the available adhesion limits of both the steered wheels, especially in a high lateral acceleration maneuver, as described in [126].

A simple PI controller is synthesized in this investigation to explore the performance potential of the AIFS concept applied to the two-axle truck. The controller is designed to provide a corrective steering action to achieve the reference yaw rate corresponding to a neutral steer condition, which is expressed as a function of forward velocity and instantaneous driver steering command δ_{st} , such that:

$$r_{ref} = \frac{V\delta_{st}}{L} \quad (3.18)$$

In the above relation δ_{st} relates to steer angles of the inner and outer wheels steer angles, δ_l and δ_r . Steering correction command, δ_C , to be distributed over the inner and outer wheels is subsequently obtained through synthesis of a PI controller, such that:

$$\delta_C = K_P \Delta\delta_{st} + K_I \int \Delta\delta_{st} \quad (3.19)$$

where K_P and K_I are proportional and integral control gains, respectively, $\Delta\delta_{st} = K_{st}\Delta r$ is the error factor relating the yaw rate error $\Delta r = r_{ref} - r$ and gain K_{st} , defined as the ratio of the steer angle and the reference yaw rate:

$$K_{st} = \frac{\delta_{st}}{r_{ref}} = \frac{L}{V} \quad (3.20)$$

In the controller synthesis r refers to the instantaneous yaw rate response of the vehicle. It should be noted that the steering correction δ_C is distributed over the left- and right-wheels through a mechanical transmission [117], while in case of an AFS control this correction is introduced following the Ackerman geometry.

Preliminary simulation results attained for a 4 degree J-turn maneuver revealed a significant overshoot in the yaw rate response, although it could easily achieve the desired target response.

This was attributed to considerations of the idealized controller, while the vehicle responses inherently show significant response delays caused by the tire lag, vehicle inertia and other mechanical components [64]. The reference model was thus refined to account for response delays considering a first-order lag function, such that:

$$r_{ref}^* = \frac{\tau r_{ref}}{1 + \tau s} \quad (3.21)$$

where τ is time constant relating the time lag between the steering input and the steady-state yaw rate response, and r_{ref}^* is the refined reference yaw rate. The simulation results of the vehicle model coupled with an AFS control using the idealized and refined reference yaw rates are shown in Fig. 3.3(a) in terms of the vehicle yaw rate. The figure also shows the ideal and refined reference yaw rates. The results were obtained using a completely filled tank truck so as to eliminate the contributions of cargo movement, while the forward speed was chosen as 57 km/h. The results clearly show that the AFS control based on the modified reference model tracks the target reasonably accurately without any overshoot. The time-histories of inner and outer front wheel steer angle responses of the AFS control based on idealized and refined reference yaw rate are further compared in Fig. 3.3(b). The results again show that addition of first-order system delays in the reference response effectively suppresses the overshoot in steer angle response.

Subsequent simulations were performed using the time-delayed reference yaw rate, while the controller gains were selected considering the frequency bandwidth of steering response of trucks of 1.5 Hz [64]. In order to ensure a consistent handling behavior under different steering

frequencies, the PI controller gains are tuned for tracking of the target yaw rate with cross-over frequency of 1.5 Hz. The gains $K_p = 1.1$ and $K_I = 16.0$ satisfied this requirement.

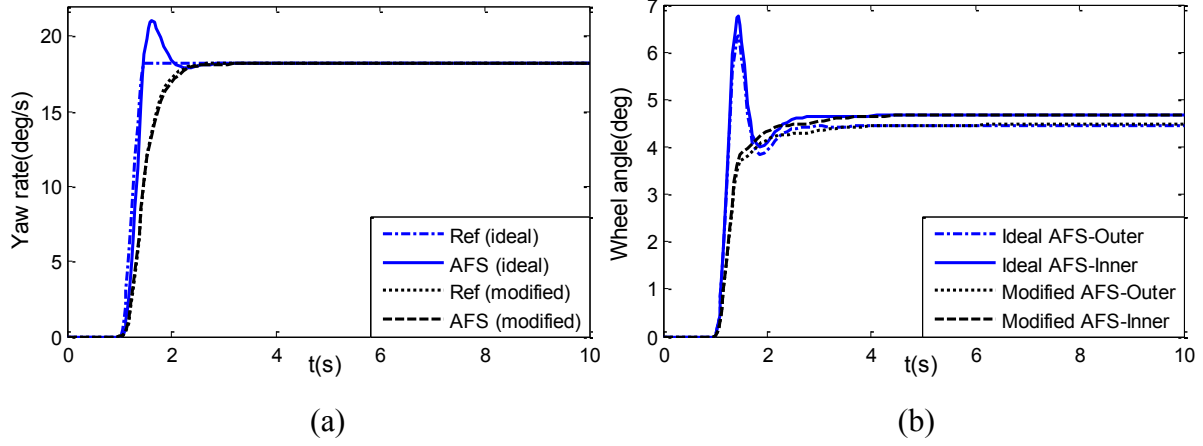


Figure 3.3: Comparisons of (a) yaw rate; and (b) steer angle responses of the model employing AFS control based upon idealized and modified time-delayed reference yaw rate.

In case of the AIFS control, the corrective steer angle δ_C , obtained from Eq. (3.19), must be distributed between the inner and outer-wheels considering the available adhesion limit of each tire. A performance parameter in terms of the tire work-load W_T is thus defined in order to determine the total force generated at a tire-road interface and its ability to generate additional forces [133]. The tire work-load is ratio of the total force developed by a tire to the maximum force a tire could generate based on the available tire-road adhesion, such that:

$$W_T = \frac{\sqrt{F_x^2 + F_y^2}}{\mu F_z} \quad (3.22)$$

where F_x and F_y are the braking/acceleration and cornering forces developed by the tire, respectively, F_z is the normal load and μ is the tire-road friction coefficient. Since the tire work-load represents utilization of the available adhesion by each tire, it can be considered as an indicator of the tire saturation. An alternate measure for tire's ability to generate maximum force

could be the saturation slip angle that may also serve as a limiting value for the steer angle applied to a wheel.

An estimate of the saturation zone of each tire may be obtained from normalized cornering stiffness q of the tire, defined as the ratio of cornering stiffness corresponding to an instantaneous slip angle to the linear cornering stiffness. Figure 3.4 presents the instantaneous normalized cornering stiffness of a truck tire as a function of tire slip angle for a wide range of normal loads. In a critical turning maneuver, the inner wheel of the steered axle will typically carry significantly less normal load compared to the outer wheel. As the figure indicates, the inner tire will thus approach the saturation zone or its adhesion limit much earlier than the outer tire. Since AIFS allows independent steering correction for each wheel, the control strategy could be synthesized to limit the steering correction so that none of the wheels approach saturation while applying greater steering correction to the outer wheel with greater normal load. The controller must also reduce the steering correction applied to the inner wheel to ensure its adequate adhesion with the road. In this study, the saturation zone is identified from the normalized cornering stiffness (Fig. 3.4) considering the tire work-load, especially that of the inner tire which tends to approach saturation relatively quickly. The limiting value of the inner tire work-load is chosen as 0.65, which corresponds to the onset of the tire force saturation, defined by the normalized stiffness, $q = 0.3$, as seen in Fig. 3.4. The chosen value of the work-load allows sufficient inner tire force adhesion for developing essential braking/acceleration forces at the inner tire-road interface. The resulting slip angle α^* at the onset of the saturation zone would also depend on the normal load, as seen in Fig. 3.4. For a given normal load, this slip

angle, referred to as ‘instantaneous saturated slip angle’ of the inner, is used to obtain the limiting value of steer angle, δ_l^* , that may be applied at the inner wheel, such that:

$$\delta_l^* = \alpha_{Fl}^* + \tan^{-1} \left[\frac{br + V_y}{V_x - T_F r} \right] \quad (3.23)$$

where V_x and V_y are the longitudinal and lateral velocity at vehicle CG. The AIFS controller is designed to introduce the corrective steering to both the wheels using the control law defined in Eq. (3.19). The steering correction applied to the inner wheel, however, is limited to δ_l^* to ensure not only its adhesion with the road but also to provide sufficient reserve for developing braking/acceleration force.

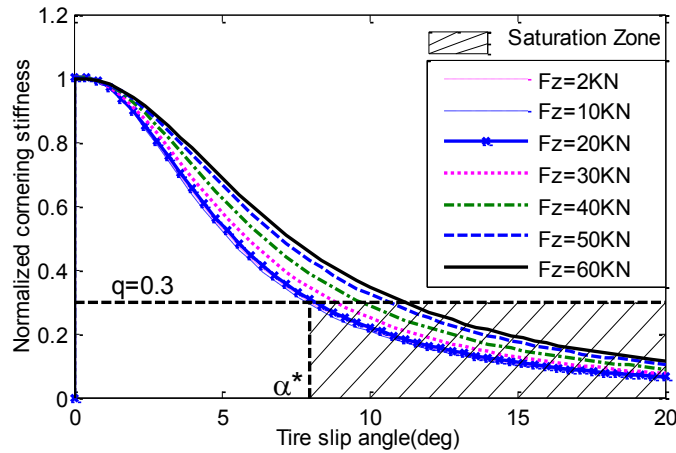


Figure 3.4: Normalized cornering stiffness and identification of saturation zone of a truck tire.

3.4 Simulation Results

Simulations are performed to investigate effectiveness of the AIFS concept for the two-axle truck with both non-moving and moving cargo. The steering responses of the truck model are obtained for three different loading conditions, while the total cargo load ($m_c = 9079.7$ kg) is held constant: (i) fully loaded tank that also represents rigid cargo with highest CG height (1.56

m); (ii) 50%-filled liquid cargo load; and (iii) 50%-filled equivalent rigid cargo load. The last two loading conditions yield substantially lower CG height compared to the first loading condition. The directional performance characteristics of the vehicle model are evaluated for a steady-turning J-turn maneuver (Fig. 3.5) on a dry road ($\mu = 0.78$). The steer input (Fig. 3.5) is applied at $t=1.0$ (s) with smooth rise and saturation at $t=1.5$ (s). Table C.2 (Appendix C) summarizes the simulation parameters [134]. The simulation results are obtained for the model integrating AFS and AIFS controllers, which are subsequently compared with those without an active steering control. The results obtained with AFS and AIFS are discussed to assess relative potential performance and effectiveness of the AIFS system for trucks, particularly under high CG loading and excessive lateral load shift conditions.

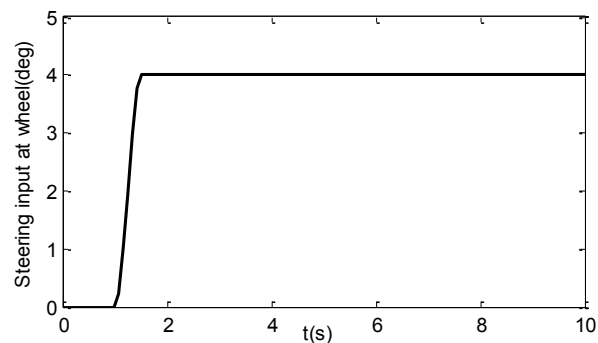


Figure 3.5: Steer angle corresponding to a J-turn maneuver.

3.4.1 Fully loaded truck

Figure 3.6 presents the lateral acceleration, yaw rate and path responses of the fully loaded truck subject to the J-turn maneuver at a forward velocity of 57 km/h. The results are obtained for the vehicle model with AFS and AIFS control systems, and without an active steering denoted as ‘NC’. The responses are also compared with those attained from the modified reference model. The lateral acceleration response in Fig. 3.6(a) may serve as an indicator of the

severity of the maneuver for the fully loaded truck considering the rollover threshold acceleration limit. The directional responses of the vehicle model with AIFS being identical to those with AFS control demonstrate that both control strategies are equally effective in realizing the target yaw rate and path responses. The effectiveness of the modified reference model in eliminating the response overshoot or oscillations is also evident from the results. The results clearly show substantial path deviation in the absence of active steering control, which is attributed to understeer nature of the vehicle (understeer coefficient = 0.012 rad).

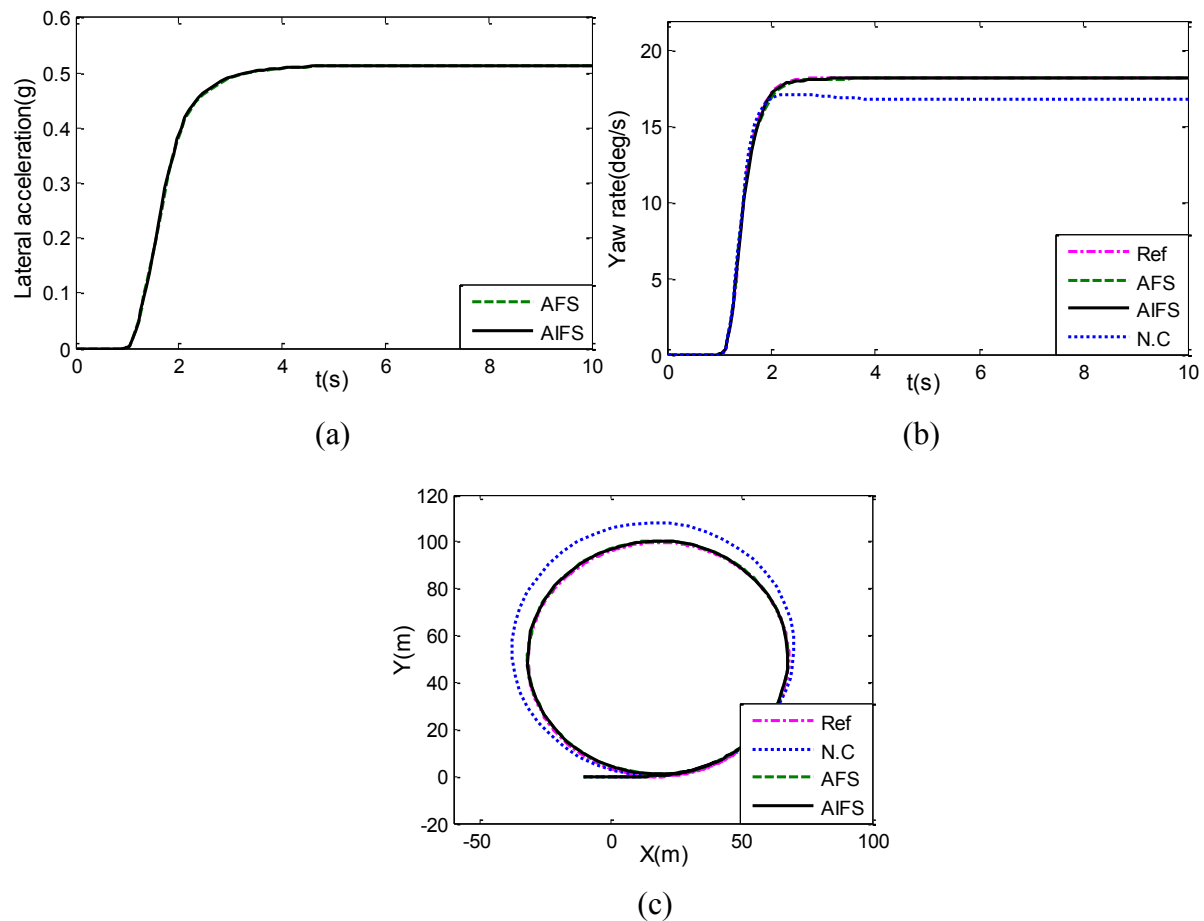


Figure 3.6: Comparisons of responses of the fully loaded truck with AFS and AIFS control with those of the reference model (Ref) and model without active steering control (NC): (a) lateral acceleration; (b) yaw rate; and (c) path trajectory.

Although both the active steering strategies achieve the desired target responses, the steered wheels in both cases are subjected to considerably different corrective steering and work-loads. As discussed earlier, the AFS control applies equal steering correction to both the wheels with no consideration of the instantaneous tire loads and tire's ability to generate lateral and longitudinal forces. Under the J-turn steering maneuver at 57 km/h, the AFS control may thus lead to saturation of the inner wheel, while the available tire-road adhesion is under-utilized by the outer wheel. The AIFS control strategy, on the other hand, applies different steering corrections to the right- and left-wheels in an independent manner considering the tire work-load and the inner wheel saturation. The tire work-loads during the maneuver are evaluated for both the controller synthesis and compared in Fig. 3.7.

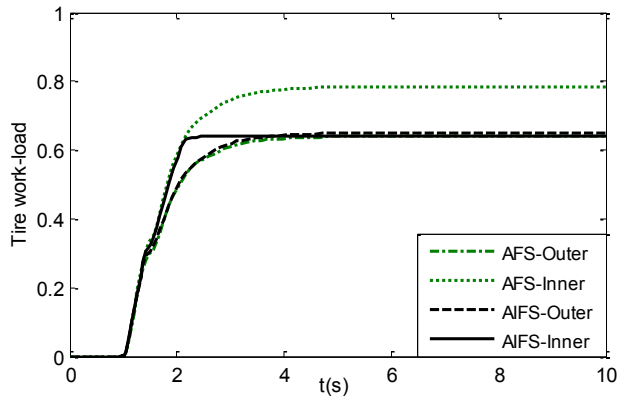


Figure 3.7: Comparison of work-loads of steered wheels of the vehicle model with AFS and AIFS control.

The results show that in generating the target response under the given steering input, the AFS control yields the inside wheel work-load of about 0.78, while that of the outer wheel is only 0.64, suggesting near saturation of the inner wheel and under-utilization of the available road adhesion by the outer wheel. The AIFS control, however, achieves the target response without any of the wheels reaching near saturation. The tire work-load of both the wheels is

comparable and limited to approximately 0.65. The AIFS control thus provides superior active steering control compared to the conventional AFS system, as it can retain a reserve capacity for both the tires for generation of additional braking/acceleration forces during the maneuver.

The steer angles developed by both the controllers are also compared in Fig. 3.8. Owing to the understeer character of the truck, the AFS controller imposes higher steer angles to both the wheels so as to achieve near Ackerman ratio. As a result the inner wheel with reduced normal load rapidly approaches force saturation. The AIFS control, however, applies significantly lower steer angle to the inner wheel so as to avoid its saturation, while increasing the steer angle of the outer wheel. The AIFS control thus reduces the inner tire work-load to the predetermined level of 0.65.

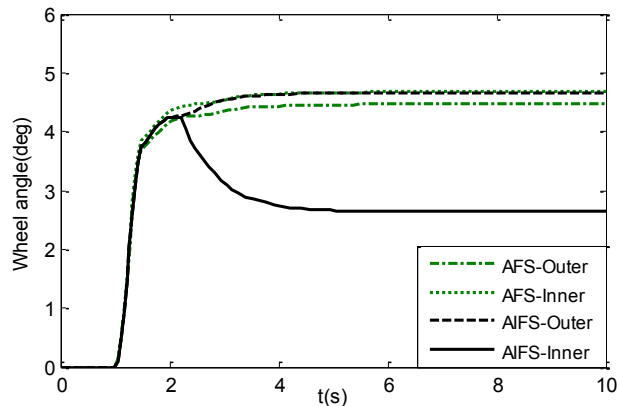


Figure 3.8: Comparison of steered wheels angle developed with AFS and AIFS control.

It should be noted that the selected maneuver causes the vehicle to operate very close to its rollover threshold limit. This is evidenced from the time-histories of the normal load on each wheel of the vehicle model with active steering control (Fig. 3.9). The results suggest substantial lateral load shift, where the inner rear wheels approach impending lift-off. A further increase in speed would likely cause the truck to roll over. It can therefore be concluded that an active

steering control can effectively realize the target vehicle responses at all speeds below the vehicle rollover threshold limit.

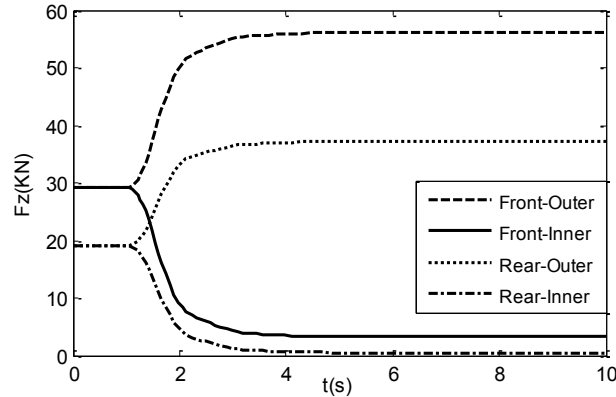


Figure 3.9: Normal load on each wheel of the vehicle model with active steering control.

In order to assess the relative significance and benefits of AIFS strategy in relation to AFS, simulations were performed at different forward speeds approaching the rollover limiting speed of nearly 61 km/h. The results are analyzed to derive the tire work-loads and the steady-state responses at different speeds that correspond to the maximum limiting value of the inner tire work-load 0.65 (Table 3.1). The results show that both the AFS and AIFS controls track the target response at moderate speeds up to 53km/h, where the inner tire work-load remains below the limiting value of 0.65. The AFS control coupled with Ackerman geometry may thus be preferred until this speed considering its relative simplicity compared to the AIFS control. The AFS control, however, causes the inner tire work-load to exceed the limiting value at speeds above 52 km/h. The inner tire work-load approaches 0.89 at 60 km/h suggesting very limited tire's ability to generate longitudinal force. The AIFS control, however, satisfies the handling performance requirements within the inner tire load limit until the vehicle approaches the rollover near 60 km/h by increasing the steer angle of outer wheel to 5.7 degrees and reducing

the inner wheel angle to 1.8 degrees. It also needs to be emphasized that the handling performance of the vehicle would strongly depend upon the tire-load limit. Increasing the inner tire load limit would adversely affect the tire's ability to generate braking/acceleration force during the maneuver. The results further show that both the control strategies yield identical steady-state responses of the vehicle in the entire speed range.

Table 3.1: Comparisons of tire work-loads and steady-state steering responses of the fully loaded truck with AFS and AIFS control.

Control	AFS W_T		AIFS W_T		AFS/AIFS directional responses		AIFS steer angle	
	Inner	Outer	Inner	Outer	ϕ (deg)	a_y (g)	Inner (deg)	Outer (deg)
50	0.58	0.48	0.56	0.49	5.6	0.39	4.1	4.1
51	0.61	0.51	0.59	0.52	5.8	0.41	4.1	4.1
52	0.63	0.53	0.62	0.54	6.0	0.43	4.1	4.2
53	0.67	0.55	0.65	0.56	6.3	0.44	4.1	4.2
54	0.70	0.56	0.65	0.58	6.5	0.46	3.8	4.3
55	0.73	0.59	0.65	0.61	6.8	0.48	3.4	4.4
56	0.76	0.62	0.65	0.63	7.0	0.50	3.0	4.6
57	0.78	0.64	0.65	0.66	7.3	0.51	2.6	4.7
58	0.82	0.67	0.65	0.69	7.6	0.53	2.3	4.8
59	0.85	0.70	0.65	0.70	7.8	0.55	2.0	5.2
60	0.89	0.73	0.65	0.73	8.1	0.57	1.8	5.7
61	0	0	0	0	8.3	0.59	1.6	6.0

3.4.2 Partially filled tank truck

The relative effectiveness of the AIFS is subsequently examined for the 50%- filled tank truck with and without liquid slosh. The steering responses are evaluated in terms of steady-state lateral cargo movement, roll angle, and inner and outer tires normal loads considering 50%-filled liquid cargo and equivalent rigid cargo vehicles. The steering responses are initially obtained in the absence of active steering control to study the effects of liquid load shift. The simulations

were performed using the parameters presented in Table C.2 (Appendix C), including the constant cargo load of 9,079.7 kg, and the J-turn maneuver shown in Fig. 3.5 at a forward speed of 60 km/h. Figure 3.10(a) illustrates the variations in lateral position of the liquid cargo CG (y_c), while the roll and yaw rate responses of the 50%-filled liquid and equivalent rigid cargo vehicles are shown in Figs. 3.10(b) and 3.10(c), respectively. As expected the steering maneuver yields significant lateral movement of the liquid cargo CG, which approaches a peak value of 0.35m within the 1 m radius tank. The steady-state lateral load shift is near 0.21 m, which causes considerably higher roll motion of the sprung mass compared to the rigid cargo vehicle, as seen in Fig. 3.10(b). It has been shown that transient fluid slosh during a steering maneuver would cause substantially higher roll angle response, which cannot be predicted from the quasi-static model used in this study. The quasi-static fluid slosh model, however, provides reasonable accurate estimation of the steady-state response [9].

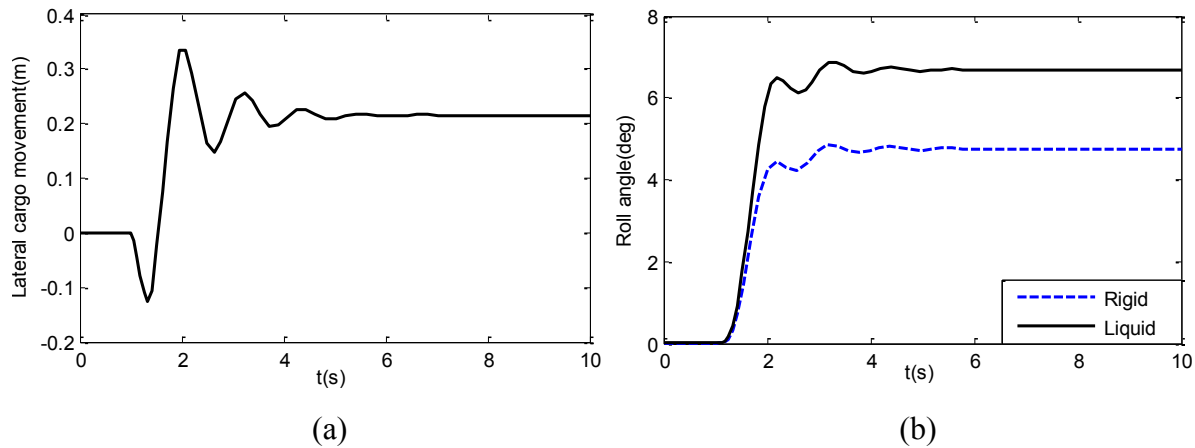


Figure 3.10: Variations in (a) lateral position of the liquid cargo CG; and (b) sprung mass roll angle responses of the 50%-filled liquid and equivalent rigid cargo vehicles.

The higher roll angle response of the liquid cargo vehicle coupled with the lateral cargo CG shift (Fig. 3.10) causes substantially higher lateral load transfer compared to the rigid cargo

vehicle, as seen in Fig. 3.11. The results suggest near lift-off of the inner wheels of the liquid cargo vehicle. This behavior is of particular interest in this investigation of the active steering system, especially the AIFS control. The yaw rate responses of both the liquid and rigid cargo vehicles show considerable deviations from the target response (Fig. 3.12). It is interesting to note that the greater load shift in the liquid cargo vehicle leads to a steering characteristic that is more understeer than the rigid cargo vehicle. A larger steering correction would thus be required for the liquid cargo vehicle, which may suggest greater effectiveness of the AIFS control.

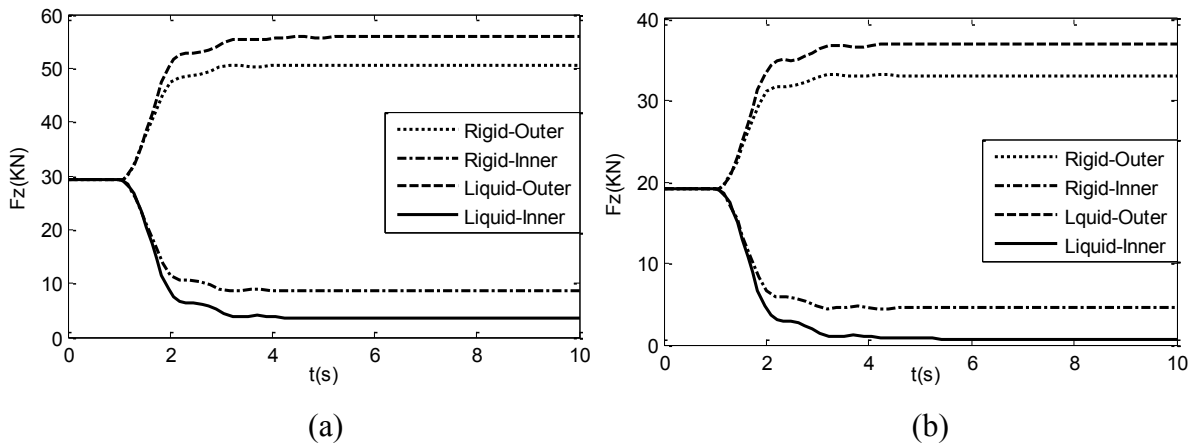


Figure 3.11: Comparison of the inner and outer wheel loads of the 50%-filled liquid and equivalent rigid cargo vehicles: (a) front axle wheels; and (b) rear-axle wheels.

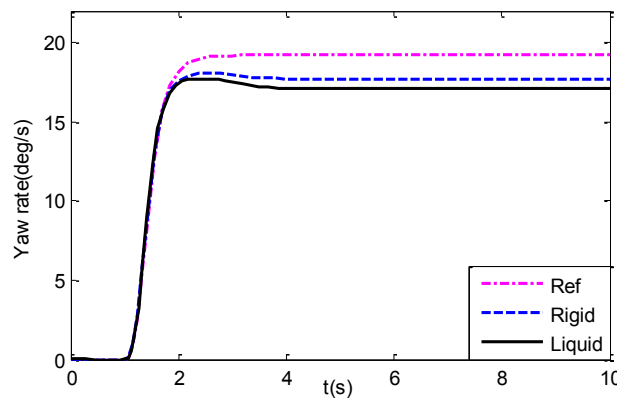


Figure 3.12: Comparison of yaw rate responses of 50%-filled liquid and equivalent rigid cargo vehicles with the reference model response.

Active steering

The yaw rate and path responses of the 50%-filled liquid truck incorporating AFS and AIFS, subject to the J-turn maneuver at a 58 km/h, are compared in Fig. 3.13 together with the target responses. The figure also presents the steering response of the vehicle in the absence of active steering control. The results suggest that vehicle can adequately track the target response with both AFS and AIFS. The two controller syntheses, however, impose different corrective steering angles and thus lead to different work-loads of the inner and outer wheels. The variations in the work-loads of the inner and outer tires are illustrated in Fig. 3.14 for both steering controls.

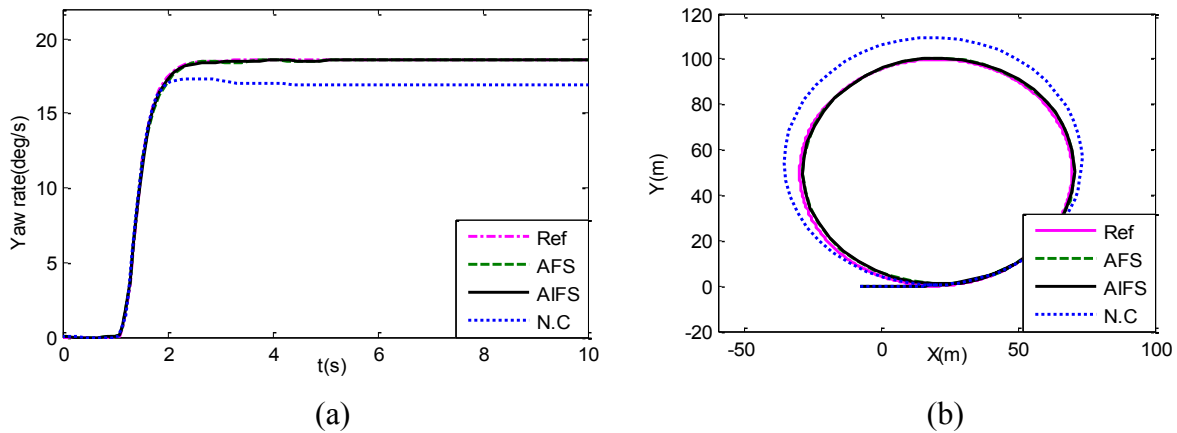


Figure 3.13: Comparisons of directional response of the 50%-filled liquid cargo truck without active steering (NC), and with AFS and AIFS control: (a) yaw rate; and (b) path trajectory.

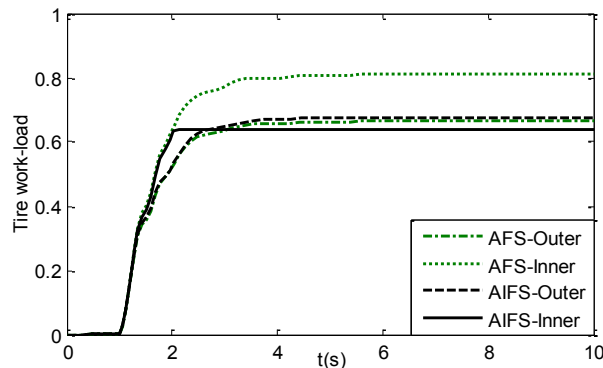


Figure 3.14: Comparisons of work-loads of the steered wheels of the 50%-filled liquid cargo truck with AFS and AIFS control.

These suggest that the inner wheel of the truck with AFS controller approaches saturation with steady-state work-load being 0.81. The work-load of the outer wheel, however, is about 0.67 suggesting underutilization of available tire-road adhesion by the outer wheel. The AIFS control, on the other hand, tracks the reference model response while maintaining comparable values of the inner and outer wheels work-loads near the limiting value of 0.65. The results show that work-load of the inner wheel with reduced normal load reduces to 0.65 at an expense of only a slight increase in work-load for the outer wheel with significantly higher normal load.

Figure 3.15 compares the steer angles of the steered wheels of the vehicle with AFS and AIFS control. The corresponding variations in the normal loads on the front and rear wheels are shown in Fig. 3.16. Both the control strategies yield identical tire loads variations, even though the steer angles are substantially different. The variations in the tire normal loads suggest substantial load shift from the inner to the outer wheels due to movement of the liquid cargo. The magnitudes of load shifts observed for the 50%-filled vehicle are quite comparable to those obtained for the fully loaded truck, shown in Fig. 3.9. It should be noted that the 50%-filled truck yields considerably lower CG height than the fully loaded truck. Considerably lower lateral load shift may thus be expected for the 50%-filled truck, while the results show comparable load shifts for the 50%-filled and the fully loaded truck. The results thus suggest that the liquid cargo load shift tends to offset the performance gain associated with lower CG height.

The steady-state handling responses of the 50%-filled tank truck with AFS and AIFS control are further analyzed to derive work-loads of the steered wheels, steering wheel angles, the roll angle and lateral acceleration responses. The results, summarized in Table 3.2, are quite comparable with those obtained for the fully loaded truck with substantially high CG (Table 3.1).

Both the 50%-filled and fully loaded vehicles also exhibit comparable rollover limit, near 61 km/h. It is further seen that the inner tire work-load of the vehicle with AFS exceeds the limiting value of 0.65 at speeds exceeding 52 km/h, while the outer wheel work-load remains relatively low. The inner wheel work-load approaches as high as 0.88 at 60 km/h suggesting very little available adhesion for generating longitudinal forces during the maneuver. In case of AIFS, the inner tire work-load is limited to 0.65 through adequate distribution of the steering correction across the steered wheels. These trends are identical to those observed for the fully loaded rigid truck, as seen in Table 3.1.

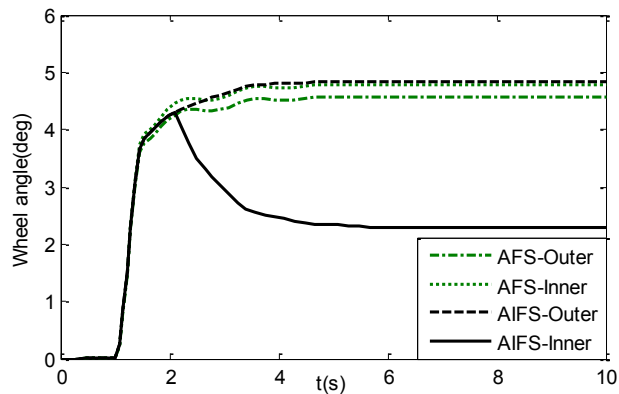


Figure 3.15: Comparisons of steered wheels angles of the vehicle with AFS and AIFS control.

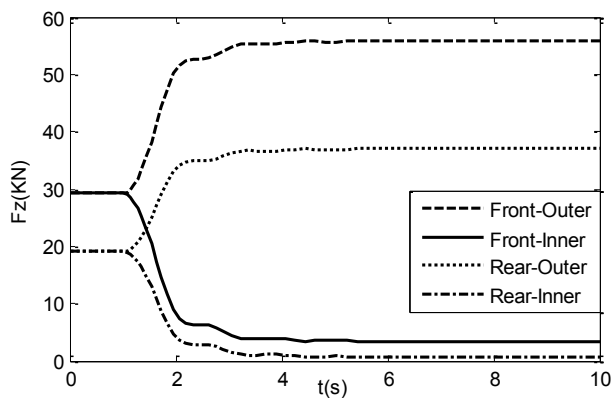


Figure 3.16: Variations in normal loads of tires of the 50%-filled vehicle with active steering control.

Table 3.2: Comparisons of tire work-loads and steady-state steering responses of the 50%-filled tank truck with AFS and AIFS control.

Control	AFS W_T		AIFS W_T		AFS/AIFS directional responses		AIFS steer angle	
	Inner	Outer	Inner	Outer	ϕ (deg)	a_y (g)	Inner (deg)	Outer (deg)
51	0.61	0.50	0.59	0.52	5.4	0.41	4.1	4.1
52	0.63	0.53	0.62	0.53	5.6	0.43	4.2	4.2
53	0.66	0.56	0.62	0.56	5.8	0.44	3.9	4.3
54	0.68	0.57	0.65	0.58	6.1	0.46	3.8	4.4
55	0.72	0.59	0.65	0.61	6.3	0.48	3.5	4.5
56	0.75	0.62	0.65	0.63	6.5	0.50	3.1	4.6
57	0.79	0.65	0.65	0.66	6.8	0.52	2.7	4.7
58	0.81	0.67	0.65	0.68	7.0	0.53	2.3	4.8
59	0.85	0.70	0.65	0.71	7.2	0.55	1.8	5.0
60	0.88	0.72	0.65	0.74	7.5	0.57	1.5	5.5
61	0.92	0.75	0.65	0.76	7.7	0.59	1.5	5.5
62	0	0	0	0	8.0	0.61	1.3	6.0

The results suggest comparable steady-state responses of both the fully loaded high CG vehicle and the 50%-filled liquid cargo vehicle (lower CG). This is evident from the lateral load shift (Figs. 3.9 and 3.16), and tire work-load (Tables 3.1 and 3.2) responses of both the vehicles. The AIFS control strategy thus yields similar potential benefits for the 50%-filled tank truck, as observed for the high CG rigid cargo vehicle. In both cases, the effectiveness of AIFS over the AFS is apparent as the former can be designed to maximize the handling performance by equalizing the work-loads of the inner and outer wheels. Furthermore, the AIFS continues to be effective until the vehicle approaches its rollover limit.

3.5 Conclusions

Unlike the active front steering (AFS) system, the Active Independent Front Steering (AIFS) strategy applies differential and independent steering corrections to inner and outer wheels

considering the normal loads and slip conditions of the individual wheels. It is shown that the AIFS strategy is more effective for commercial vehicles, which generally encounter greater lateral load shifts during steering maneuvers. The results show improved handling performance of a fully-loaded two-axle truck with high CG and that a 50%-filled liquid cargo truck. Both the vehicles revealed very similar lateral load shift and handling properties during a J-turn maneuver over the entire range of forward speeds up to the rollover limit of the vehicle. It is shown that, at high speed, the AIFS strategy helps limit the inner and outer tire work-loads so as to minimize probable saturation of the inner tire by reducing its steering correction and to maximize the available tire-road adhesion of the outer tire by increasing its steering correction. The results also revealed limitations of the AFS control under large lateral load shifts, where the inner wheel approached impending saturation with work-load as high as 0.88 at a speed of 60 km/h, while the corresponding outer wheel remained under-utilized. An AFS strategy under such situations would thus permit very limited adhesion reserve under a braking/acceleration demand during cornering. The AIFS control with predetermined work-load limit of 0.65 on the inner tire would permit reasonable reserve for meeting the longitudinal force demands under such a condition. Furthermore, the AIFS strategy offers some design flexibility through variations in the limiting value of the tire work-load, which may be varied to achieve a desired distribution of cornering and longitudinal forces during steering maneuvers.

CHAPTER 4

AN INDEPENDENTLY CONTROLLABLE ACTIVE STEERING SYSTEM FOR MAXIMIZING HANDLING PERFORMANCE LIMITS OF ROAD VEHICLES

4.1 Introduction

A vast majority of vehicle accidents are attributed to driver errors, including poor judgment and/or inadequate drivers' control action and response time, particularly under emergency-like situations. The developments in various active safety and driver assist systems (DAS) are thus increasingly being emphasized for enhancing road safety and driver comfort by reducing the control demands on the driver. Active Front Steering (AFS) systems have been proposed and widely investigated during the past decade for improved vehicle handling performance [13]. A conventional AFS introduces additional steering corrections in order to track a target handling response over a wide range of forward speeds.

The effectiveness of the AFS systems has been evaluated through both simulations and experiments using different control methods [10,55]. The reported studies have invariably shown that the AFS strategy offers beneficial handling performance of the vehicle by providing substantial yaw disturbance rejection originating from high speed turning or lane-change maneuvers or side wind force or braking on roads with asymmetric friction between the left and right tires (split- μ condition) [1,135]. Different control algorithms have also been synthesized and evaluated to realize robust AFS control under varying vehicle characteristics and uncertainties. For instance Zhang et al. [55], investigated robustness of an AFS control using

quantitative feedback based on the vehicle yaw rate considering variations in a number of uncertain parameters such as vehicle mass, forward speed and road condition. The study concluded that the proposed AFS control could yield substantial improvement in the handling quality and stability limit of the vehicle. In a similar manner, Mammar and Koeing [136] investigated stability limits of the vehicle with an active steering system under a range of operating parameters including the road-tire friction, vehicle speed and driver steering input. An integrated feed-forward and H_∞ feedback AFS control was subsequently proposed to achieve enhanced stability limits under severe road conditions, higher forward speeds, wind force disturbances and evasive steering maneuvers.

A few recent studies have also explored developments in AFS control for commercial vehicles. For instance, Kharrazi et al. [61] investigated the effectiveness of the active steering control of the towed unit axles of a long combination vehicle in view of its lateral dynamic performance. The results obtained through simulations and tests under a series of single and double-lane change maneuvers showed considerable damping of yaw velocity, rearward amplification (RWA), lateral acceleration and path trajectory responses of the towed unit when compared to those without the steering controller. Similarly, McCann et al. [137] investigated the application of AFS control for prevention of jackknife of a tractor-semitrailer combination under severe driving maneuvers, while considering interference to the driver's perception. Junjovich et al. [62] studied the handling responses of an articulated heavy vehicle incorporating active steering at all the trailer axles. The test track results revealed improved performance in terms of reduced entrance tail swing, trailer off-tracking, peak lateral force, exit settling distance and tire scrubbing. The effect of AFS control on the rollover hazard of vehicles in emergency-type of

maneuvers has also been investigated. It was shown that the AFS could yield relatively higher rollover threshold of the vehicle at the expense of reduced handling performance and lateral stability limit during an evasive maneuver [60,138].

A number of studies have also proposed integration of Active Front Steering (AFS) systems or Active Rear Steering (ARS) systems with differential braking control, referred to as the Direct Yaw-moment Control (DYC), to achieve desired stability and handling under high lateral acceleration maneuvers, where the steered wheels may approach saturation. Mokhiamar and Abe [139] investigated three different combinations of control strategies involving DYC and ARS, DYC and AFS, and DYC and ARS together with AFS to achieve enhanced vehicle stability under rapid steer inputs. The study concluded that combination of AFS, DYC and ARS control would yield better handling and stability performance of the vehicle. In a recent study, Yim et al. [38] presented an optimum yaw moment distribution considering combined AFS and DYC control together with the actuator saturation nonlinearity. While the integrated AFS and DYC control could yield definite performance gains over a broad range of operating conditions, the activation of DYC through application of the braking force tends to alter the vehicle speed, which would be undesirable especially during an obstacle avoidance maneuver. Furthermore, the vehicle equipped with DYC could lead to a level of disturbance and annoyance to the driver due to more frequent braking [5].

The reported studies have invariably shown beneficial vehicle handling performance with AFS under low to moderate lateral acceleration maneuvers. The integrated AFS and DYC control, however, has been frequently suggested for moderate to severe directional maneuvers [5,38], although the causal factors associated with performance limits of the AFS have not been

clearly illustrated. This approach, however, increases the control complexity apart from the undesirable effect of DYC in terms of reduction in the forward speed. The AFS control strategy is typically designed to introduce corrective measure to the steered wheels without altering the steering geometry. Conventional AFS system, therefore, does not consider possible saturation of the inside tire that may occur under moderate to severe directional maneuvers in addition to probable under-utilization of the available adhesion by the outer tire. The performance of an AFS system under moderate to severe maneuvers may be augmented by introducing independent variations in the inner and outer wheels steering angle. Such a control strategy, referred to as Active Independent Front Steering (AIFS) system, would further permit effective utilization of the available adhesion of both the wheels to meet the cornering demand under high-acceleration maneuvers [126]. The superior performance potentials of AIFS have been demonstrated for a rigid and liquid cargo truck subject to steady-turning maneuvers leading to high magnitudes of lateral load transfer [140].

The vast majority of the studies on active steering system propose the use of Steer-by-Wire (SBW), which has been the focus of a number of studies [106,111]. The concept of SBW, however, raises concerns related to reliability and cost due to absence of a mechanical coupling between the steering and road wheel. The implementations of steer-by-wire technology in production cars have thus been attempted together with a mechanical backup system such as the Variable Gear Ratio (VGR) mechanisms applied to the AFS systems. These include the VGR actuators based on a planetary gear, variable ratio rack and harmonic drive system [14,114,141]. A mechanical AFS system that enables automatic steering interventions without loss of coupling between the steering wheel and the road wheel has also been reported [13]. A recent study has

also reported a practically realizable fail-safe steering mechanism where the angle of each wheel can be controlled independently [117,126].

In this study, the effectiveness and performance characteristics of an AIFS system are evaluated when applied to a commercial vehicle involving high CG and high lateral load transfers over a wide range of steering maneuvers involving consistent as well as split- μ road conditions. The AIFS strategy is synthesized based on a simple PI controller considering a nonlinear yaw-plane model of a two-axle truck with limited roll DOF to realize a target handling response. The proposed control strategy permits independent control of each wheel and maximum utilization of the available tire-road adhesion.

4.2 Vehicle Model

A nonlinear yaw-plane model of a two-axle truck with roll-DOF (Fig. 4.1) is used for synthesis and evaluations of the AIFS control. The model is derived considering yaw and lateral motions of the vehicle as well as the roll motion of the sprung mass and independent steering of the right- and the left-wheels. The lateral force F_{Yij} and self-aligning moment M_{ij} due to each tire are evaluated using the Magic Formula [102] as functions of the instantaneous normal load F_{Zij} and slip angle α_{ij} . The subscript i ($i = F, R$) refers to front and rear tires, respectively, and j ($j = r, l$) denotes the right- and left-wheels, respectively. As shown in the figure, ‘RC’ refers to roll center of the sprung mass, while ϕ denotes the sprung mass roll angle. The equations of motions for the single unit truck with dual tires at the rear axle can be expressed as [140]:

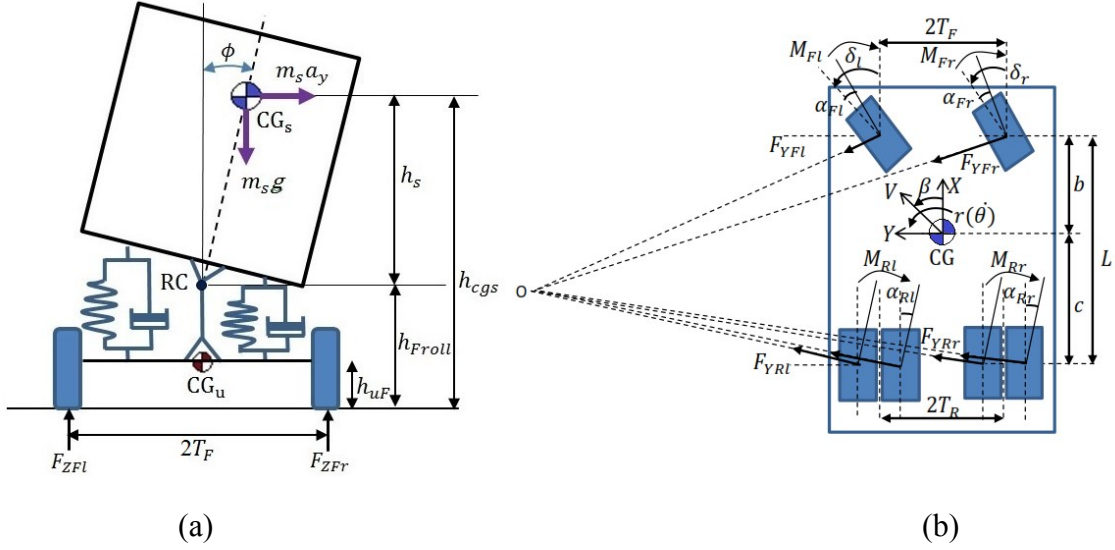


Figure 4.1: Three-DOF directional dynamic model of a two axle truck: (a) roll-plane and; (b) yaw-plane.

$$mV(\dot{\beta} + r) - m_s h_s \ddot{\phi} = F_{YFr} \cos \delta_r + F_{YFl} \cos \delta_l + 2(F_{YRr} + F_{YRl}) \quad (4.1)$$

$$(I_{xs} + m_s h_s^2) \ddot{\phi} - I_{xzs} \dot{r} - m_s h_s V(\dot{\beta} + r) = (m_s g h_s - K_{\phi F} - K_{\phi R}) \phi - (C_{\phi F} + C_{\phi R}) \dot{\phi} \quad (4.2)$$

$$(I_{zs} + I_{zu}) \dot{r} - I_{xzs} \ddot{\phi} = - \sum_{i=F}^R \sum_{j=r}^l M_{ij} + F_{YFr}(b \cos \delta_r - T_F \sin \delta_r) + \dots \quad (4.3)$$

$$F_{YFl}(b \cos \delta_l + T_F \sin \delta_l) - 2c(F_{YRr} + F_{YRl})$$

In the above equations V , r and β are the forward speed, yaw rate and side-slip angle of the vehicle, respectively. The longitudinal distances of the front and rear axles from the center of sprung mass (CG_s) are denoted by b and c , respectively. I_{xs} , I_{xzs} and I_{zs} are moments of inertia of sprung mass about x -, x - z and z -axis, respectively, about CG_s , and I_{zu} is the total yaw mass moment of inertia of the unsprung masses.

The instantaneous normal load on each tire, F_{zij} , is evaluated considering load transfers along the longitudinal and lateral axes as functions of the longitudinal (a_x) and lateral (a_y) accelerations, and suspension roll stiffness ($K_{\phi i}$) and damping ($C_{\phi i}$), such that:

$$F_{ZF_r} = \frac{W_F}{2} - \frac{a_x}{2L} (m_s h_{cgs} + m_{uF} h_{uF} + m_{uR} h_{uR}) + \frac{a_y}{2T_F} (m_{sF} h_{Froll} + m_{uF} h_{uF}) + \dots + \frac{1}{2T_F} (K_{\phi F} \phi + C_{\phi F} \dot{\phi}) \quad (4.4)$$

$$F_{ZF_l} = \frac{W_F}{2} - \frac{a_x}{2L} (m_s h_{cgs} + m_{uF} h_{uF} + m_{uR} h_{uR}) - \frac{a_y}{2T_F} (m_{sF} h_{Froll} + m_{uF} h_{uF}) - \dots - \frac{1}{2T_F} (K_{\phi F} \phi + C_{\phi F} \dot{\phi}) \quad (4.5)$$

$$F_{ZR_r} = \frac{W_R}{4} + \frac{a_x}{4L} (m_s h_{cgs} + m_{uF} h_{uF} + m_{uR} h_{uR}) + \frac{a_y}{4T_R} (m_{sR} h_{Rroll} + m_{uR} h_{uR}) + \dots + \frac{1}{4T_R} (K_{\phi R} \phi + C_{\phi R} \dot{\phi}) \quad (4.6)$$

$$F_{ZR_l} = \frac{W_R}{4} + \frac{a_x}{4L} (m_s h_{cgs} + m_{uF} h_{uF} + m_{uR} h_{uR}) - \frac{a_y}{4T_R} (m_{sR} h_{Rroll} + m_{uR} h_{uR}) - \dots - \frac{1}{4T_R} (K_{\phi R} \phi + C_{\phi R} \dot{\phi}) \quad (4.7)$$

where T_i ($i = F, R$) is the half tire track width of axle i , L is vehicle wheelbase, m_{s_i} and m_{u_i} ($i = F, R$) are the front and rear sprung and unsprung masses, respectively, and m_s is the vehicle sprung mass.

4.3 Control Strategy

The AIFS control strategy is formulated using a proportional-Integral (PI) feedback controller to track the steering response of an idealized reference model while the corrective steer angle is based upon maximum utilization of the available tire-road adhesion limits, especially during a high lateral acceleration maneuver. The dynamics of the steering actuator is also incorporated in the model considering its limited bandwidth. Figure 4.2 illustrates the overall structure of the AIFS control, while each component of the control synthesis is described below.

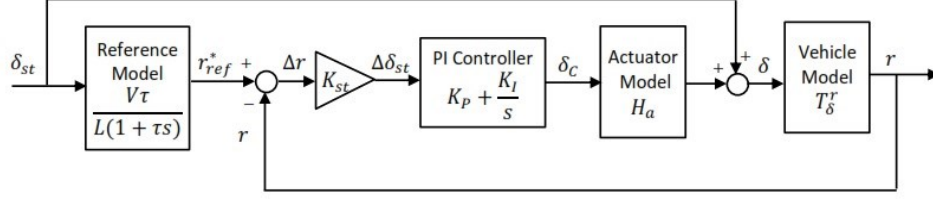


Figure 4.2: Schematic of the control structure.

4.3.1 Controller synthesis

The nonlinear equations of motion, equations (4.1) to (4.3), are linearized for the purpose of developing the control algorithm, using a three-DOF linear model of the vehicle comprising lateral, yaw and roll motions. The slip angle generated at the front and rear wheels are formulated using the kinematic relations, such that:

$$\alpha_F = \left(\delta - \beta - \frac{b}{V} r \right), \quad \alpha_R = \left(-\beta + \frac{c}{V} r \right) \quad (4.8)$$

The linearized equations of motion for the vehicle model are subsequently obtained assuming small angles, as:

$$mV(\dot{\beta} + r) - m_s h_s \ddot{\phi} = 2K_{F_o} \alpha_F + 4K_{R_o} \alpha_R = 2K_{F_o} \left(\delta - \beta - \frac{b}{V} r \right) + 4K_{R_o} \left(-\beta + \frac{c}{V} r \right) \quad (4.9)$$

$$(I_{x_s} + m_s h_s^2) \ddot{\phi} - I_{x_z s} \dot{r} - m_s h_s V (\dot{\beta} + r) = (m_s g h_s - K_{\phi_F} - K_{\phi_R}) \phi - (C_{\phi_F} + C_{\phi_R}) \dot{\phi} \quad (4.10)$$

$$(I_{z_s} + I_{z_u}) \dot{r} - I_{z_x s} \ddot{\phi} = - \sum_{i=F}^R \sum_{j=R}^l M_{ij} + 2K_{F_o} b \left(\delta - \beta - \frac{b}{V} r \right) - 4K_{R_o} c \left(-\beta + \frac{c}{V} r \right) \quad (4.11)$$

where K_{F_o} and K_{R_o} are the nominal cornering stiffness of tires. Using the Laplace transforms, equations (4.9) to (4.11) can be re-written in matrix form, as:

$$\begin{bmatrix} X_1 & X_2 & X_3 \\ X_4 & X_5 & X_6 \\ X_7 & X_8 & X_9 \end{bmatrix} \begin{bmatrix} \beta \\ r \\ \phi \end{bmatrix} = \begin{bmatrix} U_1 \\ U_2 \\ U_3 \end{bmatrix} \delta \quad (4.12)$$

where:

$$X_1 = mVs + 2(K_{Fo} + 2K_{Ro}), \quad X_2 = mV + \frac{2}{V}(bK_{Fo} - 2cK_{Ro}), \quad X_3 = -m_s h_s s^2 \quad (4.13)$$

$$X_4 = 2(bK_{Fo} - 2cK_{Ro}), \quad X_5 = (I_{zs} + I_{zu}s) + \frac{2}{V}(b^2K_{Fo} + 2c^2K_{Ro}), \quad X_6 = -I_{xz}s^2 \quad (4.14)$$

$$X_7 = -m_s h_s Vs, \quad X_8 = -I_{xz}s - m_s h_s V \quad (4.15)$$

$$X_9 = (I_{xs} + m_s h_s^2)s^2 + (C_{\phi F} + C_{\phi R})s + K_{\phi F} + K_{\phi R} - m_s g h_s$$

$$U_1 = 2K_{Fo}, \quad U_2 = 2bK_{Fo}, \quad U_3 = 0 \quad (4.16)$$

The transfer function of the vehicle model, T_{δ}^r , relating yaw rate and δ (Fig. 4.2) is subsequently obtained from Eq. (4.12), as:

$$T_{\delta}^r = \frac{(X_6 X_7 - X_4 X_9)U_1 + (X_1 X_9 - X_3 X_7)U_2 + (X_3 X_4 - X_1 X_6)U_3}{(X_1 X_5 X_9 - X_1 X_6 X_8 - X_2 X_4 X_9 + X_2 X_6 X_7 + X_3 X_4 X_8 - X_3 X_5 X_7)} \quad (4.17)$$

A PI controller is synthesized to generate a corrective steering so as to achieve the reference yaw rate corresponding to the neutral steer condition ($r_{ref} = \frac{V\delta_{st}}{L}$), which represents the dynamic behavior of the vehicle in the linear region and is considered to be predictable by most drivers [142]. A first-order lag function is further introduced to represent the steering response delay of the vehicle and to suppress the response overshoot corresponds to a given steer angle, δ_{st} , such that:

$$r_{ref}^* = \frac{V\tau\delta_{st}}{L(1 + \tau s)} \quad (4.18)$$

where τ is the time constant that primarily depends on the vehicle understeer characteristics

and r_{ref}^* is the derived reference yaw rate.

As shown in Fig. 4.2, the steering correction command, δ_C , is obtained using the simple PI feedback controller, such that:

$$\delta_C = K_P \Delta \delta_{st} + K_I \int \Delta \delta_{st} \quad (4.19)$$

where K_P and K_I are proportional and integral control gains, respectively, the steering correction $\Delta \delta_{st} = K_{st} \Delta r$ is related to the yaw rate error, $\Delta r = r_{ref}^* - r$, and K_{st} is the gain defined as the ratio of the wheelbase and velocity of the vehicle, given by:

$$K_{st} = \frac{L}{V} \quad (4.20)$$

The corrective steer angle δ_C is distributed between the inner and outer-wheels considering the available adhesion limit of each tire.

4.3.2 AIFS actuator model

The corrective steering command from the controller is constrained by the bandwidth of the steering actuator, which is approximated by a second-order system function H_a (Fig. 4.2) [64]:

$$H_a = \frac{\omega_n^2}{s^2 + 2\zeta\omega_n s + \omega_n^2} \quad (4.21)$$

where ω_n is the bandwidth and ζ is the damping ratio of the steering actuator. It has been suggested that an actuator bandwidth of about 6 Hz is required to obtain acceptable performance for a single unit truck, while the damping ratio is assumed as 0.7 [134,143].

Simulations were performed using the time-delayed reference yaw rate, r_{ref}^* , and the actuator dynamics, while the controller gains were selected considering the bandwidth of the

steering response of trucks to be 1.5 Hz [134]. In order to ensure a consistent handling behavior under different steering frequencies, the PI controller gains are tuned for tracking the target yaw rate with cross-over frequency of 1.5 Hz. The controller gains are determined using the closed loop transfer function, relating the yaw rate response to the steer input. The PI controller gains are subsequently determined by comparing the characteristics equation of the resultant closed-loop function with the optimum equation based on the minimum ITAE (Integral of Time-weighted Absolute Error) performance index as reported in [144]. The gains $K_P = 2.48$ and $K_I = 13.55$ were found to satisfy this requirement. The distribution of resulting steering correction is determined considering the saturation of the inside and outside tires. The controller synthesis is thus further refined to ensure that the steering correction is within the bounds defined by the saturation limits of the steered wheels, as described in the following section.

4.3.3 *Tire force saturation*

The tire-road adhesion limits are determined using a performance parameter in terms of the tire work-load W_T , which is also a measure of the tire's ability to generate additional force to meet possible braking or traction demands, if needed, during a severe steering maneuver [140]. The tire work-load is defined as the ratio of the total force developed by a tire to the maximum tire force based on the road adhesion limit, where the total force is estimated assuming friction circle concept:

$$W_T = \frac{\sqrt{F_x^2 + F_y^2}}{\mu F_z} \quad (4.22)$$

where F_x and F_y are the braking/traction and cornering forces developed by a tire,

respectively, and μ is the tire-road friction coefficient. Since the tire work-load represents utilization of the available adhesion by each tire, it can be considered as an indicator of the tire saturation. An alternate measure for tire's ability to generate maximum force could be the saturation slip angle that may also serve as a limiting value for the steering correction that may be applied to a wheel.

An estimate of the saturation zone of each tire may be obtained from the normalized cornering stiffness of the tire ($q = \frac{K_{ins}}{K_{int}}$), defined as the ratio of the cornering stiffness corresponding to the instantaneous slip angle to the initial cornering stiffness [140]. Figure 4.3 illustrates the normalized cornering stiffness of a truck tire as a function of the tire slip angle for a wide range of normal loads. In a critical turning maneuver, the normal load on the inner wheel of the steered axle will be significantly lower compared to the outer wheel. As the figure indicates, the inner tire would approach the saturation zone or its adhesion limit much earlier than the outer tire. Since the AIFS allows independent steering correction for each wheel, the control strategy could be synthesized to limit the steering correction so that none of the wheels approach saturation. The strategy would thus permit application of a relatively higher steering correction to the outer wheel. The controller must also reduce the steering correction to the inner wheel to ensure its adequate adhesion with the road. In this study, the limiting value of the inner tire work-load is chosen as 0.65, which corresponds to the onset of the tire force saturation, defined by the normalized stiffness, $q = 0.3$, as indicated on Fig. 4.3 [140]. This value chosen arbitrarily for limiting tire work-load would ensure that sufficient inner tire force adhesion is available for developing a braking/traction force in the presence of low normal loads, if needed. The resulting slip angle α^* at the onset of the saturation zone would also depend on the normal

load, as seen in Fig. 4.3. For a given normal load, this slip angle, referred to as ‘saturation slip angle’ of the inner tire, is used to obtain the limiting value of the inner wheel steer angle, δ_l^* , such that:

$$\delta_l^* = \alpha_{Fl}^* + \tan^{-1} \left[\frac{br + V_y}{V_x - T_F r} \right] \quad (4.23)$$

where V_x and V_y are the longitudinal and lateral velocities of the vehicle at its CG which along with vehicle yaw rate describes the side slip angle of the vehicle. The saturation limits of inside tires are subsequently implemented in the AIFS control with the nonlinear vehicle model, as seen in Fig. 4.4.

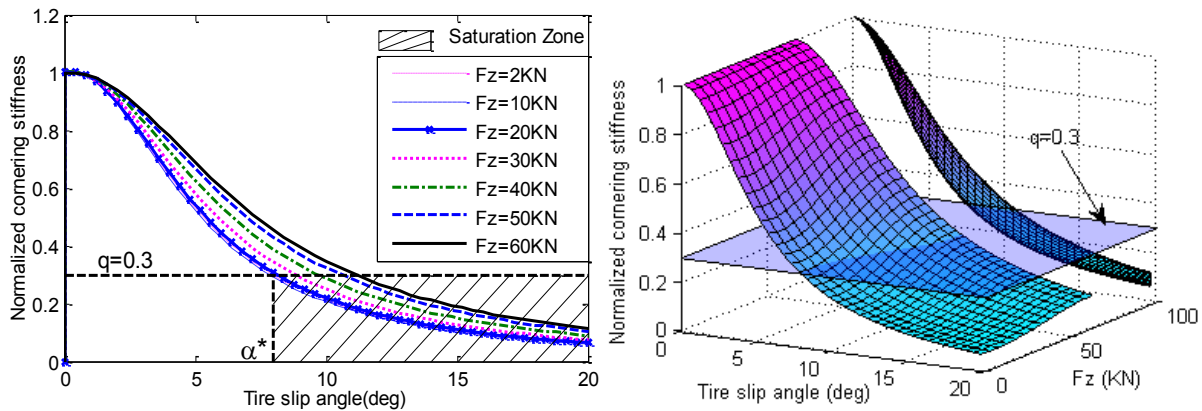


Figure 4.3: Normalized cornering stiffness and identification of the saturation zone of a truck tire [140].

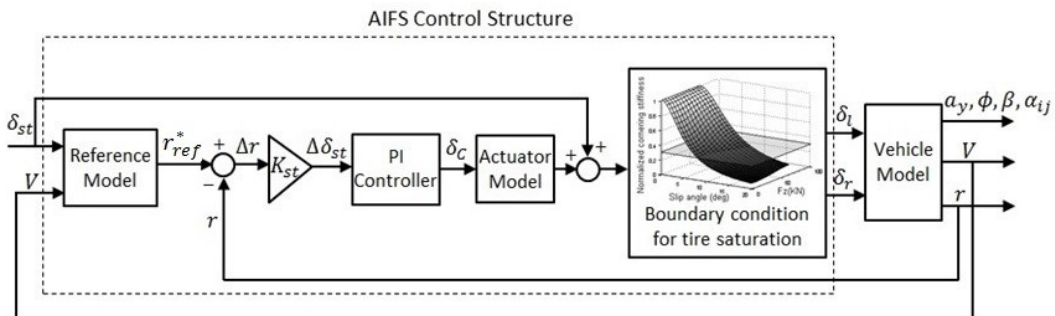


Figure 4.4: The structure of the AIFS control synthesis integrating tire-road adhesion saturation limits.

4.4 Driver Steering Input

In order to evaluate the effectiveness of AIFS concept, various pre-defined steering inputs are considered in an open-loop manner without any correction by the driver. These include: (i) a ramp-step steer input (Fig. 4.5) with 1 s delay, smoothed rise and saturation at 1.5 s, to simulate a steady-cornering maneuver; (ii) a lane-change maneuver; and (iii) an obstacle avoidance maneuver. The steer angles corresponding to the path change maneuvers are generated considering the standardized path coordinates for the given speed [145]. For this purpose, a linear vehicle model coupled with an ideal driver model, described by a PID function [146], is used to derive the required steering inputs, which are applied to the nonlinear vehicle model with AIFS in an open loop manner. The driver function could track the path reasonably well by minimizing the lateral position error, which is evaluated assuming a single-point driver preview with preview distance L^* , preview interval t_p and the vehicle forward speed, as shown in Fig. 4.6. The lateral path deviation, ε is obtained from the instantaneous lateral position y and yaw angle θ of the vehicle, and the lateral coordinate of the desired trajectory at the preview point y^* , such that [93]:

$$\varepsilon = y + L^*\theta - y^* \quad (4.24)$$

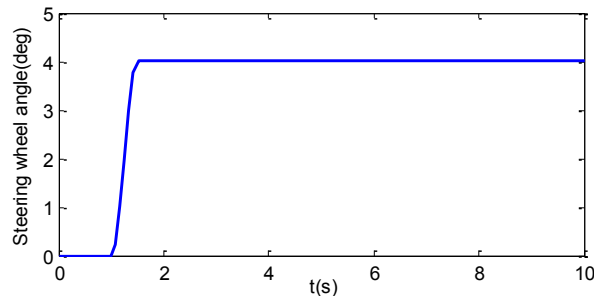


Figure 4.5: Ramp-step steer input.

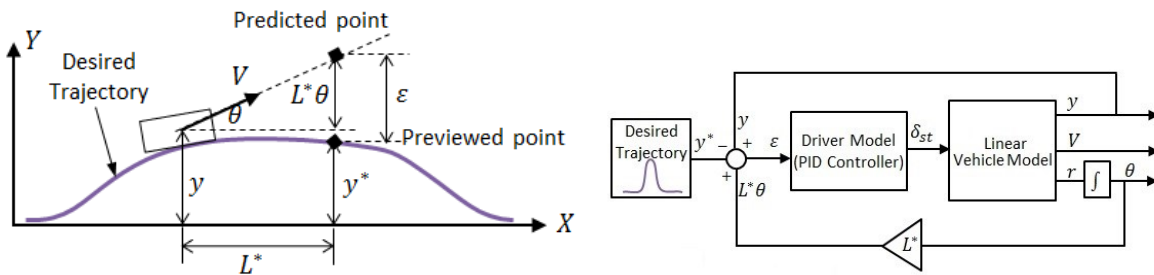


Figure 4.6: Driver path preview model coupled with the linear vehicle model.

Figure 4.7(a) illustrates the desired vehicle path for the single lane-change maneuver and the corresponding ideal steering input that is dependent on the vehicle forward speed. The time-history of the steer angle is shown in Fig. 4.7(b) for a forward speed of 83 km/h on a dry uniform friction road ($\mu=0.78$).

Figure 4.8 shows the path coordinates for the obstacle avoidance maneuver and the time-history of the steer angle at a speed of 83 km/h on the same road ($\mu=0.78$), which is obtained from the linear vehicle model coupled with the ideal driver model. The resulting time histories of the steering inputs, shown in Figs. 4.7(b) and 4.8(b) are applied to the non-linear vehicle model with AIFS for assessing the effectiveness of the AIFS under different steering maneuvers.

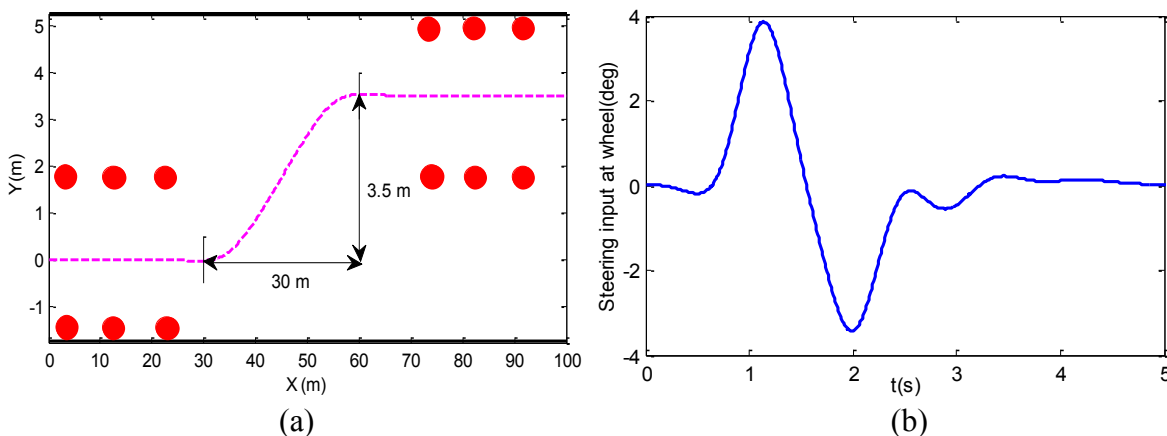


Figure 4.7: (a) Desired path trajectory; and (b) steer angle corresponding to a single-lane change maneuver derived from the ideal driver model (83 km/h).

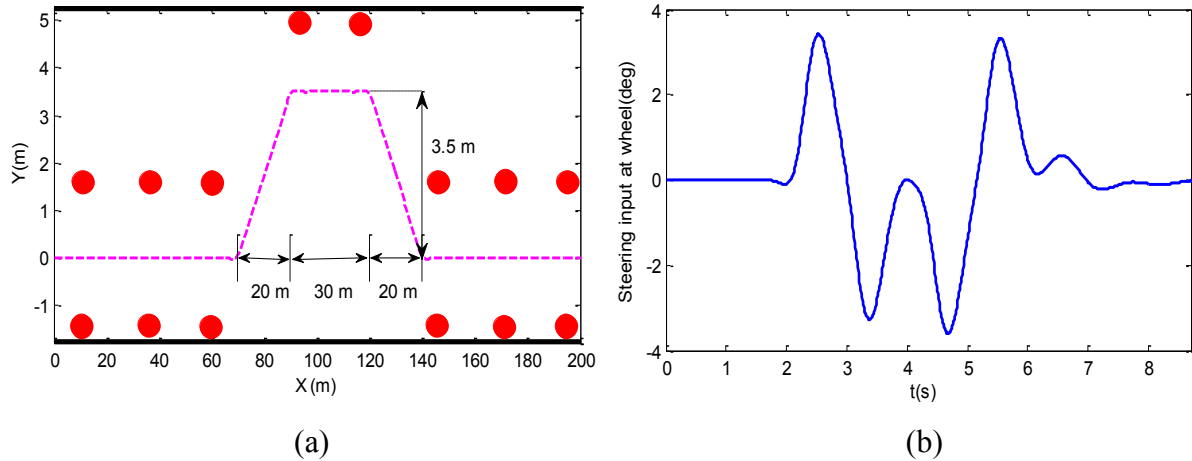


Figure 4.8: (a) Desired trajectory; and (b) steer angle corresponding to an obstacle avoidance maneuver derived from the linear vehicle model coupled with the ideal driver model.

4.5 Results and Discussion

The steering responses of the truck model are evaluated to assess the effectiveness of the AIFS relative to a conventional AFS system under the three steering maneuvers described above. The responses are also obtained in the absence of an active steering, which are denoted as ‘NC’. The responses obtained with AIFS and AFS are also compared with the reference model (target) response to assess their relative effectiveness. The simulation parameters are listed in the Table C.2 (Appendix C).

4.5.1 Ramp-step steering maneuver

The steady-turning response characteristics of the vehicle model with AFS, AIFS and without the active steering, are evaluated using the ramp-step input (Fig. 4.5) on a uniform dry road ($\mu=0.78$) and on a split- μ road condition ($\mu_r=0.78$, $\mu_l=0.4$). In case of split- μ , the lower friction is assigned to the inner tire-road interface. Figure 4.9 compares the yaw rate and path responses of the model with conventional AFS, AIFS and without active steering (NC) at a

relatively high forward speed of 57 km/h for both uniform and split- μ road surfaces. The figures also show the target responses. The results show that both the AFS and AIFS yield identical responses and can effectively tracks the target response, irrespective of the road surface friction. The results further show that there are substantial deviations in these responses when there is no control, which is attributed to understeer nature of the vehicle.

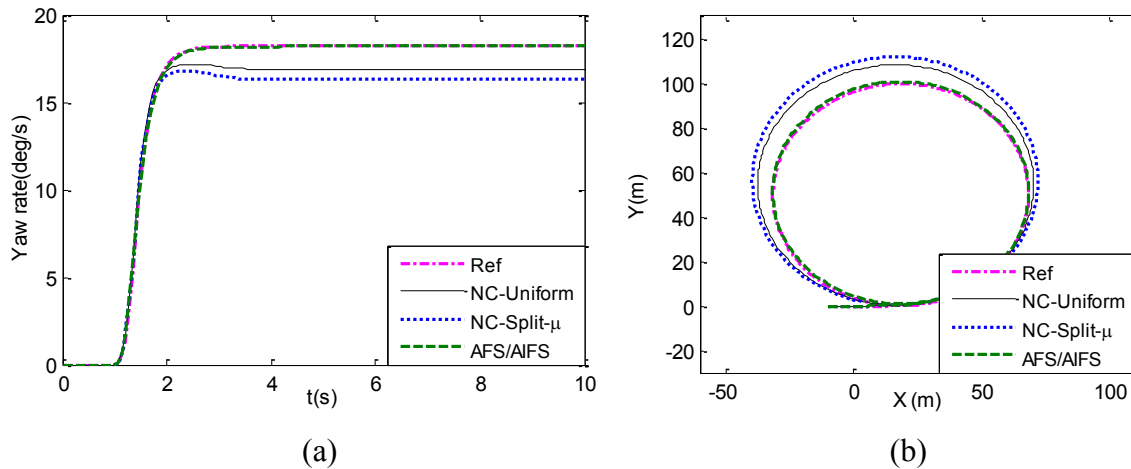


Figure 4.9: Comparisons of yaw rate and path trajectory of the truck model with conventional AFS and AIFS control and without control (NC) with those of the reference model (Ref): (a) yaw rate; and (b) path trajectory under uniform and split- μ road conditions at 57 km/h.

The steer angles generated by AFS and AIFS together with the tires' workload performance are presented in Figs. 4.10 and 4.11, respectively, for both the uniform and split- μ road surfaces. It is evident that the AFS control imposes higher steer angles of both the wheels in order to realize the target (Fig. 4.10(a)), which tends to be even higher for the split- μ surface (Fig. 4.10(b)). The AFS applies the steering corrections without the considerations of the tire's ability to generate the desired cornering force and thus it could lead to saturated inner tire as it is seen from the work load in Fig. 4.11. The AIFS system, on the other hand, limits the tire work load to the chosen upper limit of 0.65. Furthermore, the AIFS yields substantially lower steering of the inner wheel with its reduced normal load, which is compensated by an increase in the steer angle

at the outside wheel. For the given maneuver on the split- μ surface, AIFS reduced the inside steer angle to zero in order to maintain the workload limit of 0.65, while the target was realized by a moderate increase in the angle of the outside wheel. The results clearly demonstrate that the independent steering control strategy equalizes the work-load of both the steered wheels for the range of the road surface conditions considered, and ensures an adhesion reserve for generating additional traction/braking force, if required. The conventional AFS control, however, would lead to a saturated inner tire under the same maneuvers, while the adhesion at the outer tire will remain relatively under-used.

Figure 4.12 compares the side-slip angles developed at each front tire of the vehicle model employing the two control strategies. These results further show that the AFS control yields comparable slip angles of both the tires on both road surfaces, while the slip angle generated at the inner tire of the AIFS controller is dictated by the tire-road adhesion limit.

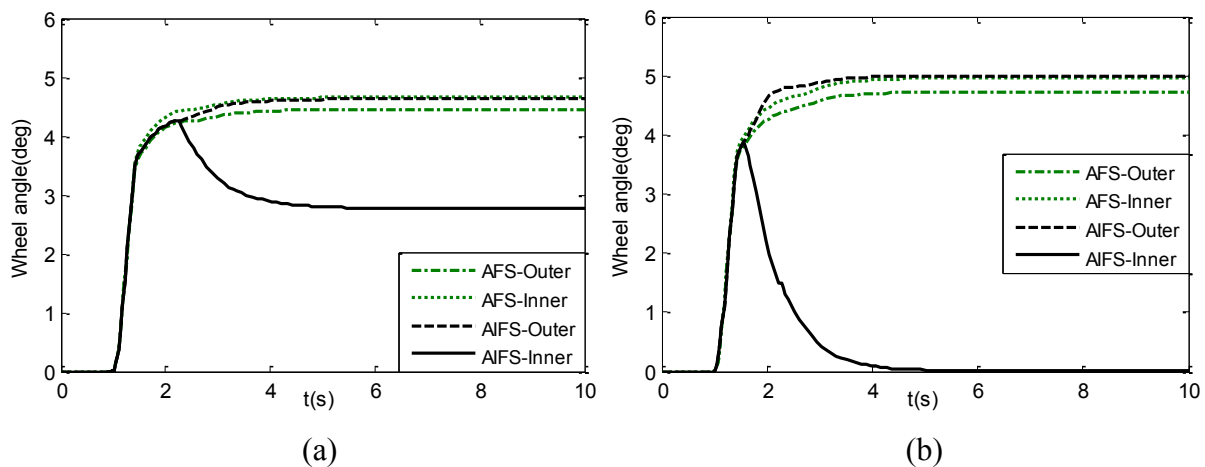


Figure 4.10: Front inner and outer wheel angle of the model on a (a) uniform; and (b) split- μ road condition with conventional AFS and AIFS control (57 km/h).

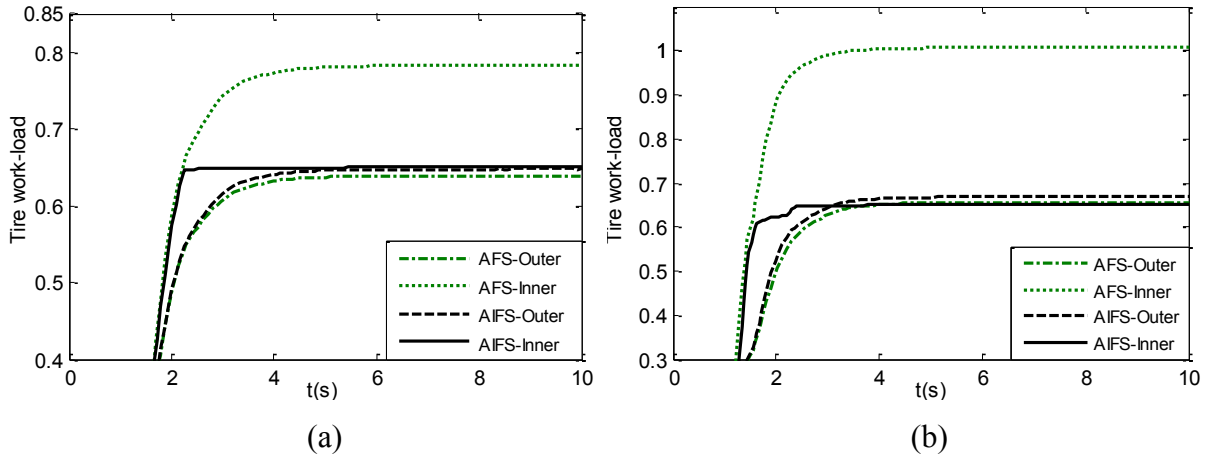


Figure 4.11: Front inner and outer wheels work-load of the model on a (a) uniform; and (b) split- μ road condition with conventional AFS and AIFS control (57 km/h).

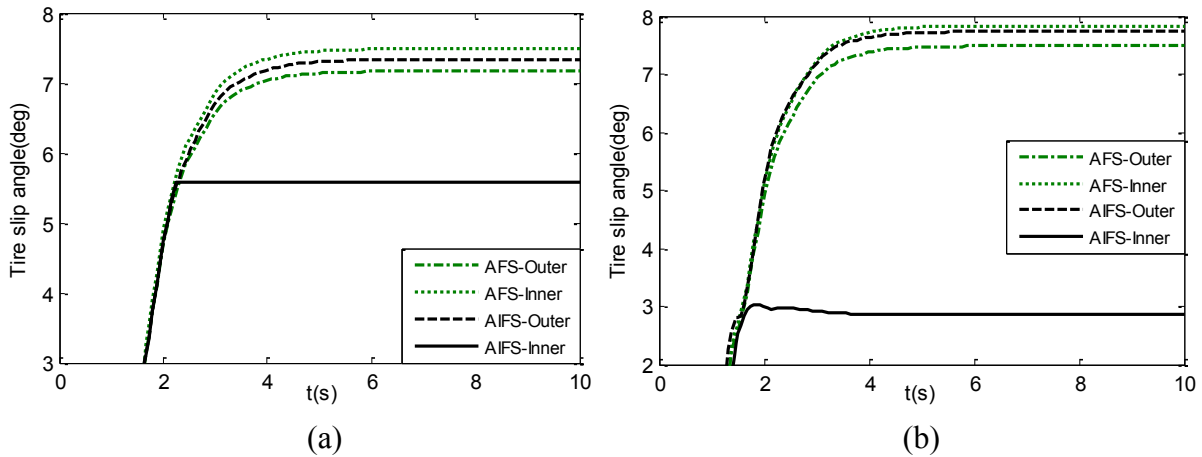


Figure 4.12: Front inner and outer wheels slip angle of the model on a (a) uniform; and (b) split- μ road condition with conventional AFS and AIFS control (57 km/h).

The relative responses of the vehicle model with AFS and AIFS are further evaluated for different speeds. Table 4.1 summarizes the responses in terms of yaw rate, turning radius, lateral acceleration, roll angle and the body slip angle for speeds ranging from 40 to speed corresponding to vehicle rollover (61 km/h). The results are presented for both the uniform and split- μ road surfaces. Both the control strategies showed identical steady-state directional responses on both road surfaces, although AFS and AIFS controls approached to substantially

different steer angles and tire work-loads, as illustrated in Table 4.2.

Table 4.1: Steady-state directional responses of the truck with conventional AFS and AIFS control on a uniform and split- μ surfaces.

Conventional AFS and AIFS directional responses ($\delta_{st}=4$ deg)						
Speed (km/h) [m/s]	r (deg/s)	R (m)	a_y (g)	ϕ (deg)	β (deg)	
					Uniform	Split- μ
40 [11.1]	12.77	49.83	0.25	3.58	-0.88	-0.97
45 [12.5]	14.37	49.83	0.32	4.53	-1.71	-1.85
48 [13.3]	15.32	49.83	0.36	5.16	-2.32	-2.50
51 [14.2]	16.28	49.83	0.41	5.82	-3.04	-3.23
52 [14.4]	16.60	49.83	0.43	6.06	-3.32	-3.50
53 [14.7]	16.92	49.83	0.44	6.29	-3.61	-3.78
54 [15.0]	17.24	49.83	0.46	6.53	-3.93	-4.08
57 [15.8]	18.20	49.83	0.51	7.28	-5.04	-5.08
60 [16.7]	19.15	49.83	0.57	8.06	-5.85	-5.85
61 [16.9]	Vehicle rollover					

Table 4.2: Variations in steady-state angles and workloads of the inside and outside wheels with increasing forward speed of the vehicle model with AFS and AIFS subject to a steady-turning maneuver on a uniform and a split- μ road surface.

Control	Uniform Road ($\delta_{st}=4$ deg)								Split- μ Road ($\delta_{st}=4$ deg)							
	Conventional AFS, W_T		AIFS, W_T		Conventional AFS, Steer angle		AIFS Steer angle		Conventional AFS, W_T		AIFS, W_T		Conventional AFS, Steer angle		AIFS Steer angle	
	Inner	Outer	Inner	Outer	Inner (deg)	Outer (deg)	Inner (deg)	Outer (deg)	Inner	Outer	Inner	Outer	Inner (deg)	Outer (deg)	Inner (deg)	Outer (deg)
Speed Km/h [m/s]																
40 [11.1]	0.35	0.30	0.35	0.30	4.12	3.96	4.12	3.96	0.63	0.31	0.63	0.31	4.15	3.98	4.15	3.98
45 [12.5]	0.45	0.39	0.45	0.39	4.17	4.00	4.17	4.00	0.76	0.40	0.62	0.43	4.22	4.05	3.20	4.30
48 [13.3]	0.52	0.44	0.52	0.44	4.21	4.05	4.21	4.05	0.84	0.46	0.62	0.49	4.30	4.12	2.52	4.46
51 [14.2]	0.60	0.50	0.60	0.50	4.29	4.12	4.29	4.12	0.91	0.52	0.62	0.55	4.34	4.16	1.77	4.62
52 [14.4]	0.63	0.52	0.63	0.52	4.33	4.15	4.33	4.15	0.93	0.55	0.63	0.57	4.38	4.20	1.50	4.66
53 [14.7]	0.66	0.54	0.65	0.55	4.37	4.19	4.21	4.22	0.97	0.57	0.65	0.59	4.43	4.24	1.34	4.71
54 [15.0]	0.69	0.57	0.65	0.57	4.42	4.24	3.90	4.32	0.96	0.59	0.65	0.61	4.48	4.29	1.04	4.77
57 [15.8]	0.78	0.64	0.65	0.65	4.65	4.45	2.77	4.63	1.00	0.66	0.65	0.67	4.72	4.51	0.00	5.00
60 [16.7]	0.89	0.72	0.65	0.72	5.93	5.60	1.93	5.68	1.04	0.72	0.65	0.73	5.17	4.92	-0.79	5.79
61 [16.9]	Rollover								Rollover							

It is evident that the conventional AFS system achieves the target response for the understeer vehicle by increasing the steer angles at the wheels while maintaining the pro-Ackerman geometry. Consequently, the AFS control causes saturation of the inner wheel at

speeds above 52 km/h on the uniform road surface and at a substantially lower speed on the split- μ surface ($WT > 0.65$), as seen in Table 4.2. The available tire-road adhesion, however, is underutilized by the outer wheel up to relatively higher speeds, particularly in case of the split- μ surface. Unlike the conventional AFS control, the AIFS applies steering correction following pro-Ackerman geometry only until the inner tire reaches the predefined work-load. Unequal steering corrections are then applied to the inner and outer wheels, while limiting the inner wheel work-load to the pre-defined limit of 0.65, shown as highlighted columns in Table 4.2. The AIFS control also applies relatively greater correction to the outer wheel so as to increase the tire-road adhesion utilization. The AIFS thus not only provides superior active steering control, it affords a reserve capacity for both the tires for generation of additional braking/traction forces during the maneuver, if required. The superiority of the proposed AIFS control over the conventional AFS system is more evident from the results presented for split- μ road surface. These results clearly demonstrate significant advantage of AIFS control during a severe maneuver, when tire-road friction level is relatively low and non-uniform.

The higher steering correction applied to the outer wheel by the AIFS control permits considerable reduction in the steer angle of the inner wheel, which is either saturated or is near saturation at higher speeds. For example, under the turning maneuver at 60 km/h on the uniform road surface, the AIFS control applies slightly higher outer wheel steer angle (5.68 degrees) compared to the AFS control (5.60 degrees), which allows substantially lower inner wheel steer of 1.93 degrees compared to 5.93 degrees in case of the AFS control. For the maneuver conducted on the split- μ road condition with lower friction at the inner tire, the conventional AFS causes inner tire saturation at speeds above 40 km/h, while the AIFS limits the inner tire

work-load to the desired value by reducing its steer angle gradually with increasing speed, as seen in Table 4.2. The inner wheel steer angle reduces 0 degree at 57 km/h. The target response in this case is realized by increasing the outer tire steer angle from 4.51 to 5 degrees.

Figure 4.13 illustrates the time histories of the inner and outer wheels' steer angles and the resulting tire work-loads, attained for the proposed AIFS control at speeds corresponding to onset of the inner wheel saturation (52 km/h) and when both the wheels approach the limiting value of the work load (57 km/h). On the uniform friction road surface, the inner tire work-load approaches 0.63 at 52 km/h, prior to its saturation, and consequently the controller maintained the inner and outer wheels angles following pro-Ackerman steering ratio. This, however, resulted in significantly different work-loads of the inner and outer wheels, which remain below the selected threshold value. Subsequently, at 57 km/h, the AIFS introduces anti-Ackerman steering by imposing significantly larger steering angle to the outer wheel than the inner wheel. The results suggest comparable tire work-loads for both wheels, while the reduced cornering force at the inner tire is compensated by increasing the outer tire cornering for realization the target response.

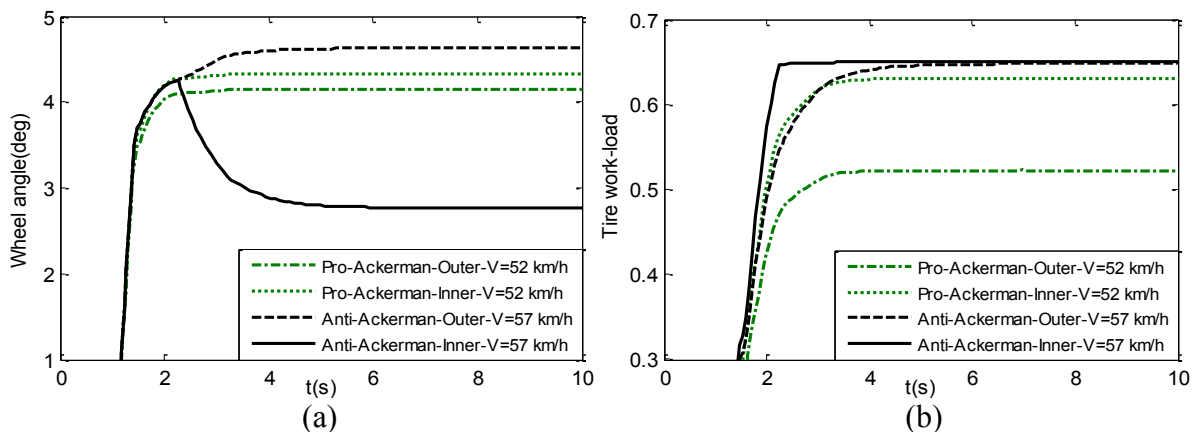


Figure 4.13: Comparisons of the inner and outer wheels (a) steering angles; and (b) work-loads of the model with AIFS control at 52 km/h and 57 km/h on a uniform road.

4.5.2 Single-lane change maneuver

Figure 4.14 illustrates the handling responses of the vehicle model without and with active steering control (AFS and AIFS) in terms of yaw rate and path trajectory under the lane-change maneuver conducted at 83 km/h on a dry road ($\mu=0.78$). Relatively high speed of 83 km/h for lane change was selected to generate a severe turning maneuver where the tire work-load of the inner wheel in each cycle would reach close to saturation.

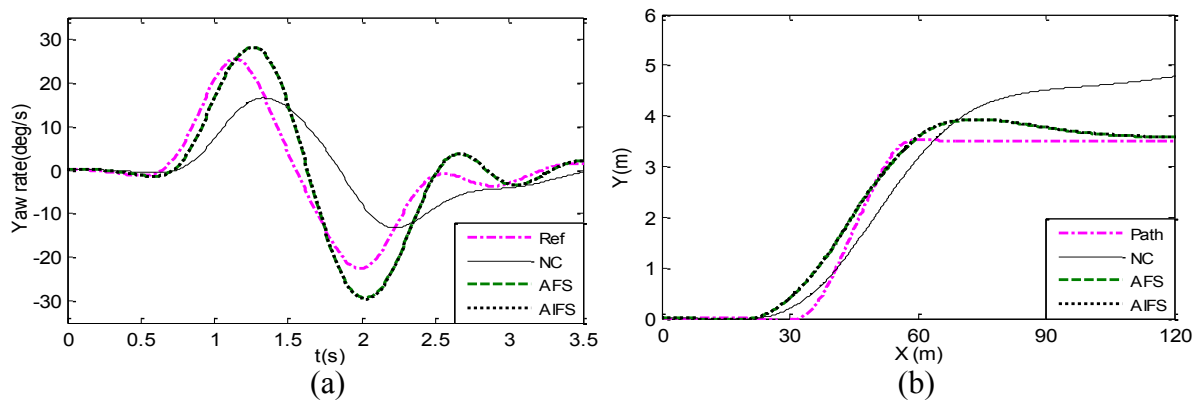


Figure 4.14: Comparisons of (a) yaw rate; and (b) path trajectory responses of the vehicle model without active steering (NC), and with conventional AFS and AIFS control (Lane-change maneuver at 83 km/h).

The results are attained for the steering input estimated from the linear model, as shown in Fig. 4.7(b). The figures also show the target path, reference model yaw rate and responses of the model without the active steering (NC). The results suggest that both the AFS and AIFS can effectively track the desired path, while the responses of the model without active steering exhibit substantial deviations from the desired path.

The two active controller syntheses, however, exhibit notable differences in the corrective steering angles and thereby the peak work-loads of the inside and outside wheels (left- and right-wheels depending upon the direction of the steering input), as seen in Fig. 4.15. The work-load of the inside wheel of the model with conventional AFS approaches the saturation zone during

the initial steering cycle, which is evident from its workload approaching 0.78, as seen in Fig. 4.15(a). The corresponding work-load of the outer or the right-wheel, shown in Fig. 4.15(b), is about 0.64 suggesting slight underutilization of the available tire-road adhesion by the outer wheel. The AIFS control, on the other hand, tracks the reference model response while maintaining comparable values of the inner and outer wheels work-loads near the limiting value of 0.65. The results further show that the work-load of the inner wheel reduces to 0.65 at the expense of only slightly higher work-load of the outer wheel. From the variations in the wheels angles, shown in Fig. 4.15(c), it is evident that both the controllers impose substantially higher steer angles to realize the target response.

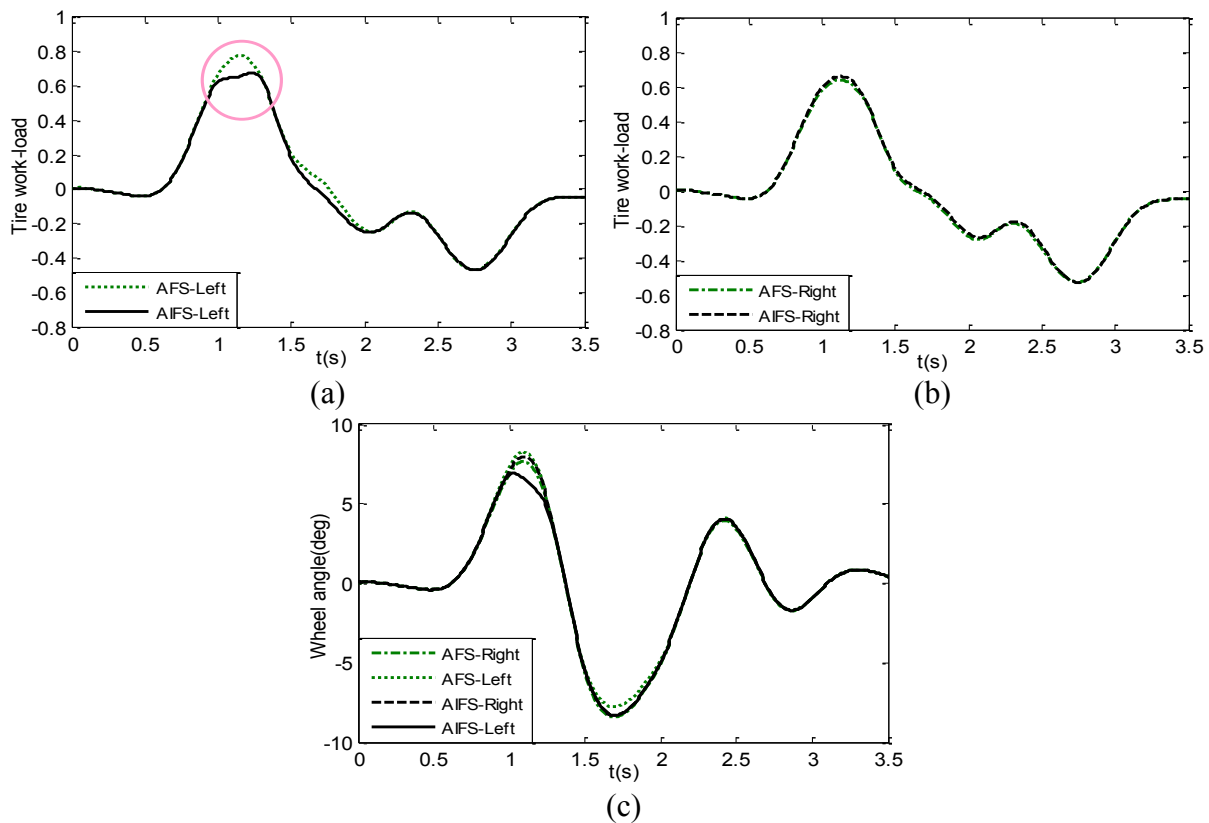


Figure 4.15: Variations in work-loads of the (a) left-; and (b) right-steered wheels; and (c) the corresponding steer angles developed with conventional AFS and AIFS (Lane-change maneuver at 83 km/h, uniform road).

Figure 4.16(a-c) shows the work-load and steer angle responses of the left- and right-wheels for the given maneuver on split- μ surface ($\mu_r=0.78$, $\mu_l=0.5$) while realizing the same target as presented in Fig. 4.14. While the AFS control generates the increase in wheel angles following the Ackermann geometry throughout the steering cycle, the AIFS controller yields relatively lower steering correction to the inside (left) wheel during the first cycle in order to limit the tire-work load to 0.65. At the same time, the AIFS controller imposed higher correction to the outside wheel in order to track the desired path. The AIFS leads to anti-Ackerman geometry near the extreme values of steering angles in order to limit the tire work-load to predefined value.

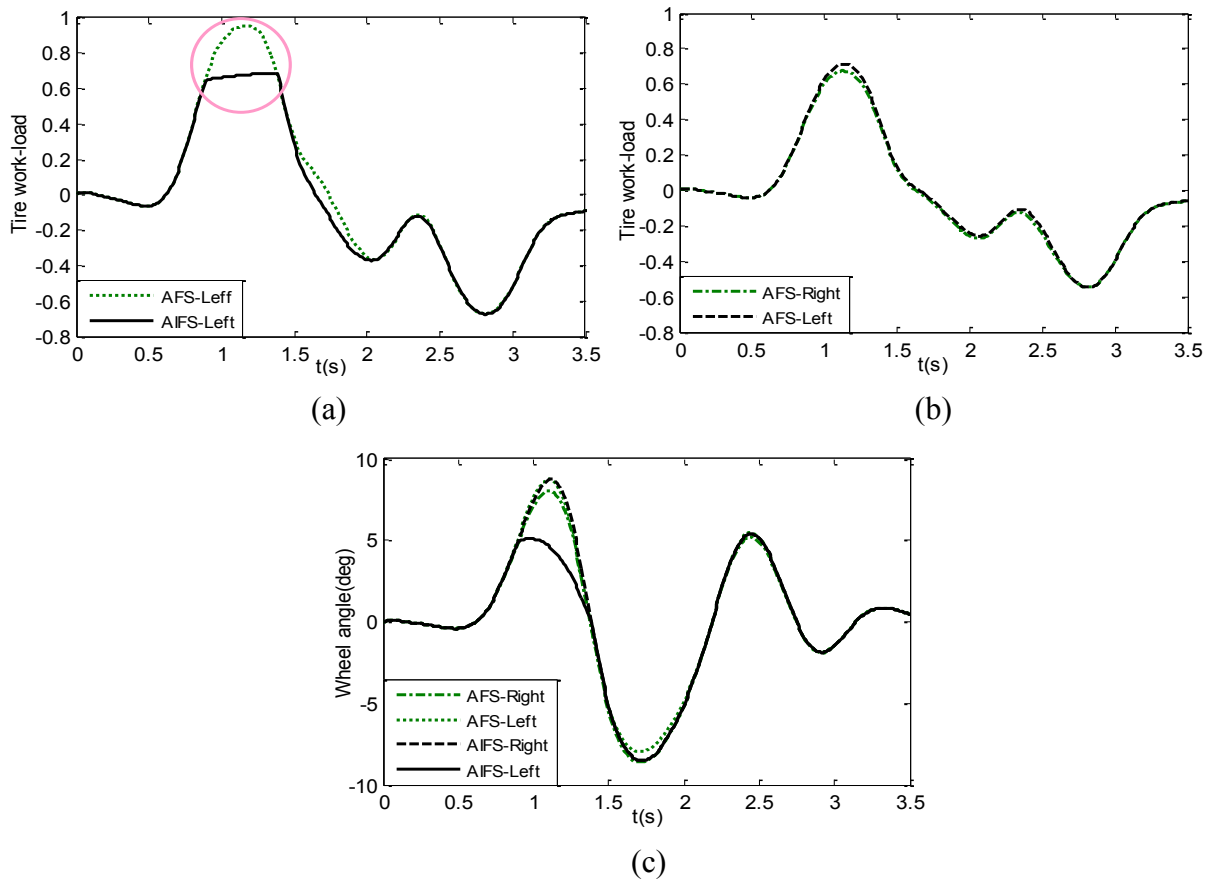


Figure 4.16: Variations in work-loads of the (a) left-; and (b) right-steered wheels; and (c) the corresponding steer angles developed with conventional AFS and AIFS (Lane-change maneuver at 83 km/h, split- μ road).

4.5.3 Double-lane change maneuver

Figure 4.17 illustrates the yaw rate and path responses of the vehicle models with AFS and AIFS control subject to the standardized double lane-change maneuver at 83 km/h on the dry road ($\mu=0.78$). The results are obtained under the steering input estimated from the linear model coupled with an ideal driver tracking the desired path trajectory, as described in Figs. 4.8(a) and 4.8(b). It is evident that both the AFS and AIFS controls can effectively track the desired trajectory reasonably well, as observed in the case of lane-change and steady-turning maneuvers. The vehicle model without the active steering control, however, exhibits substantial path deviations and path divergence, which is attributable to high vehicle CG and high lateral load transfer during the maneuver.

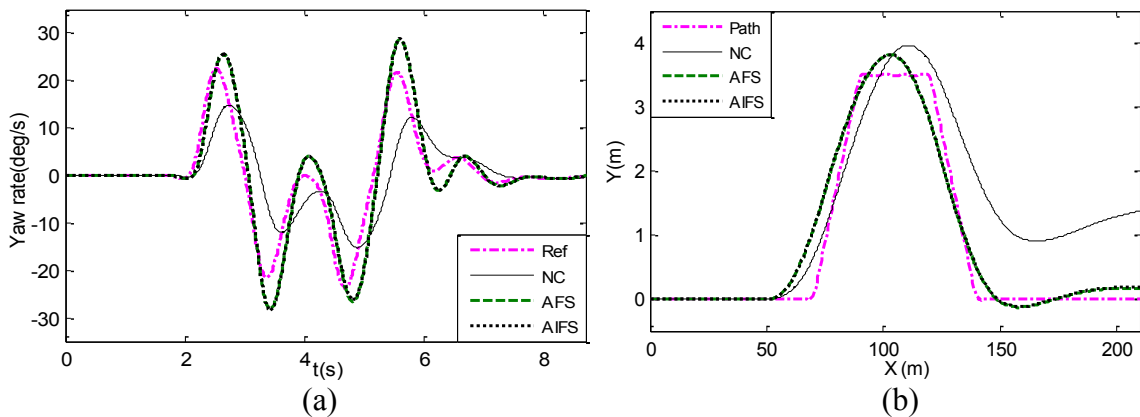


Figure 4.17: (a) Yaw rate; and (b) path trajectory responses of the vehicle model without active steering (NC), and with conventional AFS and AIFS (double lane-change at 83 km/h).

Despite tracking the target responses well, the two steering control strategies yield notable differences in the peak tire work-load generated, as it was observed under the lane-change maneuver. As illustrated in Figs. 4.18(a) and 4.18(b), the conventional AFS control causes the left- and right-wheels approach the saturation zone during the first and second cycle of the steering input. Relatively greater saturation of the left (outer) and right- (inner) wheels is evident

during the initial and second steering cycles, respectively. Consequently, the intervention of the AIFS for limiting the right wheel work-load during the second cycle is particularly more significant. The same trend is also evident from the time history of steering angles generated by the two control strategy as illustrated in Fig. 4.18(c). The AIFS controller was observed to generate anti-Ackerman steering geometry around the extreme peak steer angles, where the lateral load transfer was most significant. The severity of this trend is more evident from the results presented for split- μ road surface ($\mu_r=0.78$, $\mu_l=0.5$), as shown in Fig 4.19(a-c). These results also demonstrate significant advantage of AIFS control over the AFS system when tire-road friction is low or non-uniform.

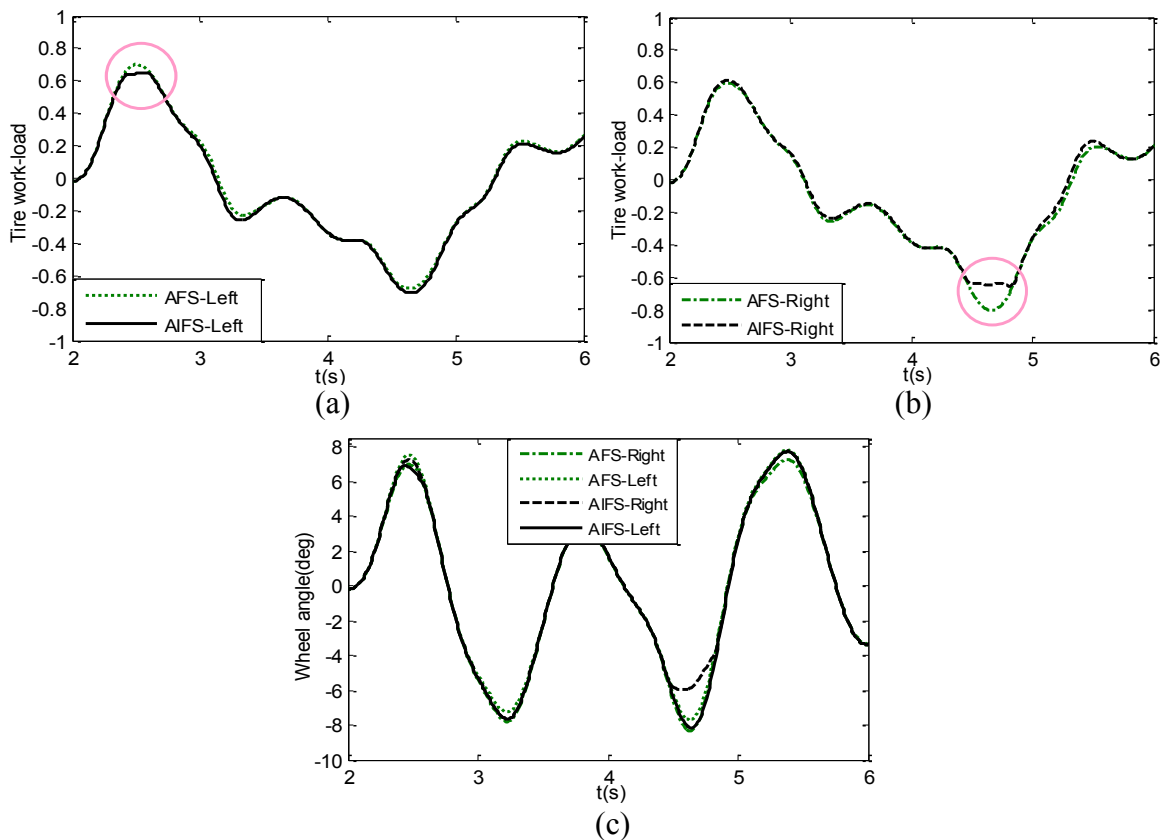


Figure 4.18: Work-loads of the (a) left; (b) right steered wheels; and (c) the corresponding steer angles developed with conventional AFS and AIFS (double lane-change maneuver at 83 km/h, uniform road).

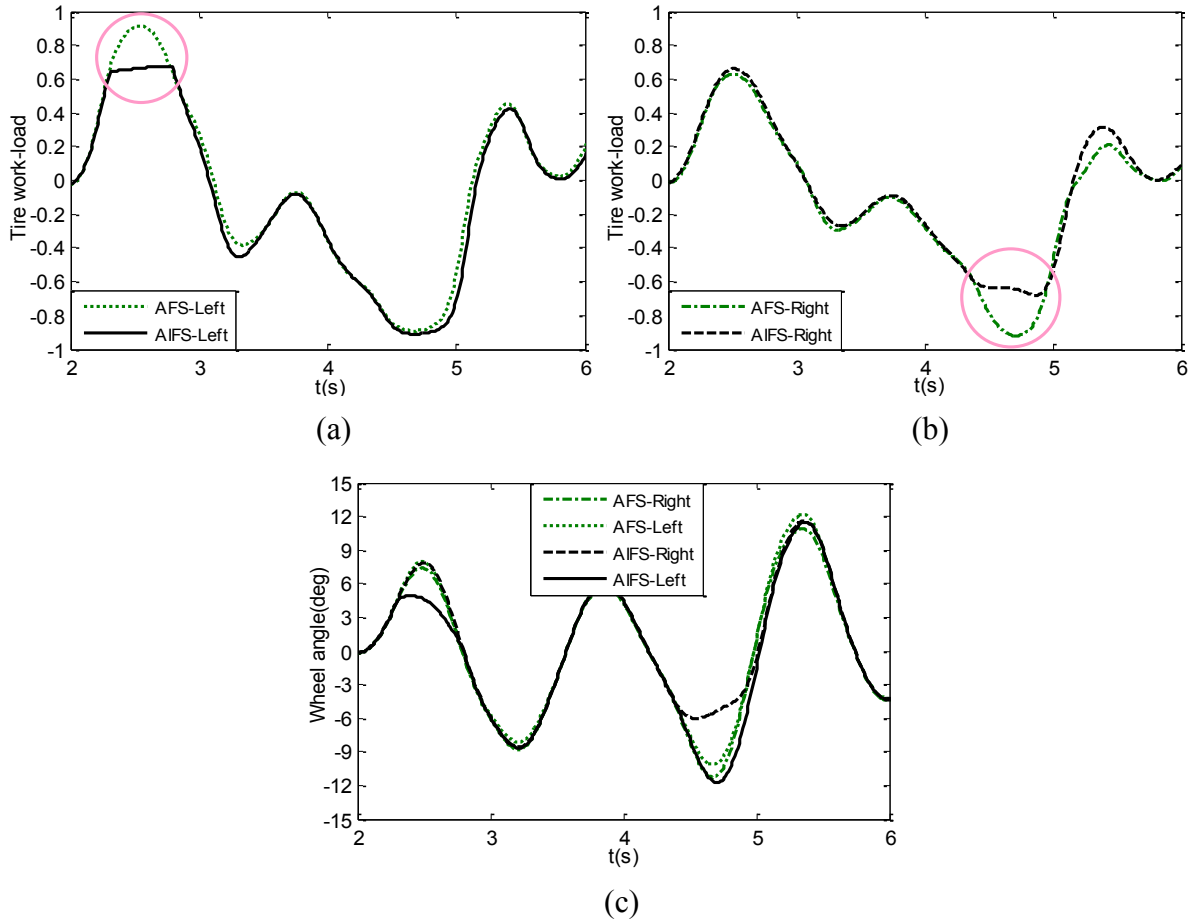


Figure 4.19: Work-loads of the (a) left; (b) right steered wheels; and (c) the corresponding steer angles developed with conventional AFS and AIFS (double lane-change maneuver at 83 km/h, split- μ road).

The results demonstrate that the proposed AIFS control strategy can enhance the handling performance of a vehicle under both the steady and transient steering maneuvers including the double lane change. Its effectiveness is particularly meritorious under the lane-change and evasive maneuvers conducted at relatively higher speeds, as the vehicle encounters higher lateral load transfers. The most notable merit of the AIFS compared to AFS lies in its ability to provide sufficient tire-load reserve so as to enable the tire to develop braking/traction forces during a relatively severe directional maneuver.

4.6 Conclusion

The directional performance potentials of the Active Independent Front Steering (AIFS) system are evaluated using a nonlinear yaw-plane model of a two-axle truck. The AIFS control strategy is synthesized based on a simple PI controller in order to track the steering response of an idealized reference model. Simulation results are obtained for a truck model integrating AFS and AIFS systems subjected to a range of steering maneuvers, namely: a J-turn maneuver, path change and obstacle avoidance maneuvers on uniform as well as split- μ road condition. Unlike the conventional Active Front Steering (AFS), the proposed AIFS system permits maximum utilization of the available tire-road adhesion at both the steered wheels, while eliminating potential of tire saturation. The AIFS could thus lead to improved handling performance under severe maneuvers through unequal distribution of steering correction over the inside and outside wheels when required. The results also show that the AIFS can be designed to maintain a desired tire-work load over the entire range of speed up to the vehicle rollover limit. The results obtained for various maneuvers on different surface conditions suggest that independent steering control strategy is desirable under severe maneuvers and once a threshold value of tire workload is reached at the inner tire. It is therefore suggested that the AIFS control strategy should be designed to generate proportional steer angle for the inner and outer wheels following pro-Ackerman geometry until a threshold value for the inner tire workload is reached. Beyond which the proposed independent control may be applied to enhance the active steering system performance limit. At higher speeds, the same active controller may be designed to enhance the rollover threshold by relaxing the target requirement at the expense of directional control. This potential is not explored in this investigation. The most meritorious feature of the AIFS lies in

the fact that it can provide a target response under severe maneuvers while equalizing the workloads at the steered wheels. The results thus suggest that the performance of an AIFS system would be highly promising under more severe maneuvers involving simultaneous braking and steering, since it permits a desired adhesion reserve at each wheel to meet a braking demand during the steering maneuver.

CHAPTER 5

BRAKING AND STEERING PERFORMANCE ANALYSIS OF A ROAD VEHICLE WITH ACTIVE INDEPENDENT FRONT STEERING (AIFS)

5.1 Introduction

The vehicle handling performance benefits of active front steering (AFS) systems have been widely investigated through both simulations and experiments [45,55]. The reported studies have invariably shown that the AFS strategy offers beneficial handling performance by providing substantial yaw disturbance rejection originating from high speed turning or lane-change maneuvers or side wind forces. The AFS systems are designed to apply corrective steering angles to realize a target handling response under ranges of steer angle and forward velocity. The steering corrections, however, are applied to both wheels having fixed geometrical ratio, which may cause saturation of the inside wheel and under-utilization of the available adhesion at the other wheel. It has been shown that application of independent steering corrections to the two steered wheels could yield significant improvement in the handling performance during high speed maneuvers [140,147]. The steering corrections in the reported studies were established considering the tire saturation limits in terms of the tires' workload. The concept, referred to as active independent front steering (AIFS) could yield target responses that are either similar to or better than the conventional AFS. Furthermore, AIFS would ensure sufficient adhesion reserve at each wheel for generating a longitudinal force, when needed in an emergency-type maneuver. The AIFS could thus be beneficial in realizing enhanced braking performance during a steering maneuver. While the majority of the studies on AFS have suggested the use of steer-by-wire

(SBW), a few studies have expressed concerns related to high cost and reliability due to lack of mechanical coupling between the steering and the road [106]. A mechanical system based on tandem planetary gear systems that can be readily adapted for AIFS control has been proposed by Farazandeh et al. [126].

The studies reporting handling performance analyses of AFS systems have mostly considered steering inputs in the absence of braking. The effectiveness of the AFS systems under braking during steering maneuvers or braking in a straight line driving in the presence of asymmetric friction between the left and right tires (split- μ condition) have been investigated in only a few studies [1,49,135]. A severe braking input during turning may impose considerable demands on both the driver's skill and the vehicle performance, which is largely dependent on the road adhesion level available at the tire-road interface. During an emergency-type braking-in-turn maneuver, such as that encountered while avoiding a potential collision, it is essential to ensure handling and stability limits so as to limit the vehicle path deviations to minimum, while minimizing the stopping distance by realizing maximum deceleration. Application of braking while turning may cause the resultant friction demand to approach the available adhesion limit leading to tire saturation. In such situations, the vehicle can no longer be steered along the desired path and it may exhibit a directional instability. A number of studies have shown the loss of directional stability and spin-out, as the vehicle changes from understeer to a limit oversteer condition under a hard braking input [47,148]. These have also emphasized the need to distribute the braking force based on the load of each wheel to achieve effective steering operation, particularly with the novice drivers [149]. El-Gindy [150] suggested to limit the friction demand

during steering to a maximum of 80% so as to allow a safety margin for additional tractive or braking effort requirements, particularly for the drive-axles of the heavy vehicle combinations.

In the AFS design, the inner wheel may approach saturation and thereby provide limited braking force, while the adhesion available at the outer wheel would be under-utilized. Several studies have demonstrated the effectiveness of different active chassis systems in realizing greater stability limits during combined braking and steering maneuvers under a range of driving conditions [151-153]. These include the AFS, active rear steering (ARS), four wheel steering (4WS) and yaw moment-based vehicle stability systems with differential braking control namely, DYC (direct yaw-moment control) and ESP (electronic stability program). Xia et al. [151] investigated the maneuverability and stability of the conventional front wheel steering (FWS) and four wheel steering (4WS) vehicles using a non-linear bicycle model under an obstacle avoidance maneuver involving a panic braking together with the steering input. The study concluded enhanced stability limit and shortest stopping distance of the vehicle with the closed-loop 4WS based on the vehicle yaw rate and front wheel steer angle compared to that with open-loop 4WS or FWS. More recently, Tardy [47] examined the directional performance of a vehicle with AFS and rear wheel steering (RWS) under different maneuvers with and without a driver model using a PI controller based on the yaw rate feedback. Both controllers showed significant improvement in the vehicle responses to hard braking during turning or lane change maneuvers, while the AFS with the driver model revealed limited performance due to driver delays.

Anstrom [153] investigated the stability of a hybrid electric vehicle with a proportional yaw rate controller for distributing the front-right and left motor torques as well as anti-lock braking control systems (ABS). The study showed improved responsiveness and stability limit of the

vehicle in terms of yaw rate, and longitudinal and lateral accelerations during braking-in-turn maneuvers but relatively higher stopping distance due to the ABS control. Hancock et al. [142] compared the yaw stability limit of a vehicle with an active brake control (ABC) with that of an active rear differential using distribution of driveline torque, under braking-in-turn and lane change maneuvers. The ABC was judged undesirable during braking at a high lateral acceleration turning maneuver, which was attributed to application of braking torque via the rear inside wheel prior to the brake application in order to generate the required yaw moment during turning. The rear inside tire thus rapidly approached saturation under braking. The study thus suggested the use of the active rear differential, which generating the required yaw moment through two wheels instead of the single wheel. Nuessle et al. [148] assessed the active safety of the vehicle equipped with an electronic stability program (ESP) through tests under acceleration in a turn on both high- and low friction roads, and braking in a turn at high speeds. The ESP controller compensated the vehicle oversteering tendency by applying the brake force mainly through the outside wheel to simultaneously realize the required yaw rate. The brake pressure on the rear wheels with lower normal load was also limited so as to increase the vehicle stability.

The aforementioned studies have emphasized the enhancement of stability and/or braking performance of vehicles using different active chassis control systems. Only limited efforts, however, have been made towards realizing a target handling response, while simultaneously maximizing the braking performance. This study investigates the braking efficiency and handling characteristics of a road vehicle equipped with the AIFS system under a wide range of braking-in-turn maneuvers and different road adhesion coefficients, including the split- μ roads. The response characteristics are compared with those of the vehicle with the conventional AFS. The

sensitivity of the AIFS controller responses are further evaluated under variations in selected vehicle design parameters. The robustness of the AIFS control synthesis is also evaluated considering variations in the tire properties, external disturbances and tires interactions with roads with asymmetric friction properties.

5.2 Vehicle Dynamic Modeling

A directional dynamic model of a heavy truck is considered for the analysis of braking and steering performance of the AIFS, since it could lead to large lateral load shift during a turn and thus potential tire saturation. The vehicle model in the yaw-plane with limited roll degree-of-freedom (DOF), and incorporating lateral and longitudinal load transfers, was judged adequate to study the independent steering control of the left and right wheels. Figure 5.1 illustrates the 8-DOF model of a two-axle truck in the yaw and roll planes.

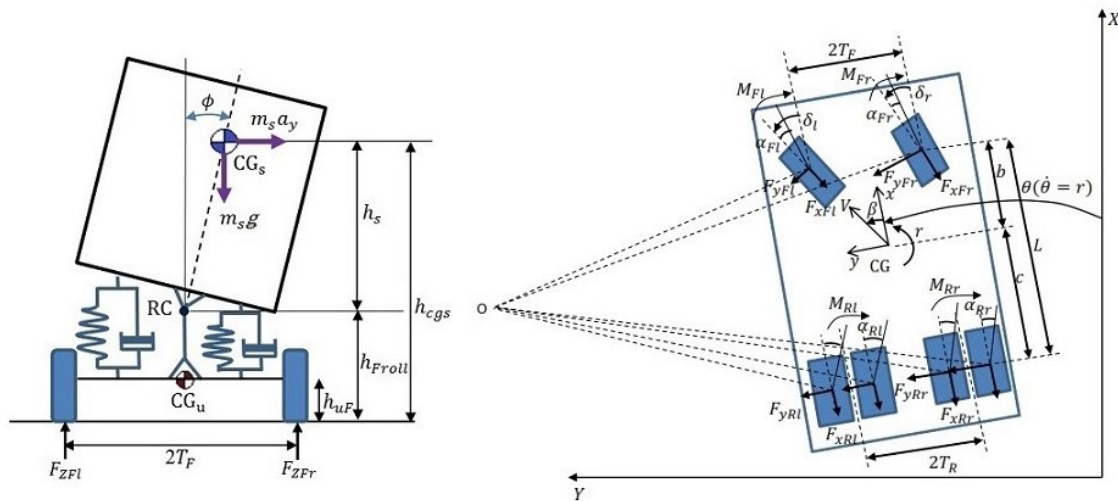


Figure 5.1: Full vehicle model for braking and turning maneuver.

The model is formulated considering the longitudinal, lateral, yaw and roll motions of the vehicle and rotational motions for each of the four wheels. As shown in the figure, δ_r and δ_l

refer to two independent steering inputs applied to the right- and left-wheels, respectively. The high magnitude load transfers coupled with severe braking/steering maneuvers also necessitated a nonlinear tire model.

The ‘‘Magic Formula’’ tire model is applied to describe the longitudinal (F_{Xij}) and lateral (F_{Yij}) forces, and self-aligning moment M_{ij} ($i = F, R; j = r, l$) properties of the tire as functions of the normal load (F_{Zij}), slip angle (α_{ij}), longitudinal slip ratio (λ_{ij}) and road-tire friction coefficient (μ). The subscript, $i = F, R$, denotes the front and rear wheels, respectively, while $j = r, l$, refers to right- and left-wheels. The equations of motions describing the longitudinal, lateral, roll and yaw motions of the vehicle may be expressed as:

$$m(\dot{V}_x - rV_y) + m_s h_s \dot{\phi} r = -F_{YFr} \sin \delta_r - F_{YFl} \sin \delta_l + F_{XF r} \cos \delta_r + F_{XF l} \cos \delta_l + 2F_{XRr} + 2F_{XRl} \quad (5.1)$$

$$m(\dot{V}_y + rV_x) - m_s h_s \ddot{\phi} = F_{YFr} \cos \delta_r + F_{YFl} \cos \delta_l + 2(F_{YRr} + F_{YRl}) + F_{XF r} \sin \delta_r + F_{XF l} \sin \delta_l - F_w \quad (5.2)$$

$$(I_{xs} + m_s h_s^2) \ddot{\phi} - I_{xzs} \dot{r} - m_s h_s (\dot{V}_y + rV_x) = (m_s g h_s - K_{\phi F} - K_{\phi R}) \phi - (C_{\phi F} + C_{\phi R}) \dot{\phi} \quad (5.3)$$

$$(I_{zs} + I_{zu}) \dot{r} - I_{xzs} \ddot{\phi} = - \sum_{i=F}^R \sum_{j=r}^l M_{ij} + F_{YFr} (b \cos \delta_r - T_F \sin \delta_r) + \dots \\ F_{YFl} (b \cos \delta_l + T_F \sin \delta_l) - 2c (F_{YRr} + F_{YRl}) + F_{XF r} (b \sin \delta_r + T_F \cos \delta_r) - \dots \\ - F_{XF l} (-b \sin \delta_l + T_F \cos \delta_l) + 2T_R (F_{XRr} - F_{XRl}) - e_w F_w \quad (5.4)$$

In the above equations V_x and V_y are the longitudinal and lateral velocities; and ϕ and r are the roll angle and yaw rate of the vehicle, respectively. The longitudinal distances of the front and rear axles from the center of sprung mass (CG_s) are denoted by b and c , respectively. T_i ($i = F, R$) is the half tire track width of axle i . m and m_s are the total and sprung masses of the vehicle, respectively, while h_s is the CG height of the sprung mass from the roll center. I_{xs} , I_{xzs}

and I_{zs} are moments of inertia of sprung mass about x -, x - z and z -axis, respectively, about CG_s , and I_{zu} is the total yaw mass moment of inertia of the unsprung masses.

The model is subjected to side force excitation, F_W , due to cross wind and e_W is the yaw moment arm, the distance between the geometric center and the CG coordinate along the x -axis. The instantaneous normal load on each tire is expressed in terms of longitudinal (a_x) and lateral (a_y) accelerations, and suspension roll stiffness ($K_{\phi i}$) and damping ($C_{\phi i}$), such that:

$$F_{Zij} = \frac{W_i}{n} \mp \frac{a_x}{nL} (m_s h_{cgs} + m_{uF} h_{uF} + m_{uR} h_{uR}) \pm \dots \quad (5.5)$$

$$\frac{a_y}{nT_i} (m_{si} h_{iroll} + m_{ui} h_{ui}) \pm \frac{1}{nT_i} (K_{\phi i} \phi + C_{\phi i} \dot{\phi})$$

where, W_i ($i = F, R$) is the total load on front and rear axle, while $n= 2$ for the front and $n=4$ for rear axle tires. L is the vehicle wheelbase, and m_{si} and m_{ui} ($i = F, R$) are the front and rear sprung and unsprung masses, respectively. As shown in Fig. 5.1, h_{cgs} is the CG height of the sprung mass from the ground, h_{iroll} is the sprung roll center height and h_{ui} ($i = F, R$) is the unsprung mass CG height from the ground. The lateral (F_{Yij}) and longitudinal forces (F_{Xij}), and the aligning moments (M_{ij}) developed at each wheel, in equations (5.1) to (5.4), are computed using ‘‘Magic Formula’’ [102] as functions of the normal load F_{Zij} , longitudinal slip ratio λ_{ij} and slip angle α_{ij} , given by (Fig. 5.2):

$$\alpha_{Fr} = \delta_r - \tan^{-1} \left[\frac{br+V_y}{V_x+T_{Fr}} \right]; \quad \alpha_{Fl} = \delta_l - \tan^{-1} \left[\frac{br+V_y}{V_x-T_{Fr}} \right] \quad (5.6)$$

$$\alpha_{Rr} = \tan^{-1} \left[\frac{cr-V_y}{V_x+T_{Rr}} \right]; \quad \alpha_{Rl} = \tan^{-1} \left[\frac{cr-V_y}{V_x-T_{Rr}} \right] \quad (5.7)$$

$$\lambda_{ij} = \frac{V_x - R_w \Omega_{ij}}{V_x} \quad (5.8)$$

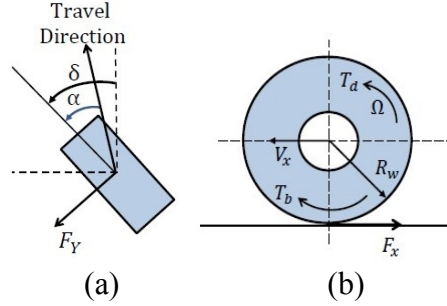


Figure 5.2: (a) Tire slip angle; and (b) rotational dynamics of the wheel.

Furthermore, the equation of the angular motion of each wheel is given by:

$$I_w \dot{\Omega}_{ij} = -R_w F_{Xij} + T_{ij} \quad (5.9)$$

where I_w is mass moment of inertia of each wheel, Ω_{ij} is angular velocity and $T_{ij} = T_{dij} - T_{bij}$ is the net torque considered as the difference between the driving T_{dij} and braking T_{bij} torques. The braking torque applied to wheel j of axle i , is computed as a function of the total torque T_b and the ideal braking torque distribution factor k_{bi} of the front and rear axles. Moreover, the gain k_{bRj}^* is applied to rear wheels to ensure that these wheels do not lock-up during braking, such that [7]:

$$T_{bFj} = k_{bF} T_b; \quad T_{bRj} = k_{bRj}^* k_{bR} T_b$$

$$\frac{k_{bF}}{k_{bR}} = \frac{\frac{c}{L} + \frac{h_{cg}}{L} \mu}{\frac{b}{L} - \frac{h_{cg}}{L} \mu} \quad (5.10)$$

where h_{cg} is the overall CG height of the vehicle.

5.3 Controller Synthesis and Method of Analysis

A detailed synthesis of the AIFS controller has been presented in [140,147]. Briefly, the AIFS control strategy was synthesized using a proportional-integral (PI) yaw rate feedback controller to generate a corrective steering, δ_c , based on tracking a reference yaw rate response

corresponding to the neutral steer condition. A first-order lag function was further introduced to compensate for the steering response delay of the vehicle. The dynamics of the steering actuator was also incorporated in the model considering its limited bandwidth. In addition to realizing the target response, the corrective steer angle for a given wheel generated by the AIFS controller was limited by the available tire-road adhesion based on the instantaneous normal load. The tire-road adhesion limits were determined using a performance parameter in terms of the tire work-load (W_T), defined as the ratio of the total force developed by a tire to the maximum available tire force based on the road adhesion limit and the normal load, where the total force is estimated assuming the friction circle concept:

$$W_T = \frac{\sqrt{F_X^2 + F_Y^2}}{\mu F_Z} \quad (5.11)$$

During a high lateral acceleration maneuver, the normal load on the inner wheel of the steered axle will be significantly lower compared to the outer wheel. The inner tire may thus approach the saturation zone or its adhesion limit much earlier than the outer tire. Since the AIFS allows independent steering correction for each wheel, the control strategy was synthesized to limit the steering correction so that none of the wheels approach saturation. The AIFS control strategy in general reduces the steering correction to the inner wheel while applying relatively higher steering correction to the outer wheel in order to ensure the target response. The limiting value of the inner tire work-load was chosen as 0.65 for realizing the target handling responses to different steering inputs [140,147]. This value permitted for a reasonable adhesion reserve for developing tractive or braking force that may be needed in emergency-type of maneuvers involving simultaneous braking and steering. The limiting value of the tire work-load was

identified from the nonlinear cornering characteristics of the tire. A schematic of the control structure is summarized in Fig. 5.3. In this figure, the steering correction $\Delta\delta_{st} = K_{st}\Delta r$ is related to Δr , the yaw rate deviation from the reference value r_{ref}^* , and the gain $K_{st} = \frac{L}{v}$, defined as the ratio of the wheelbase to the vehicle velocity. The external disturbance caused by side wind force is also considered in the model structure.

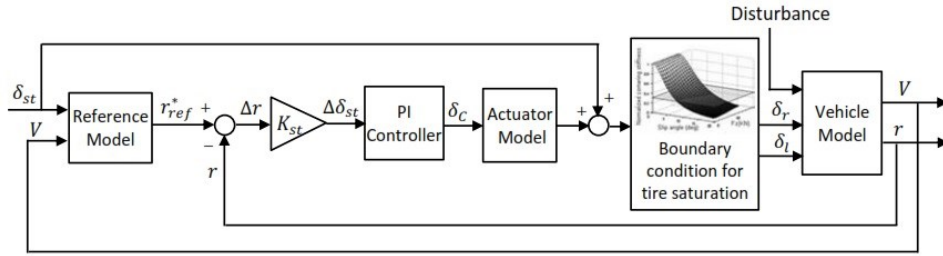


Figure 5.3: Schematic of the AIFS control structure.

In the present study, a wheel slip controller is integrated to the above AIFS controller such that the rear wheels do not approach lock-up during a hard braking input. For this purpose, the rear axle brake gain factor k_{BRj}^* ($j = l, r$) is defined as a function of the longitudinal wheel slip and the road-tire friction coefficient μ . Owing to wide variations in the road surface friction coefficient, a generalized gain function is defined considering the lower and upper limits of the slip ratio, λ_L and λ_U , such that [7]:

$$k_{BRj}^* = \begin{cases} 1, & \text{if } \lambda_{Rj} \leq \lambda_L \\ \frac{\lambda_U - \lambda_{Rj}}{\lambda_L}, & \text{if } \lambda_L < \lambda_{Rj} < \lambda_U \\ 0 & \text{if } \lambda_{Rj} \geq \lambda_U \end{cases} \quad (5.12)$$

The lower and upper limiting values of the longitudinal slip are taken as 0.15 and 0.3, respectively, for road surface with adhesion coefficient above 0.5, and 0.05 and 0.1 for low friction roads ($\mu \leq 0.5$). The vehicle model together with the AIFS controller was analyzed under

different braking-in-turn maneuvers and road surface coefficients in the Matlab/Simulink platform, as illustrated in Fig. 5.4. The simulations were performed considering a standardized braking-in-turn maneuver, where a sudden braking input was applied in an open-loop manner while the vehicle is negotiating a constant-speed steady-state turn of specified lateral acceleration, as described in ISO-14794 [145]. For this purpose, a PI controller is introduced to track the desired vehicle speed so as to apply controlled driving torque T_d , distributed between right- and left-wheels of the drive-axle. The simulation parameters were taken as those of a two-axle truck, which are summarized in the Table C.2 (Appendix C).

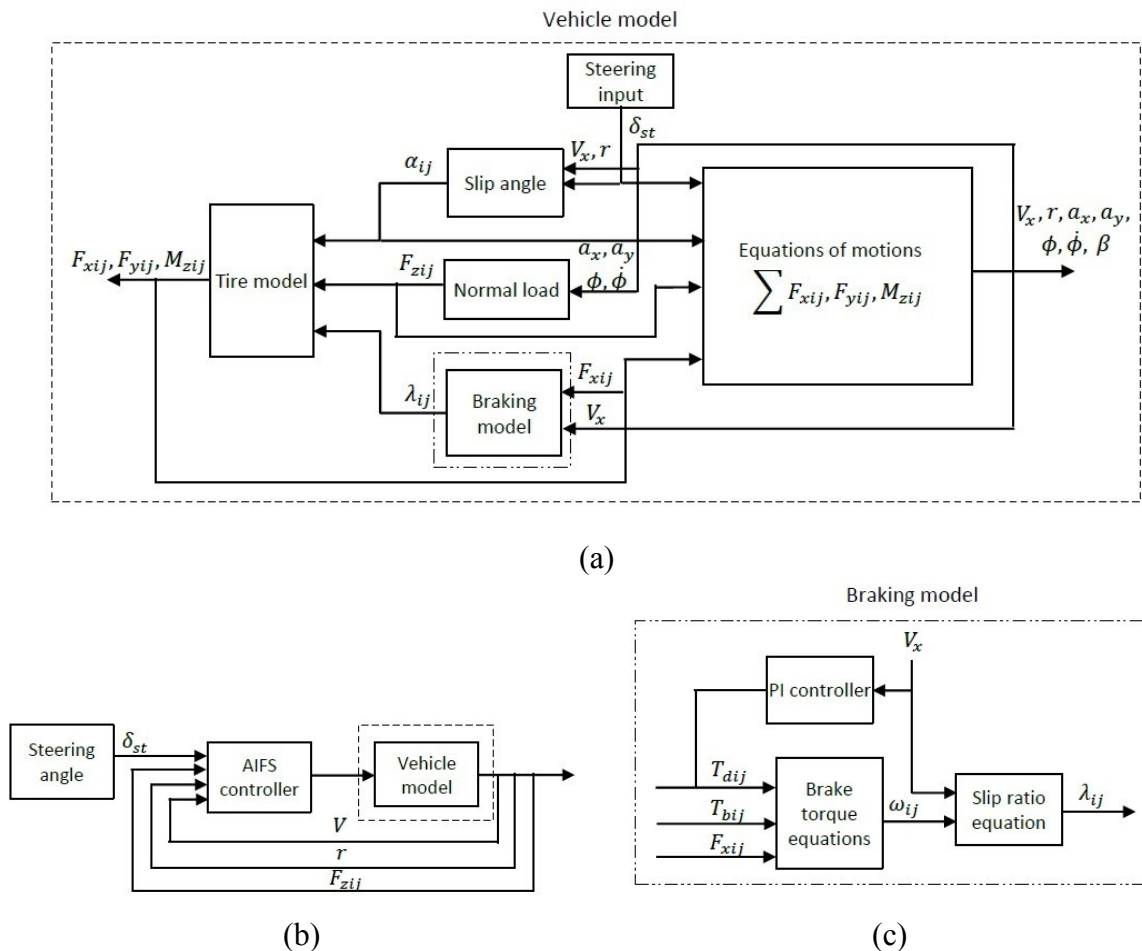


Figure 5.4: Simulink diagrams illustrating: (a) the full vehicle model; (b) AIFS controller block; and (c) the brake system model.

The standardized test permits the assessment of the effects of braking on course-holding and directional behavior of a vehicle, in particular, the sensitivity of vehicle's yaw response to braking. The results are obtained mainly in terms of path deviation (lane keeping), stopping distance, deceleration and rollover limit. In this investigation, the maneuver is initiated with a constant-speed steady turn steering input, as shown in Fig. 5.5(a). After a period of 10 seconds, a braking torque, T_b , is applied in a ramp-step manner with rise time of 1 s, as shown in Fig. 5.5(b). The braking torque, however, is limited to 20% longitudinal slip ratio ($\lambda^* = 0.2$) for the front wheels on a dry road. This in general corresponds to the peak tire force generated during braking. At a relatively high speed of 57 km/h and a steering input of 4 degrees, $T_b = 5580$ Nm resulted in $\lambda^* = 0.2$ for the front inner wheel of the vehicle equipped with AFS.

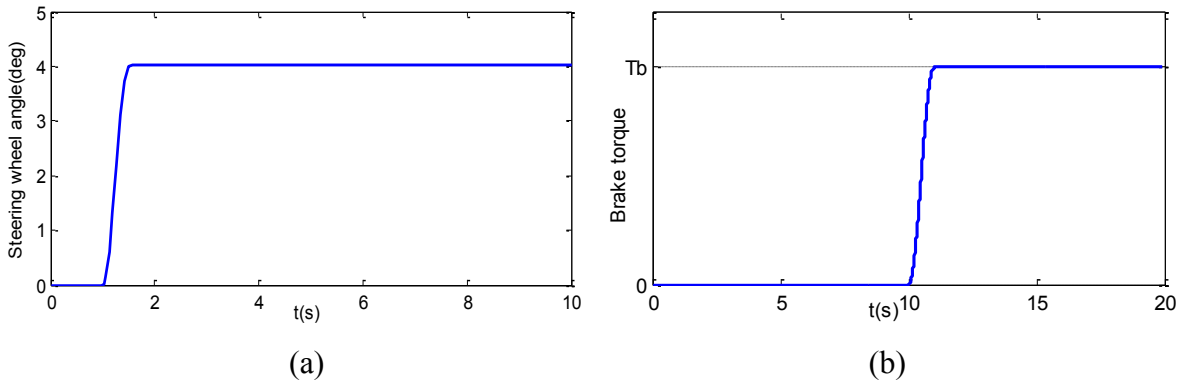


Figure 5.5: (a) Steer angle; and (b) braking torque during the braking in a turn maneuver.

Figure 5.6 compares the longitudinal slip ratio developed at the inner wheels of the vehicle with conventional AFS and AIFS systems under the inputs described in Fig. 5.5 and $\mu=0.78$. The figure also shows the rear wheels slip ratio. Furthermore, it is necessary to maintain certain tractive force at the rear wheels in order to maintain the constant forward speed during steady turning prior to application of the braking torque. These results further show that the front tire of the vehicle equipped with AIFS develops the least slip ratio and could thus accommodate

relatively higher braking torque before reaching the slip ratio limit. This is attributed to the fact that AIFS, by its design, limits the work-load at the inner tire during turning and thereby permits sufficient adhesion reserve.

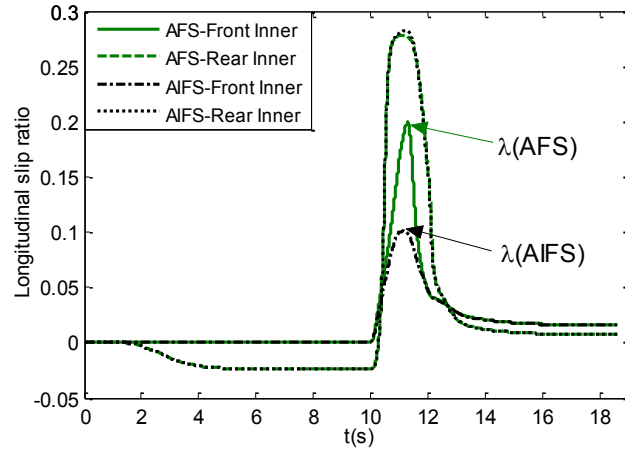


Figure 5.6: Comparisons of longitudinal slip ratios of the inside tires of the vehicle with AFS and AIFS control ($T_b=5580$ Nm, $\mu=0.78$ at 57 km/h).

Braking-in-turn simulations are carried out considering a range of road-tire adhesion levels at the highest possible vehicle speed prior to the potential rollover (57 km/h for $\mu=0.78$). A parametric study is also carried out to verify the performance limits of the AIFS for a range of operating conditions such as vehicle weight and location of vehicle center of gravity. In all cases, the performance characteristics of the AIFS system are compared with those of the conventional AFS control to highlight the potential merits of the AIFS control.

5.4 Results and Discussions

Table 5.1 compares the braking-in-turn performance of the vehicle with AFS, AIFS and in the absence of the steering control (NC) in terms of the stopping time and distance on road surfaces with $\mu=0.78$ and $\mu=0.5$ at speeds of 57 and 52 km/h, respectively. Lower speed for the

low friction road is considered to ensure safer handling response, where the inner tire work-load approached 0.94 for the vehicle with the AFS control. The table also presents the maximum braking torque that could be applied prior to the front inner tire reaching the limiting value of the slip ratio in each case. The slip ratio for the dry road was limited to 0.2 and 0.125 for the low friction road. The results suggest that the vehicle without the steering control can be given considerably larger braking torque than the conventional AFS, which would lead to shorter stopping time. This is, however, achieved at the expense of poor directional control and relatively larger radius turn compared to the active steering systems. The stopping distances for the vehicle without the control are thus not presented in the table. An opposite trend, however, is evident on the low friction road. The results show that the AIFS control allows significantly larger braking torque for both the road surfaces, when compared to the AFS. As a result, the AIFS yields over 17% reduction in the stopping distance compared to the conventional AFS. The AIFS could thus lead to superior handling performance under braking during a turn.

Table 5.1: Comparisons of the braking characteristics of the vehicle with conventional AFS, AIFS and without steering control (NC) on two different road surfaces ($\delta_{st} = 0.07$ rad).

Adhesion coefficient, vehicle speed and longitudinal slip ratio limit	$\mu = 0.78; V = 57 \text{ km/h}; \lambda^* = 0.2$			$\mu = 0.5; V = 52 \text{ km/h}; \lambda^* = 0.125$		
	Without Control	AFS	AIFS	Without Control	AFS	AIFS
Max T_b , Nm	6270	5580	6945	4020	6575	8155
Stopping time, s	7.7	8.6	7.1	9.1	6.4	5.4
Stopping distance, m	NA	69.3	58.9	NA	49.3	27.9

Further in-sight on the relative performances of the steering controllers can be obtained from the time histories of the selected directional responses. Figure 5.7 illustrates variations in the path trajectory, yaw rate, forward speed, and longitudinal and lateral acceleration responses of the

vehicle with the two steering controllers. The path trajectory and yaw rate responses of the vehicle without the steering control are also presented. The results show that the vehicle without control cannot achieve the target response (Figs. 5.7(a) and 5.7(b)), while both the active steering systems yield similar direction responses, except that the AIFS can be given larger braking torque leading to lower stopping distance while closely following the handling target. This is evident from the forward speed and longitudinal acceleration responses in Figs. 5.7(c) and 5.7(d).

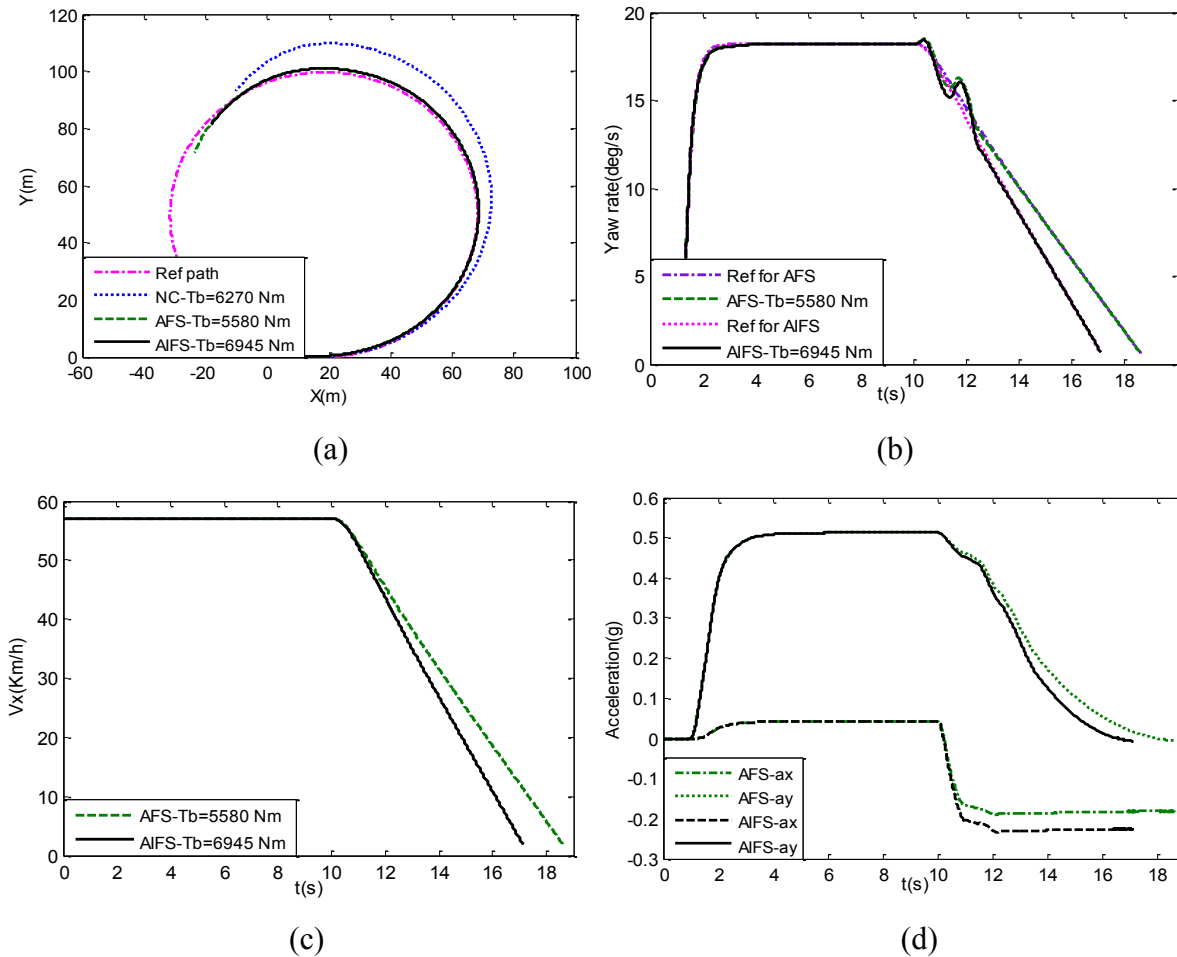


Figure 5.7: Comparisons of directional responses of the vehicle with conventional AFS and AIFS control and without steering control: (a) path trajectory; (b) yaw rate; (c) longitudinal velocity; and (d) longitudinal and lateral accelerations ($V=57$ km/h, $\mu=0.78$).

Although both the active control strategies track the target path and the yaw rate for the given steering input, major differences exist between the two systems in terms of how the target response is realized and the effect of braking immediately after the brakes are applied. Figure 5.8 presents the time histories of the corrective steering angles generated by AFS and AIFS, and the resulting tire work-loads of the steered wheels. The conventional AFS system increases the steer angles at both the wheels considering the fixed pro-Ackerman geometry in order to realize the target response at a given speed, as seen in Fig. 5.8(a). The oscillations in the steer angles are observed immediately following the braking application ($t \geq 10$ s) as the speed decreases and the vehicle tends to deviate slightly from the target path. As the vehicle speed becomes very low, little or no steering correction is required for tracking the target.

The AIFS control, on the other hand, generates the steer angles following anti-Ackerman geometry to track the target response, while limiting the inner tire work-load to a predefined level of 0.65 during constant speed turning. The work-load of the inner steered tire tends to be considerably higher with the AFS control, as seen in Fig. 5.8(b). The work-load limit of 0.65 was chosen for AIFS to ensure sufficient adhesion reserve to meet the braking demand [140,147]. The oscillations in the steer angles occur following the application of braking to compensate for the reduced speed of the vehicle. The AIFS correction, however, follows the pro-Ackerman ratio similar to the AFS control, when steady braking torque is achieved. The peak inner tire work-load approaches near 1 for both systems, although the AIFS imposes considerably higher braking torque compared to the AFS corresponding to the slip limit of 20%, as seen in Table 5.1.

Considerable differences in the inner wheel slip angle and slip ratio are further evidenced in Fig. 5.9. While the front wheel slip angles of the vehicle with AFS and AIFS controllers differ

considerably, the inner wheels of both the systems approach the limiting longitudinal slip ratio. The longitudinal slip ratios of the outer tire with significantly larger normal load, however, approach a very low value near 0.03. It should be pointed out that no attempt is made maximize the braking performance of the vehicle equipped with the AIFS system.

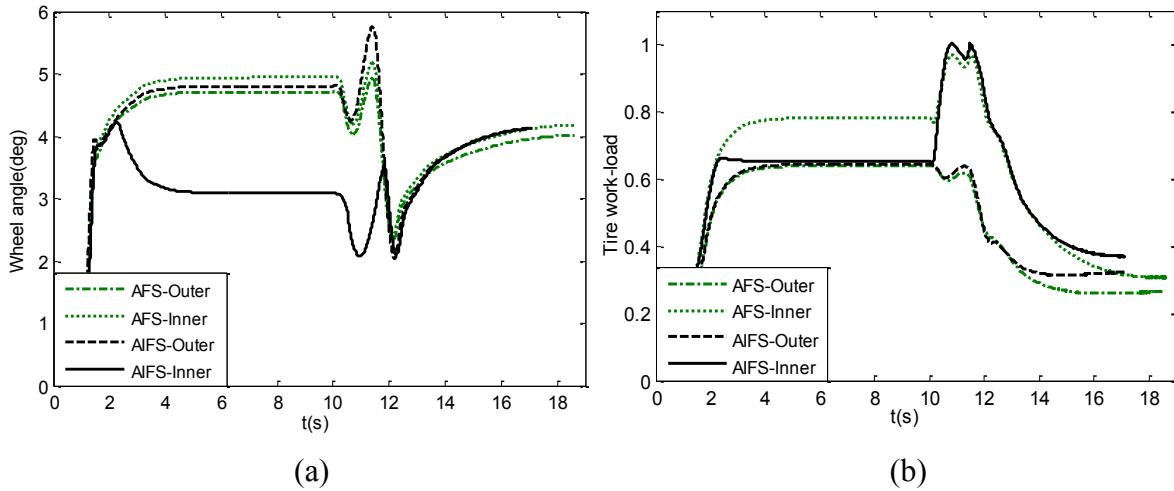


Figure 5.8: Inner and outer wheels (a) steer angle; and (b) work-load responses of the vehicle models with conventional AFS and AIFS control ($V=57$ km/h, $\mu=0.78$).

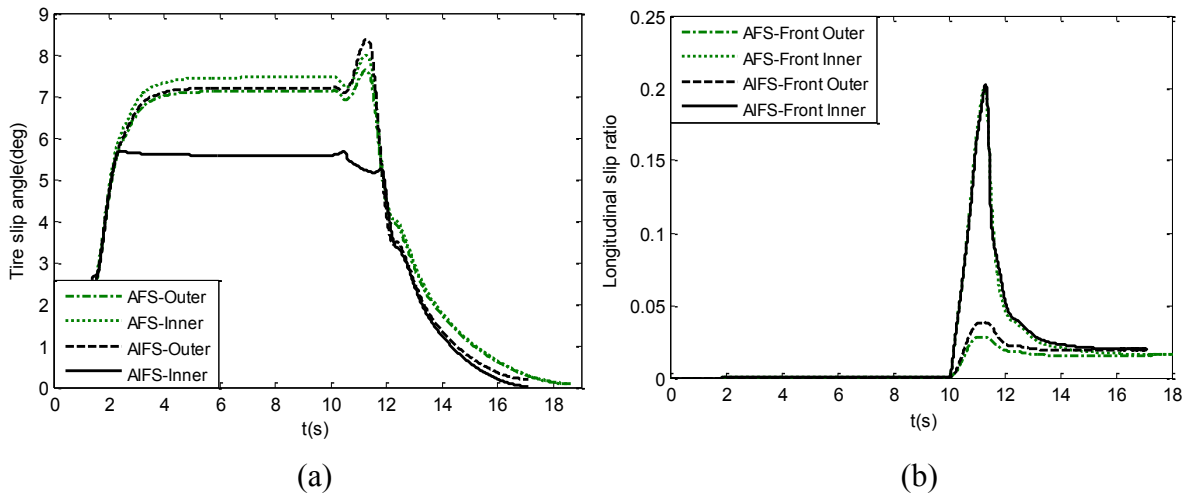


Figure 5.9: Comparisons of (a) tire slip angle; and (b) longitudinal slip ratio responses of the vehicle model with conventional AFS and AIFS control ($V=57$ km/h, $\mu=0.78$).

5.4.1 Effect of road friction

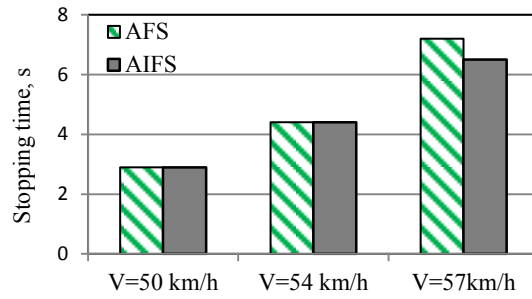
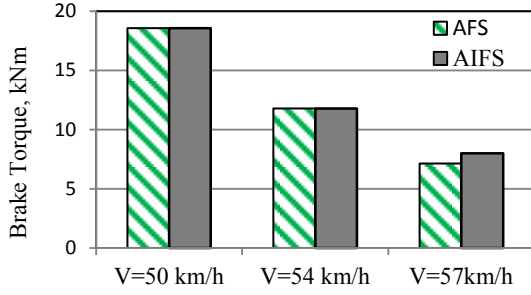
The effectiveness of the AIFS is examined for a range of road-tire adhesion coefficients considering uniform as well as split- μ road conditions at different forward speeds ($V = 50, 54$ and 57 km/h). For the given steady turn input, the braking responses of the vehicle are evaluated in terms of maximum brake torque and stopping time for uniform and split- μ road conditions with adhesion coefficient ranging from 0.5 to 0.9. Simulations are performed considering the maximum allowable braking torque corresponding to the inner front tire slip ratio (λ^*) along with ideal braking force distributions, which are summarized in Table 5.2.

Table 5.2: Critical slip ratio and braking distribution for different road adhesion coefficients ($\delta_{st} = 0.07$ rad)

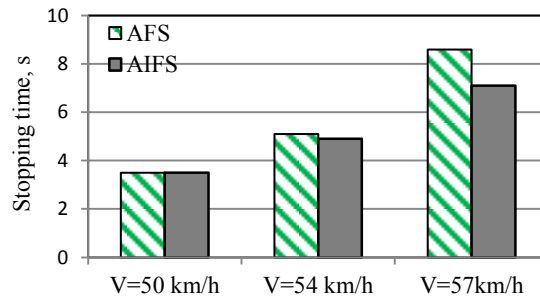
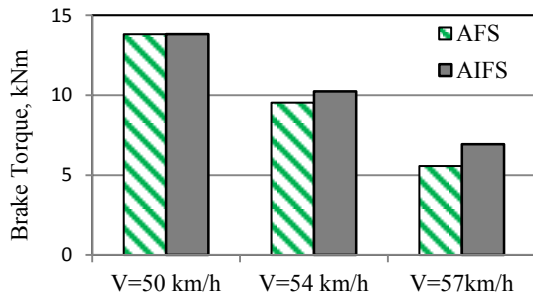
Adhesion coefficient	λ^*	k_{bF}	k_{bR}
0.9	0.25	0.83	0.17
0.78	0.20	0.78	0.22
0.6	0.15	0.70	0.30
0.5	0.125	0.66	0.34
Split-road 0.78/0.5	0.15	0.66	0.34

Figure 5.10 compares the maximum braking torque and the stopping distance responses of the vehicle model with the AFS and AIFS for different forward speeds: 50, 54 and 57 km/h. As it would be expected, the braking effort that can be applied decreases with decreasing adhesion coefficient or increasing handling demand. The AIFS outperforms the conventional AFS system, irrespective of the road adhesion coefficient considered in the simulation. The effectiveness of the AIFS system on a dry road surface, however, is evident only at the higher speed. The AIFS system yields relatively better braking performance compared to the AFS system on lower friction roads. For instance, the maximum brake torque for the AIFS is 57.7% larger than that of

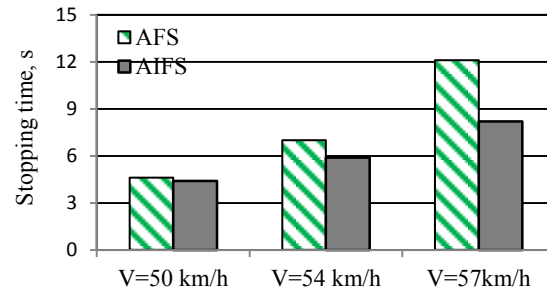
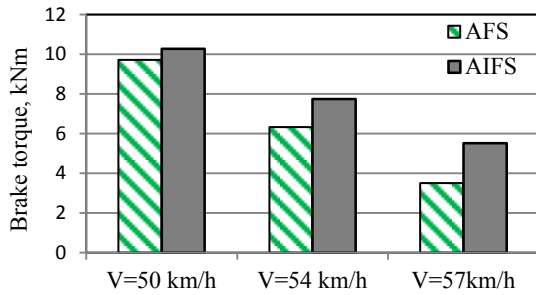
$\mu = 0.9$



$\mu = 0.78$



$\mu = 0.6$



Split- μ

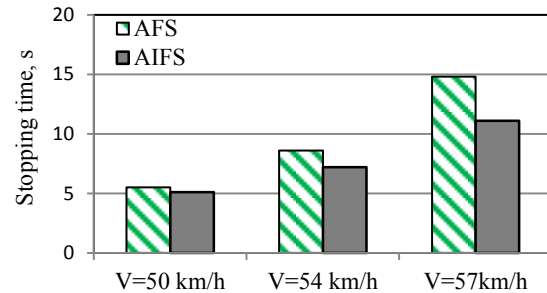
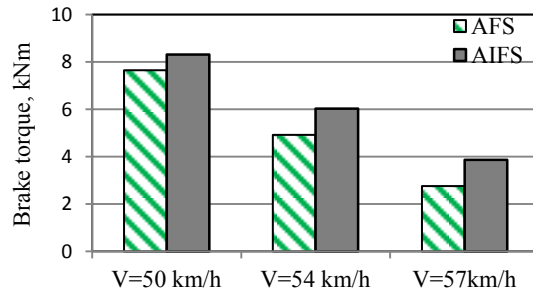


Figure 5.10: Comparisons of maximum brake torque and stopping time of the vehicle model with conventional AFS and AIFS systems for a range of speeds and adhesion coefficients.

the AFS for road surface with adhesion coefficient of 0.6, while the stopping time is 32.2% lower. Furthermore, the braking performance of the vehicle with AIFS on the split- μ road surface, with lower friction at the inner tire, is very similar to that on a uniform low friction surface.

Despite the substantial gains in the maximum braking torque and thereby the stopping distance on low friction surfaces, as seen in Table 5.1 and Fig. 5.10, the AIFS control yields handling responses similar to those of the vehicle with the conventional AFS. In the absence of the steering control, the vehicle maneuver on road surface with $\mu=0.5$ develops very high side-slip angle and tends to become unstable, as seen in Fig. 5.11. Both the active steering systems, however, yield comparable side-slip angle and path tracking performance. Further simulation results obtained for a braking-in-turn maneuver on road surfaces with $\mu \leq 0.2$ revealed that the baseline vehicle tends to be less understeer. Consequently, the active steering controllers would be more beneficial in reducing the steer angles at higher speeds. The relative advantages of the AIFS over the AFS would thus diminish for very low friction surfaces.

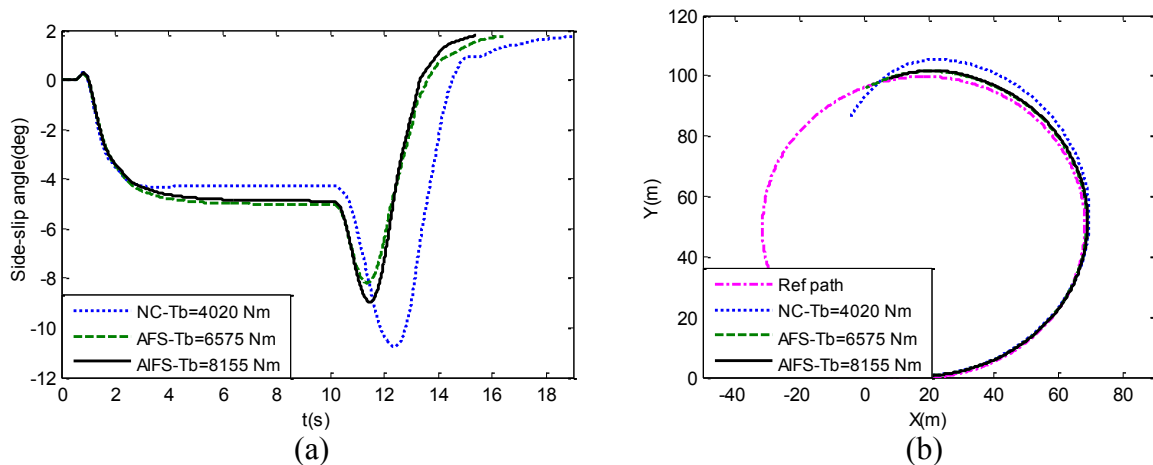


Figure 5.11: Comparisons of (a) side-slip angle; and (b) path trajectory of the vehicle model without active steering (NC), conventional AFS and AIFS control on a low friction road ($\mu = 0.5, V=52$ km/h).

5.4.2 Vehicle weight and mass center coordinates

It has been shown that the AIFS is particularly beneficial in situations leading to greater load transfers [140]. The AIFS response characteristics are thus investigated considering variations in the vehicle load, and longitudinal and vertical coordinates of the mass center (CG). Figure 5.12(a) illustrates the variations in the steering demand of the vehicle with AIFS in order to track the target responses during a braking and turning maneuver under three different load conditions: full-load, half-load and no-load. As the results show, the steer angles required for the half-load and no-load cases are significantly lower, which also lead to significantly lower inside wheel tire-work load (Fig. 5.12(b)). The results clearly demonstrate the increasing oversteer tendency of the vehicle as the load is decreased.

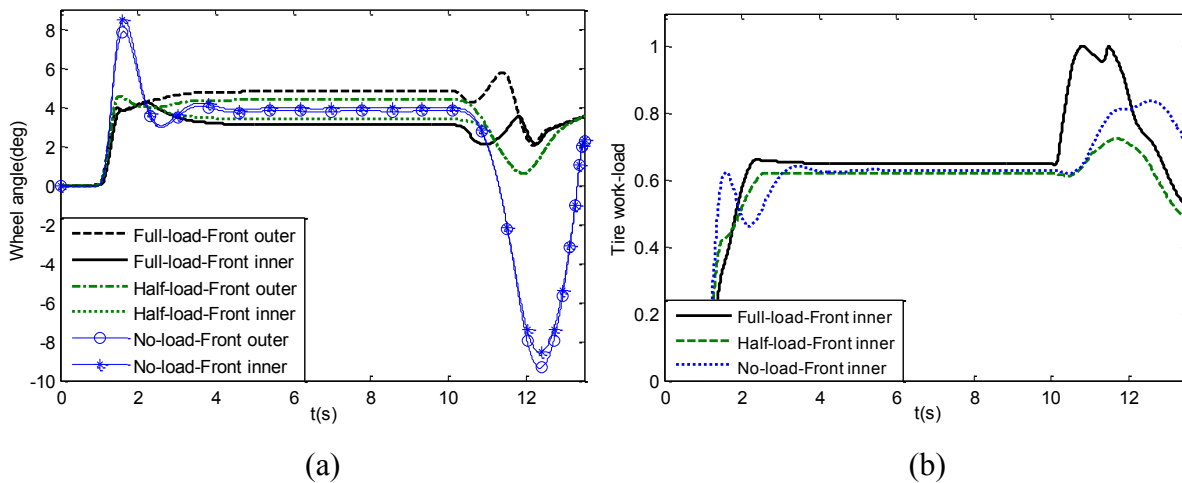


Figure 5.12: Comparisons of (a) steered wheel angles; and (b) inner tire work-load developed with AIFS for different loading conditions ($T_b=6945$, $V =57$ km/h and $\mu =0.78$).

The AIFS yields greater performance gains for vehicles with relatively higher load transfers, which are strongly dependent upon the mass center coordinates (CG). The effects of variations in the CG coordinates are thus investigated for the fully loaded baseline truck. Simulation results obtained for the nominal vehicle ($h_{cg} = 1.56$ m) at 57 km/h revealed vehicle rollover for

$b < 1.91$ m (longitudinal distance between the front axle and the CG) and oversteer response for $b > 2.07$ m. The braking performance characteristics of the vehicle are thus evaluated for these extreme values of b , which are summarized in Table 5.3 in terms of the braking torque corresponding to limiting slip ratio and the stopping time. The second column lists the responses of the fully-loaded baseline vehicle, which show over 24% higher braking torque and 17% lower stopping time for the AIFS compared to the AFS control. The results suggest that the brake torque and stopping time of the vehicle with AIFS are, respectively, nearly 32% higher and 21% lower than that of the vehicle with AFS, when the CG shifted only slightly forward from 1.98 m to 1.91 m. Shifting the CG towards the rear axle ($b = 2.07$ m) deteriorated the braking performance of the both the steering controllers, which is attributed to oversteer behavior of the vehicle. In this situation, the advantage of AIFS over the AFS is relatively less significant. The AFS control resulted in nearly 11% lower brake torque and 7% higher stopping time compared to the baseline vehicle and accordingly, the corresponding changes with the AIFS control are nearly 18% and 17%.

The influence of CG height on the relative braking performance of AFS and AIFS control is also evaluated considering a lower CG height ($h_{cg} = 1.34$ m) and the higher limiting speed of 62 km/h. The results are also obtained for the lower speed of 57 km/h and summarized in Table 5.3. Reducing the CG height diminishes the lateral load transfer and thereby the performance gains of the AIFS control. The performance benefits of the AIFS are evident when the speed is increased to 62 km/h, which is due to higher load transfer. The AIFS control in this case yields nearly 24% lower stopping time and 40% higher brake torque compared to the AFS control. The results

confirm that the AIFS control is more beneficial under more severe maneuver conditions that cause greater load transfers.

Table 5.3: Effect of variations in CG height and longitudinal coordinate on the stopping time and brake torque of the vehicle with AFS and AIFS control ($\delta_{st} = 0.07$ (rad), $\mu = 0.78$).

Speed (km/h)	57		57		57		62			
b	1.98		1.91	2.07	1.98					
hcg	1.56		1.56		1.34					
Steering control	AFS	AIFS	AFS	AIFS	AFS	AIFS	AFS	AIFS	AFS	AIFS
Stopping time (s)	8.6	7.1	8.4	6.6	9.2	8.3	5.0	4.6	9.0	6.8
Braking torque (kNm)	5.6	6.9	5.9	7.8	5.0	5.7	10.3	11.2	5.5	7.7

5.4.3 Robustness of the AIFS control

Apart from the variations in the operating parameter, a road vehicle is often subjected to undesired external disturbances and design parameters uncertainties. The robustness of the simple PI controller synthesis used in this study is evaluated considering uncertainties in a vehicle parameter through sensitivity analyses. In particular, the analysis is performed considering variations in the tire cornering stiffness, which is widely known to be less certain [55]. The sensitivity of the AIFS control to variations in a vehicle parameter is investigated using the additive perturbation control method, where a parametric uncertainty is described by a perturbation function $\Delta M(s)$ bounded in magnitude to obtain the transfer function of the perturbed system, as [144]:

$$M^*(s) = M(s) + \Delta M(s) \quad (5.13)$$

where $M(s)$ is the open loop transfer function incorporating the transfer functions of the plant $D(s)$ and the controller $D_c(s)$ in a closed-loop unity feedback arrangement, as seen in Fig.

5.13(a). $M^*(s)$ is the transfer function of the perturbed system.

It is assumed that $M^*(s)$ and $\Delta M(s)$ have the same number of poles in the right-hand side in the s -plane, if any. The stability of the system will be retained in the entire frequency range, provided:

$$|\Delta M(j\omega)| < |1 + M(j\omega)| \quad (5.14)$$

where ω is the frequency. The relative sensitivity S of the closed-loop system N to a perturbation in the plant model $D(s)$ can be expressed as:

$$S(s) = \frac{\Delta N/N}{\Delta D/ND} = \frac{1}{1 + M(s)} \quad (5.15)$$

where ΔD and ΔN , respectively, denote the changes in plant transfer function $D(s)$, and the closed-loop transfer function of the system $N(s)$, which can be expressed as:

$$N(s) = \frac{D(s)D_c(s)}{1 + D(s)D_c(s)} \quad (5.16)$$

Equations (5.14) and (5.15) yield following relation between the sensitivity and perturbation functions in frequency domain:

$$|\Delta M(j\omega)| < \left| \frac{1}{S(j\omega)} \right| \quad (5.17)$$

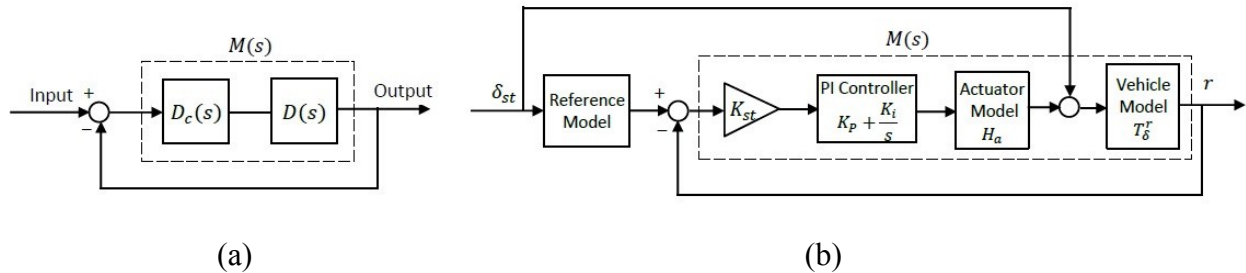


Figure 5.13: (a) Unity-feedback plant and controller functions; and (b) closed-loop system integrating the AIFS controller and actuator model.

Figure 5.13(b) shows the transfer function of the system comprising the vehicle model, the PI controller and the AIFS actuator model H_a . The closed-loop transfer function of the system then could be defined considering nominal cornering stiffness, while the variations in the tire cornering stiffness could be expressed by a bounded perturbation function.

The sensitivity analysis and the controller robustness is investigated considering $\pm 80\%$ variations in the front and rear tires' stiffness, ranging from 34 to 306 kN/rad and 23 to 207 kN/rad, respectively, with side-slip angle ranging from 0° to 15° . The nominal cornering stiffness of each front and rear tires are taken as 170 and 115 kN/rad, respectively. The stability limit of the closed loop system is evaluated in the 0.01 to 10 rad/s frequency range considering the above-stated variations in the cornering stiffness. Figure 5.14 illustrates the magnitude responses of the perturbation function $\Delta M(j\omega)$ corresponding to minimum and maximum values of tires' cornering stiffness.

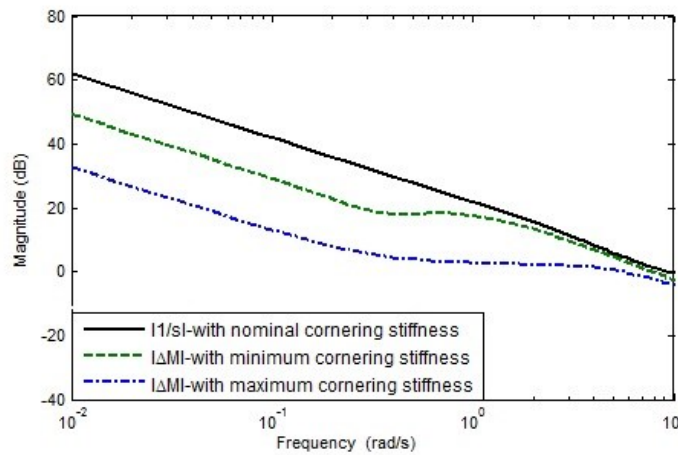


Figure 5.14: The robust stability criterion showing magnitudes of the perturbation function with maximum and minimum tire cornering stiffness.

The figure also presents the inverse sensitivity function, $1/S(j\omega)$, of the closed-loop system with nominal tires' cornering stiffness. It is evident that the magnitudes of the perturbation

functions are less than those of the inverse sensitivity function over the entire frequency range considered. It can thus be concluded that the controller synthesis would assure stability of the closed-loop system over a wide range of variations in the tire cornering stiffness. The simulation results also revealed varying the stiffness beyond 80% would violate the stability criterion.

5.4.4 Disturbance rejection

Disturbance attenuation performance of the controller is further examined in the presence of a side wind force as well as straight-line braking on a split- μ surface (left track- $\mu_l = 0.2$; right-track- $\mu_r = 0.78$). Although μ is not an input to the system, it may change arbitrarily depending on change in road condition. A change in this parameter is thus considered as a disturbance to the system. For the straight line driving maneuvers, a simple driver model, described by a PID function [146], was integrated in the vehicle model. The gains of driver model were tuned considering an average driver with minimal driving effort such that $K_p = 0.02$, $K_I = 0.01$ and $K_D = 0.01$. The cross-wind disturbance was described by a 8 kN impulse force with 3.5 s duration and center of pressure located 0.5 m ahead of the vehicle mass center so as to impose a yaw moment disturbance. Figure 5.15 compares the lateral path deviation of the vehicle models with AIFS and without a steering controller (NC), when subjected to the side force at forward speeds of 80 and 120 km/h on a road with $\mu = 0.78$. The results clearly illustrate beneficial performance of the AIFS control in limiting the side-wind disturbance effect, irrespective of the vehicle speed considered. The AIFS control thus yields enhanced directional stability compared to the performance that may be expected from the driver model representing an average driver.

The lateral path deviations of the vehicle models with AIFS and without the steering control,

while braking on a split- μ road surface are compared in Fig. 5.16. The results are obtained considering $T_b=6000$ Nm and $V=100$ km/h. The results suggest that in the absence of the AIFS there exist the potential for instability during braking on split- μ surface at a high speed even with simple driver model. The proposed AIFS controller, however, effectively tracks the desired path and compensates for the destabilizing moment.

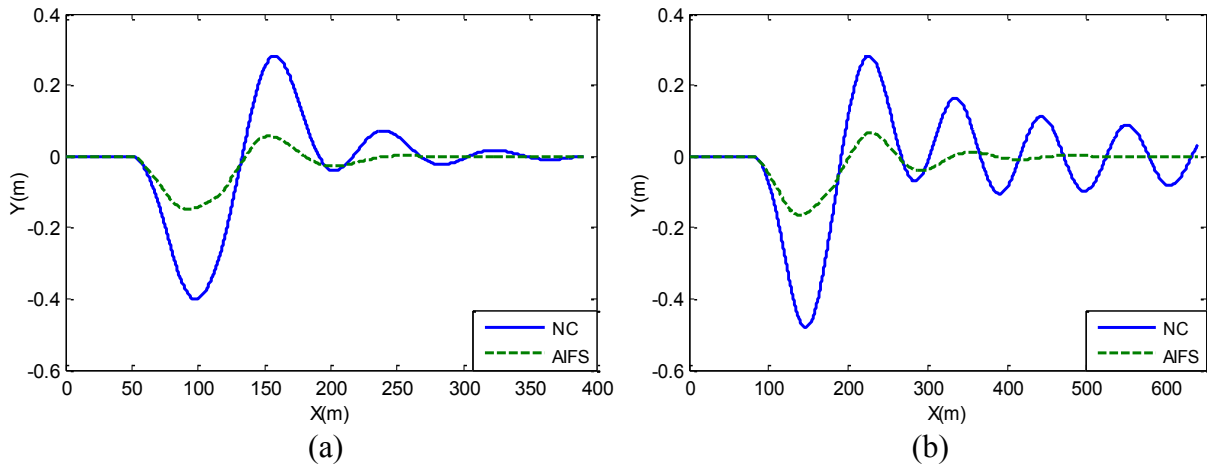


Figure 5.15: Comparisons of the lateral path deviations of the vehicle models with AIFS and without a steering control (NC) under a 8 kN side force disturbance: (a) $V=80$ km/h; and (b) $V=120$ km/h.

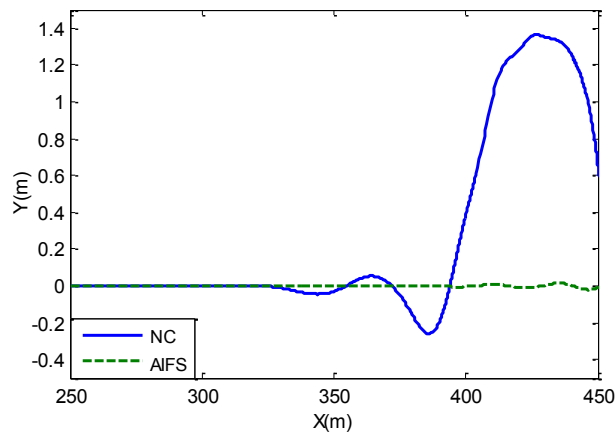


Figure 5.16: Comparison of path deviations of the vehicle models with AIFS and without a steering control (NC) under braking on a split- μ surface ($V=100$ km/h, $T_b=6$ kNm).

5.5 Conclusion

The performance gains of the active independent front steering (AIFS) system are investigated under braking through simulation of a nonlinear three-dimensional model of a two-axle truck. The AIFS control strategy was synthesized using a proportional-integral (PI) yaw rate feedback controller to generate corrective steering of the left and right wheels through tracking of the reference yaw rate. The steering corrections were synthesized considering the tires saturation limit, while ensuring sufficient adhesion reserve for meeting the braking force demand. The effectiveness of the AIFS system was evaluated under braking-in-turn maneuvers for a range of road-tire adhesion limits at the highest vehicle speed prior to the potential rollover. The AIFS control permitted greater braking torque and thereby resulted in substantially lower stopping time compared to the conventional AFS system. The results suggested that the independent control of steer angles could yield improved braking performance of a heavy vehicle compared to the AFS, particularly at higher speeds. The effectiveness of the AIFS on dry road surfaces was apparent only at very high speeds representing braking during extreme handling maneuvers. The AIFS control however revealed superior braking performance on low friction surfaces. From the simulation results, it was further concluded that the AIFS control could yield enhanced braking performance during extreme maneuvers on all the road surfaces provided that the vehicle handling characteristics remain understeer. The AIFS revealed performance similar to that of the AFS when the vehicles characteristics become less understeer, which is due to reduced steering correction demand of the less understeer or oversteer vehicle. The AIFS controller synthesis also revealed stability of the closed-loop vehicle system over a wide range of variations in the tire cornering stiffness, and while braking on a split- μ road surface.

CHAPTER 6

CONCLUSIONS AND RECOMMENDATIONS

6.1 Highlights and Major Contributions of the Dissertation Research

This dissertation research contributes towards the development of a comprehensive active chassis control system for enhancement of safety performance of road vehicles under emergency-type steering and braking maneuvers. The study particularly focused on an active steering system that could realize near optimal cornering and braking/traction force distributions between the two steered wheels while realize a target response. An extensive critical review of recent developments in active chassis system technologies demonstrated the limitations of conventional active front steering (AFS) system under extreme maneuvers. Although AFS integrated with direct yaw-moment control (DYC) by selective braking have been shown to improve the performance range, several related disadvantages and drawbacks have also been reported. The present investigation thus proposed an innovative alternative active steering system using Active Independent Front Steering (AIFS) concept that could introduce a corrective steer angle at each wheel in an independent manner. A PI controller was synthesized to generate corrective steer angle for the left- and right-wheels such that the work-load at the steered tires were nearly equal ensuring reserve for longitudinal force capability if required. The study is conducted through extensive simulations of a four-wheel vehicle model with the controller to examine the effectiveness of the AIFS during extreme maneuvers over a wide range of operating conditions. The study was next extended to examine the effectiveness of the proposed concept for braking in a turn performance of a heavy vehicle under different conditions. The robustness

of the controller was also tested for possible uncertainties. A mechanical system design that can be adapted for implementation for the AIFS concept was finally explored in this investigation. The major highlights of the dissertation work are summarized below, which is followed by specific conclusions drawn and recommendations for future studies.

- A four-wheel yaw plane model incorporating the effects of lateral and longitudinal load shifts was developed to study the concept of AIFS where independent steering of the right- and the left-wheels could be assigned. Limited validation was carried out by comparing the results with those of CarSim and ADAMS.
- The nonlinear tire model for the vehicle was formulated using “Magic Formula” where the coefficients were established based on actual experimental data acquired from other research groups for car and truck tires. The capability of the model to include the interaction between the longitudinal and the lateral forces generated under combined braking and steering inputs was retained.
- The AIFS control strategy for equalizing work-load was formulated using a PI feedback controller to track the reference yaw rate corresponding to the neutral steer condition. The dynamics of the steering actuator was incorporated in the model considering its limited bandwidth. A first-order function was also used to compensate for the system delay and making the simulation response to change more realistic.
- Upon identification of the inner and outer wheel during a maneuver, the synthesized controller distributed the correction between the inner and outer wheels based on maximum utilization of the available tire-road adhesion limits. Normalized cornering stiffness was thus introduced to identify the saturated slip angle based on instantaneous normal load on tire. By

tuning this parameter, tire work-load equal to 0.65 was chosen as the limit for inner tire saturation with an objective of near equalizing the tire work-loads.

- In view of preliminary results and sensitivity to load transfer, the model was extended to simulate heavy cargo truck to examine the effects of load as well as partially-filled liquid cargo on the effectiveness of AIFS.
- Extensive simulation results were obtained for the truck model integrating with conventional AFS control and the proposed AIFS systems subjected to a range of steering maneuvers, namely: a J-turn maneuver on uniform and split- μ road condition, as well as path change and obstacle avoidance maneuvers to demonstrate the effectiveness of AIFS during extreme cases.
- For the purpose of the combined braking in a turn study, a single-unit truck model with 8-DOF was formulated including the longitudinal, lateral, yaw and roll motions of the vehicle as well as rotational motions for each of the four wheels.
- The effectiveness of the vehicle equipped with the proposed AIFS system was evaluated for braking-in-turn maneuvers under a range of road-tire adhesion levels. The brake torque limit that can be applied to the front axle was dictated by longitudinal slip corresponding to peak tire force. The braking performance during a handling maneuver was established in terms of peak brake torque and stopping distance.
- A parametric study of braking performance was also carried out to verify the performance limits for a range of operating parameters such as vehicle weight and location of vehicle center of gravity. In all cases, the results of the AIFS system are compared with those of conventional AFS control in order to highlight the advantages of the AIFS control.

- The robustness of the AIFS controller synthesis was studied over a wide range of variations in the tire cornering stiffness, and while braking on a split- μ road surface.
- An extensive review of literature was carried out to explore possible steering system configurations to realize independent control of steering angles required for the AIFS concept. A mechanical system using planetary gears was explored for application of AIFS concept for road vehicles in a fail-safe manner. A first prototype has been developed to examine the functionality of the mechanism for AIFS concept.

6.2 Conclusion

Numerous simulation studies carried out in this investigation and analysis of results for conventional AFS and AIFS systems led to many observations and conclusions regarding limitations of AFS and performance potentials of AIFS concepts. The major conclusions drawn on various aspects of this study are summarized in the following:

- The results for pure handling (steering) maneuver show that while both the AFS and AIFS can theoretically generate the target response to a steering command, the AFS control causes the inner wheel to saturate under high lateral acceleration maneuvers as the normal load on the wheel diminishes, while the adhesion at the outer tire will remain underutilized.
- A simple PI controller monitoring the tire force saturation was found adequate to effectively limit the work-load at the inner wheel and simultaneously generate the required lateral force for target response by introducing additional correction at the outer wheel.
- It is concluded that the best control approach would be to use AIFS controller to generate and apply the steering corrections following the Ackerman geometry at low to moderate speeds similar to a conventional AFS. At higher speeds or extreme maneuvers, however, the

controller will introduce the correction at the outer wheel to generate the required lateral force and reduce the steering angle applied to the inner wheel to ensure its adequate adhesion with the road.

- The threshold value for the inner tire work-load was selected as 0.65, since this was found to nearly equalize the tire work-loads at both the wheels prior to reaching the stability or rollover threshold for the vehicle-tire combination considered. Such a strategy in AIFS control would ensure a reserve at both tires for generating longitudinal force for traction or braking during the handling maneuver.
- The results obtained for heavy vehicles with solid and liquid cargo including partial loads, show superior active control performance of the vehicle with AIFS systems. This is attributed to the fact that the concept of independent control based on normal load on tires is more appropriate for vehicles with higher CG and greater lateral load transfer during a turn.
- The effectiveness of the proposed control strategy was evaluated under extreme driving conditions such as high-speed turning, single and double lane change maneuvers and on different road conditions including uniform as well as split- μ surfaces to demonstrate the superiority of the AIFS system
- The results obtained in terms of maximum brake torque that can be applied, stopping time and stopping distance attained during braking-in-turn maneuvers suggested that the independent control of steer angle could provide highly significant improvement when compared with that of conventional AFS system as well as the vehicle without a controller.
- The superiority of AIFS in comparison to a conventional AFS system for braking-in-turn performance was demonstrated during all extreme maneuvers and on all road surfaces as

long as the vehicle handling characteristics remain understeer. Its effectiveness, furthermore, was shown to increase rapidly as the friction between the tire and road is reduced.

- The parametric study performed with respect to different loading conditions and the longitudinal and vertical location of the CG also demonstrated that AIFS concept will be superior under all design and operating conditions as long as the vehicle remains understeer. As the vehicles characteristics become less understeer or even oversteer, the AIFS performance approaches same as that of conventional active steering systems.
- The robustness of the designed PI controller was finally evaluated by examining its sensitivity to parameter perturbations such as tire cornering stiffness and in the presence of external disturbance such as lateral wind force and straight-line braking on split- μ surface. The controller was found to be robust for the uncertainties considered in this investigation as long as the rear wheels are not locked.
- The functionality of the mechanical steering mechanism was evaluated using its first prototype to demonstrate the feasibility of implementing AIFS concept in a fail-safe manner.

6.3 Recommendations for Future Studies

The proposed AIFS concept and mechanism offer attractive potentials for enhancing the directional responses of road vehicles especially those with higher propensity for load transfer. The synthesized AIFS control can further ensure sufficient adhesion reserve in the event of a braking demand. Although the simulation results obtained with the AIFS controller revealed enhanced directional and longitudinal dynamic response under a wide range of steering and braking maneuvers, further studies are essential prior to any implementation of such concept. A

number of further studies including testing are thus recommended in the following that may be undertaken for successful implementation of the AIFS system.

- The model used for the simulation studies can be enhanced by including roll and pitch dynamics as well as suspension compliances for improved prediction of instantaneous tire normal loads. Although this will not change the outcome or conclusions drawn from this study, it will help to design and implement a real time controller more accurately.
- It would be important to integrate the driver model with the AIFS controller in a closed-loop manner and study the effects of the driver interference based on his/her perception to vehicle responses with those generated by AIFS control.
- The effectiveness of the synthesized PI controller could be compared with other robust controllers such as robust H_∞ or MPC controllers in the presence of both internal and external perturbations.
- Alternate indicators can be explored for possible improvement in the prediction of instantaneous tire saturation level. In order to improve the directional stability of the vehicle, the side-slip angle may also be controlled along with the yaw rate response of the vehicle in critical turning maneuvers.
- It is suggested to develop a virtual multi-body model of the vehicle so as to evaluate the dynamic responses of the vehicle considering the kinematics and dynamics of the proposed AIFS mechanism.
- As a follow up to the first prototype, a more refined design of steering mechanism incorporating worm gear and appropriate step motors should be manufactured for

experimental study such as hardware-in-the-loop-simulations (HILS) prior to further possible road test of the AIFS concept.

REFERENCES

- [1] Ackermann, J., Bünte, T. and Odenthal, D. (1999) Advantages of active steering for vehicle dynamics control, *In Proceedings of International Symposium on Automotive Technology and Automation*, Vienna, Austria.
- [2] Kasselmann, J. and Keranen, T. (1969) Adaptive steering, *Bendix Technical Journal*, 2(3), 26–35.
- [3] Shibahata, Y., Shimada, K. and Tomari, T. (1993) Improvement of vehicle maneuverability by direct yaw moment control, *Vehicle System Dynamics*, 22(5-6), 465-481.
- [4] Van Zanten, A., Erhardt, R. and Pfaff, G. (1995) VDC, the vehicle dynamics control system of BOSCH, *SAE Technical Paper no. 950759*.
- [5] Bedner, E. and Chen, H.H. (2004) A supervisory control to manage brakes and four-wheel-steer systems, *SAE Technical Paper no. 2004-01-1059*.
- [6] Mirzaei, M. (2010) A new strategy for minimum usage of external yaw moment in vehicle dynamic control system, *Transportation Research Part C: Emerging Technologies*, 18(2), 213-224.
- [7] Ding, N. and Taheri, S. (2010) An adaptive integrated algorithm for active front steering and direct yaw moment control based on direct lyapunov method, *Vehicle System Dynamics*, 48(10), 1193-1213.
- [8] Huang, J., Huang, Q. and Cheng, A. (2011) Robust braking/driving force distribution and active front steering control of vehicle system with uncertainty, *SAE Technical Paper no. 2011-01-2145*.
- [9] Selby, M., Manning, W.J., Brown, M.D. and Crolla, D.A. (2001) A coordination approach for DYC and active front steering, *SAE Technical Paper no. 2001-01-1275*.
- [10] Zheng, B. and Anwar, S. (2009) Yaw stability control of a steer-by-wire equipped vehicle via active front wheel steering, *Mechatronics*, 19(6), 799-804.
- [11] Oncu, S., Guvenc, L., Otosan, S.E.F., Otosan, N.K.F. and Otosan, M.S.F. (2007) Steer-by-wire control of a light commercial vehicle using a Hardware-in-the-Loop test setup, *SAE Technical Paper no. 2007-01-4198*.

- [12] Oh, S.W., Yun, S., Chae, H.C., Jang, S.H. and Jang, J.H. (2003) The development of an advanced control method for the steer-by-wire system to improve the vehicle maneuverability and stability, *SAE Technical Paper no. 2003-01-0578*.
- [13] Klier, W., Reimann, G. and Reinelt, W. (2004) Concept and functionality of the active front steering system, *SAE Technical Paper no. 2004-21-0073*.
- [14] Austin, M. (Sept 2008) A style worth repeating: Audi makes a few changes to the recipe with the new A4, *Car and Drive Magazine*.
- [15] New test procedures for handling of vehicles with variable ratio steering systems, www.fev.com, accessed in September 2011.
- [16] Guglielmino, E., Sireteanu, T., Stammers, C.W., Ghita, G. and Giuclea, M. (2008) Semi-active suspension control: improved vehicle ride and road friendliness, Springer-Verlag, London.
- [17] Beamish, T. (2004) Active roll control for sport utility vehicles, Ph.D Thesis, Harvard University, USA.
- [18] Yamazaki, I., Kushihiro, I. and Kunihiro, Y. (2009) Electronic power steering compensating control for influence of vehicle dynamics on steering torque, *SAE International Journal of Passenger Cars-Mechanical Systems*, 2(1), 239-246.
- [19] Austin, L. and Morrey, D. Recent advances in antilock braking systems and traction control systems, *Proceedings of the Institution of Mechanical Engineers, Part D: Journal of Automobile Engineering*, 214(6), 625-638.
- [20] Furukawa, Y. and Abe, M. (1997) Advanced chassis control systems for vehicle handling and active safety, *Vehicle System Dynamics*, 28(2-3), 59-86.
- [21] Esmailzadeh, E., Goodarzi, A. and Vossoughi, G.R. (2003) Optimal yaw moment control law for improved vehicle handling, *Mechatronics*, 13(7), 659-675.
- [22] Abe, M. (1999) Vehicle dynamics and control for improving handling and active safety: from four-wheel steering to direct yaw moment control, *Journal of Multi-body Dynamics*, 213(2), 87-101.
- [23] Dang, J.N. (2004) Preliminary results analyzing the effectiveness of Electronic Stability Control (ESC) systems, US Department of Transportation, National Highway Traffic Safety Administration.

- [24] Van Zanten, A.T. (2000) Bosch ESP systems: 5 years of experience, *SAE Technical Paper no. 2000-01-1633*.
- [25] He, J., Crolla, D.A., Levesley, M.C. and Manning, W.J. (2004) Integrated active steering and variable torque distribution control for improving vehicle handling and stability, *SAE Technical Paper no. 2004-01-1071*.
- [26] Zeyada, Y., Karnopp, D.C., El-Arabi, M. and El-Behiry, E. (1998) A combined active-steering, differential-braking yaw rate control strategy for emergency maneuvers, *SAE Technical Paper no. 980230*.
- [27] Snyder, A., Jones, B., Grygier, P., W. and Riley, G. (June 2005) NHTSA light vehicle ABS performance test development, National Highway Traffic Safety Administration.
- [28] Mirzaei, M., Alizadeh, G., Eslamian, M. and Azadi, S. (2008) An optimal approach to non-linear control of vehicle yaw dynamics, *Proceedings of the Institution of Mechanical Engineers, Part I: Journal of Systems and Control Engineering*, 222(4), 217-229.
- [29] Abe, M., Kano, Y., Suzuki, K., Shibahata, Y. and Furukawa, Y. (2001) Side-slip control to stabilize vehicle lateral motion by direct yaw moment, *JSAE Review*, 22(4), 413-419.
- [30] Zheng, S., Tang, H., Han, Z. and Zhang, Y. (2006) Controller design for vehicle stability enhancement, *Control Engineering Practice*, 14(12), 1413-1421.
- [31] Hamzah, N., Aripin, M.K., Sam, Y.M., Selamat, H. and Ismail, M.F. (2012) Vehicle stability enhancement based on second order sliding mode control, *Presented at Control System, Computing and Engineering (ICCSCE), 2012 IEEE International Conference on*, 580-585.
- [32] Tamaddoni, S.H., Taheri, S. and Ahmadian, M. (2011) Optimal direct yaw controller design for vehicle systems with human driver, *SAE Technical Paper no. 2011-01-2149*.
- [33] CarSim user manual, www.carsim.com, accessed in December 2011.
- [34] Chen, B.C. and Peng, H. (2001) Differential-braking-based rollover prevention for sport utility vehicles with human-in-the-loop evaluations, *Vehicle System Dynamics*, 36(4-5), 359-389.
- [35] Hopkins, B., Taheri, S., Ahmadian, M. and Reid, A. (2010) Yaw stability control and emergency roll control for vehicle rollover mitigation, *SAE Technical Paper no. 2010-01-1901*.

- [36] Hayama, R., Nishizaki, K., Nakano, S. and Katou, K. (2000) The vehicle stability control responsibility improvement using steer-by-wire, *In Proceedings of the IEEE Intelligent Vehicles Symposium*, Dearborn, USA, 596-601.
- [37] Hebden, R.G., Edwards, C. and Spurgeon, S.K. (2004) Automotive steering control in a split- μ manoeuvre using an observer-based sliding mode controller, *Vehicle System Dynamics*, 41(3), 181-202.
- [38] Yim, S., Cho, W., Yoon, J. and Yi, K. (2010) Optimum distribution of yaw moment for unified chassis control with limitations on the active front steering angle, *International Journal of Automotive Technology*, 11(5), 665-672.
- [39] Yih, P. (2005) Steer-by-wire: implications for vehicle handling and safety, Ph.D Thesis, Stanford University, USA.
- [40] Grip, H.F., Imsland, L., Johansen, T.A., Fossen, T.I., Kalkkuhl, J.C. and Suissa, A. (2008) Nonlinear vehicle side-slip estimation with friction adaptation, *Automatica*, 44(3), 611-622.
- [41] Nguyen, B.M., Wang, Y., Oh, S., Fujimoto, H. and Hori, Y. (2012) GPS based estimation of vehicle side slip angle using multi-rate kalman filter with prediction of course angle measurement residual, *In Proceedings of the FISITA 2012 World Automotive Congress*, Springer Berlin Heidelberg, 597-609.
- [42] Ryu, J., Rossetter, E.J. and Gerdes, J.C. (2002) Vehicle side slip and roll parameter estimation using GPS, *In Proceedings of the International Symposium on Advanced Vehicle Control (AVEC)*, Tokyo, Japan.
- [43] Jazar, R.N. (2008) *Vehicle dynamics: theory and application*, Springer, New York.
- [44] ZF active steering in the steering column for mid-size and luxury cars, www.zf-lenksysteme.com/en/products/car-steering-systems/active-steering, accessed in June 2011.
- [45] Oraby, W.A.H. (2007) Improvement of vehicle lateral stability during overtaking process by active front steering system, *SAE Technical Paper no. 2007-01-0810*.
- [46] Fukao, T., Miyasaka, S., Mori, K., Adachi, N. and Osuka, K. (2001) Active steering systems based on model reference adaptive nonlinear control, *In Proceedings of IEEE Intelligent Transportation Systems*, Oakland, USA, 502-507.
- [47] Tardy, S. (2007) *Active steering for vehicle stability control*, Cranfield University, UK.

- [48] Lin, W.C. and Chen, S.K. (2007) Active front steering damping control, *Presented at ASME 2007 International Mechanical Engineering Congress and Exposition*, Seattle, Washington, USA, 235-241.
- [49] Chen, D., Yin, C. and Zhang, J. (2008) Controller design of a new active front steering system, *WSEAS Transactions on Systems*, 7(11), 1258-1268.
- [50] Reinelt, W., Klier, W., Reimann, G., Lundquist, C., Schuster, W. and Großheim, R. (Apr 2004) Active front steering for passenger cars: system modelling and functions, *In Proceedings of the First IFAC Symposium on Advances in Automotive Control*, Salerno, Italy.
- [51] Tagawa, Y., Ogata, H., Morita, K., Nagai, M. and Mori, H. (1996) Robust active steering system taking account of nonlinear dynamics, *Vehicle System Dynamics*, 25(S1), 668-681.
- [52] Oraby, W.A.H., El-Demerdash, S.M., Selim, A.M., Faizz, A. and Crolla, D.A. (2004) Improvement of vehicle lateral dynamics by active front steering control, *SAE Technical Paper no. 2004-01-2081*.
- [53] Ackermann, J. and Bunte, T. (1997) Yaw disturbance attenuation by robust decoupling of car steering, *Control Engineering Practice*, 5(8), 1131-1136.
- [54] Ackermann, J. (1998) Active steering for better safety, handling and comfort, *In Proceedings of Vehicle Control and Safety*, France, 1-10.
- [55] Zhang, J.Y., Kim, J.W., Lee, K.B. and Kim, Y.B. (2008) Development of an active front steering (AFS) system with QFT control, *International Journal of Automotive Technology*, 9(6), 695-702.
- [56] Odenthal, D., Bunte, T. and Ackermann, J. (1999) Nonlinear steering and braking control for vehicle rollover avoidance, *Presented at European Control Conference*, Karlsruhe, Germany, 1-6.
- [57] Zhao, J. and Taheri, S. (2012) A multi-objective LMI-based antiroll control system, *SAE International Journal of Commercial Vehicles*, 5(2), 421-428.
- [58] Solmaz, S., Corless, M. and Shorten, R. (2007) A methodology for the design of robust rollover prevention controllers for automotive vehicles with active steering, *International Journal of Control*, 80(11), 1763-1779.

- [59] Shim, T. and Toomey, D. (2004) Investigation of active steering/wheel torque control at the rollover limit maneuver, *SAE Technical Paper no. 2004-01-2097*.
- [60] Ackermann, J. and Odenthal, D. (1998) Robust steering control for active rollover avoidance of vehicles with elevated center of gravity, *In Proceedings of the International Conference on Advances in Vehicle Control and Safety*, Amiens, France, 118-123.
- [61] Kharrazi, S., Lidberg, M., Roebuck, R., Fredriksson, J. and Odhams, A. (2012) Implementation of active steering on longer combination vehicles for enhanced lateral performance, *Vehicle System Dynamics*, 50(12), 1949-1970.
- [62] Jujnovich, B., Odhams, C., Roebuck, R. and Cebon, D. (2008) Implementation of active rear steering of a tractor/semi-trailer, *In Proceedings of the 10th international symposium of Heavy Vehicle Transport Technology*, Paris, France, 358-367.
- [63] Mccann, R. and Nauven, S. (2004) Jackknife avoidance in large trucks using active front steering, *SAE Technical Paper no. 2004-01-2639*.
- [64] Yu, N. (2007) Yaw-control enhancement for buses by active front-wheel steering, Ph.D Thesis, Pennsylvania State University, USA.
- [65] Azad, N.L. (2006) Dynamic modelling and stability controller development for articulated steer vehicles, Ph.D Thesis, University of Waterloo, Canada.
- [66] Shibahata, Y., Irie, N., Itoh, H. and Nakamura, K. (1986) The development of an experimental four-wheel-steering vehicle, *SAE Technical Paper no. 860623*.
- [67] Irie, N. and Shibahta, Y. (1986) Improving vehicle stability and controllability through active rear wheel steering, *JSAE Review*, 40(3), 360-369.
- [68] Hirano, Y. and Fukatani, K. (1997) Development of robust active rear steering control for automobile, *JSME International Journal Series C*, 40(2), 231-238.
- [69] Sano, S., Furukawa, Y. and Shiraishi, S. (1986) Four wheel steering system with rear wheel steer angle controlled as a function of steering wheel angle, *SAE Technical Paper no. 860625*.
- [70] Lee, S.H., Lee, U.K., Ha, S.K. and Han, C.S. (1999) Four-wheel independent steering (4WIS) system for vehicle handling improvement by active rear toe control, *JSME International Journal Series C*, 42(4), 947-956.

- [71] Shibahata, Y. (2005) Progress and future direction of chassis control technology, *Annual Reviews in Control*, 29(1), 151-158.
- [72] Boada, M.J.L., Boada, B.L., Munoz, A. and Díaz, V. (2006) Integrated control of front-wheel steering and front braking forces on the basis of fuzzy logic, *Journal of Automobile Engineering*, 220(3), 253-267.
- [73] Goodarzi, A. and Alirezaie, M. (2009) Integrated fuzzy/optimal vehicle dynamic control, *International Journal of Automotive Technology*, 10(5), 567-575.
- [74] Hirano, Y., Harada, H., Ono, E. and Takanami, K. (1993) Development of an integrated system of 4WS and 4WD by H_∞ control, *SAE Technical Paper no. 93-0267*.
- [75] Lv, H.M., Chen, N. and Li, P. (2004) Multi-objective H_∞ optimal control for four-wheel steering vehicle based on yaw rate tracking, *Proceedings of the Institution of Mechanical Engineers, Part D: Journal of Automobile Engineering*, 218(10), 1117-1123.
- [76] Goodarzi, A., Sabooteh, A. and Esmailzadeh, E. (2008) Automatic path control based on integrated steering and external yaw-moment control, *Proceedings of the Institution of Mechanical Engineers Part K-Journal of Multi-Body Dynamics*, 222(2), 189-200.
- [77] Yang, X., Wang, Z. and Peng, W. (2009) Coordinated control of AFS and DYC for vehicle handling and stability based on optimal guaranteed cost theory, *Vehicle System Dynamics*, 47(1), 57-79.
- [78] Zhao, Y., Chen, S. and Shim, T. (2011) Investigation of trailer yaw motion control using active front steer and differential brake, *SAE International Journal of Materials and Manufacturing*, 4(1), 1057-1067.
- [79] Baslamisli, S.Ç., Köse, İ.E. and Anlaş, G. (2009) Gain-scheduled integrated active steering and differential control for vehicle handling improvement, *Vehicle System Dynamics*, 47(1), 99-119.
- [80] Poussot-Vassal, C., Sename, O., Dugard, L. and Savaresi, S.M. (2011) Vehicle dynamic stability improvements through gain-scheduled steering and braking control, *Vehicle System Dynamics*, 49(10), 1597-1621.
- [81] Nagai, M., Shino, M. and Gao, F. (2002) Study on integrated control of active front steer angle and direct yaw moment, *JSAE Review*, 23(3), 309-315.

- [82] Nagai, M. and Yamanaka, S. (1996) Integrated control law of active rear wheel steering and direct yaw moment control, *Presented at the Proceedings of the 3rd International Symposium on Advanced Vehicle Control (AVEC)*, Aachen, Germany.
- [83] Gao, Y., Gray, A., Tseng, H.E. and Borrelli, F. (2014) A tube-based robust nonlinear predictive control approach to semiautonomous ground vehicles, *Vehicle System Dynamics, ahead of print*, 1-22.
- [84] Di Cairano, S., Tseng, H.E., Bernardini, D. and Bemporad, A. (2013) Vehicle yaw stability control by coordinated active front steering and differential braking in the tire sideslip angles domain, *Control Systems Technology, IEEE Transactions on*, 21(4), 1236-1248.
- [85] Cho, W., Choi, J., Kim, C., Choi, S. and Yi, K. (2012) Unified chassis control for the improvement of agility, maneuverability, and lateral stability, *IEEE Transactions on Vehicular Technology*, 61(3), 1008-1020.
- [86] Wang, Y.Q. and Nagai, M. (1996) Integrated control of four-wheel-steer and yaw moment to improve dynamic stability margin, *In Proceedings of the 35th Conference on Decision and Control*, Kobe, Japan, 1783-1784.
- [87] Zhi-Wei, G., Chun-Hui, L. and Feng, D. (2012) Optimal Control of Four-wheel Steering Tractor-semitrailer with Direct Yaw-moment Control, *In Proceedings of the 2012 Third International Conference on Mechanic Automation and Control Engineering. IEEE Computer Society*, 1069-1072.
- [88] Ono, E. and Hosoe, S. (1998) Bifurcation in vehicle dynamics and robust front wheel steering control, *IEEE Transactions on Control Systems Technology*, 6(3), 412-420.
- [89] Nishio, A., Tozu, K., Yamaguchi, H., Asano, K. and Amano, Y. (2001) Development of vehicle stability control system based on vehicle side slip angle estimation, *SAE Technical Paper no. 2001-01-0137*.
- [90] Allen, R.W. and Rosenthal, T. (1993) A computer simulation analysis of safety critical maneuvers for assessing ground vehicle dynamic stability, *SAE Technical Paper no. 930760*.
- [91] Singh, S. (2000) Design of front wheel active steering for improved vehicle handling and stability, *SAE Technical Paper no. 2000-01-1619*.

- [92] Qu, Q. and Liu, Y. (2000) On lateral dynamics of vehicles based on nonlinear characteristics of tires, *Vehicle System Dynamics*, 34(2), 131-141.
- [93] Abe, M. (2009) *Vehicle handling dynamics: theory and application*, Butterworth-Heinemann.
- [94] Wong, J.Y. (2008) *Theory of ground vehicles*, John Wiley and Sons, New York.
- [95] Brown, G.L. and Hung, J.C. (1994) A mathematical model for vehicle steering control, *Presented at 20th International Conference on Industrial Electronics, Control and Instrumentation*, Bologna, Italy, 2027-2032.
- [96] Rossetter, E.J. and Gerdes, J.C. (2002) A Study of lateral vehicle control under a ‘virtual’ force framework, *In Proceedings of the International Symposium on Advanced Vehicle Control*, Hiroshima, Japan.
- [97] Mammar, S., Baghdassarian, V.B. and Aacc, A. (2000) Two-degree-of-freedom formulation of vehicle handling improvement by active steering, *In Proceedings of the American Control Conference*, Chicago, Illinois, 105-109.
- [98] Gianone, L., Palkovics, L. and Bokor, J. (1995) Design of an active 4WS system with physical uncertainties, *Control Engineering Practice*, 3(8), 1075-1083.
- [99] Chu, T. and Jones, R. (2008) Analysis and simulation of nonlinear handling characteristics of automotive vehicles with focus on lateral load transfer, *Vehicle System Dynamics*, 46(S1), 17-31.
- [100] Zhang, J., Zhang, Y., Chen, L. and Yang, J. (2007) A fuzzy synthesis control strategy for active four-wheel steering based on multi-body models, *SAE Technical Paper no. 2008-01-0603*.
- [101] Dugoff, H., Fancher, P. and Segel, L. (1970) Tire performance characteristics affecting vehicle response to steering and braking control inputs, Final Report, Transportation Research Institute (UMTRI), No. CST-460.
- [102] Pacejka, H.B. (2006) *Tyre and vehicle dynamics*, Butterworth Heinemann, Oxford, UK.
- [103] Saglam, F. and Unlusoy, Y.S. (2011) Identification of low order vehicle handling models from multibody vehicle dynamics models, *Presented at 2011 IEEE International Conference on Mechatronics (ICM)*, Istanbul, Turkey, 96-101.

- [104] Hegazy, S., Rahnejat, H. and Hussain, K. (2000) Multi-body dynamics in full-vehicle handling analysis under transient manoeuvre, *Vehicle System Dynamics*, 34(1), 1-24.
- [105] Seacord, C.L. (1976) Preliminary system design study for a digital fly-by-wire flight control system for an F-8C aircraft, National Aeronautics and Space Administration (NASA) Technical Report.
- [106] Amberkar, S., Bolourchi, F., Demerly, J. and Millsap, S. (2004) A control system methodology for steer by wire systems, *SAE Technical Paper no. 2004-01-1106*.
- [107] Oh, S.W., Chae, H.C., Yun, S.C. and Han, C.S. (2004) The design of a controller for the steer-by-wire system, *JSME International Journal Series C*, 47(3), 896-907.
- [108] Mousavinejad, I. and Kazemi, R. (2014) Variable structure controller design for steer-by-wire system of a passenger car *Journal of Mechanical Science and Technology*, 28(8), 3285-3299.
- [109] Kader, A. (2006) Steer-by-wire control system, Swarthmore College, Academic Report.
- [110] Asai, S., Kuroyanagi, H., Takeuchi, S., Takahashi, T. and Ogawa, S. (2004) Development of a steer-by-wire system with force feedback using a disturbance observer, *SAE Technical Paper no. 2004-01-1100*.
- [111] Dominke, P. and Ruck, G. (1999) Electric power steering-the first step on the way to "steer by wire", *SAE Technical Paper no. 1999-01-0401*.
- [112] Feick, S., Pandit, M., Zimmer, M. and Uhler, R. (2000) Steer-by-wire as a mechatronic implementation, *SAE Technical Paper no. 2000-01-0823*.
- [113] Coudon, J., Canudas-de-Wit, C. and Claeys, X. (2006) A new reference model for steer-by-wire applications with embedded vehicle dynamics, *Presented at Proceedings of the American Control Conference*, Minnesota, USA, 14-16.
- [114] Koehn, P. and Eckrich, M. (2004) Active steering—the BMW approach towards modern steering technology, *SAE Technical Paper no. 2004-01-1105*.
- [115] Jamson, A.H., Whiffin, P.G. and Burchill, P.M. (2007) Driver response to controllable failures of fixed and variable gain steering, *International Journal of Vehicle Design*, 45(3), 361-378.

- [116] Shen, B. and Ji, P. (2011) The analysis and modeling of active front steering system, *Presented at IEEE 2nd International Conference on Computing, Control and Industrial Engineering (CCIE)*, Wuhan, China, 237-242.
- [117] Ahmed, W.A.K., Rawat, V. and Bhat, R.B. (2012) Steering system and method for independent steering of wheels, US Patent No. 8 126 612 B2.
- [118] Abdel-Rahman, A. (2009) Pulsed active steering hardware in the loop experiment, Master thesis, Waterloo University, Canada.
- [119] Shindo, M., Matsuda, M., Kawamuro, J. and Kojo, T. (2000) Vehicle steering apparatus, US Patent No. 6164150.
- [120] Tuttle, T.D. (1992) Understanding and modeling the behavior of a harmonic drive gear transmission, Massachusetts Inst. of Tech., Cambridge. Artificial Intelligence Lab, 1365.
- [121] Aga, M., Kusunoki, H., Satoh, Y. and Saitoh, R. (1990) Design of 2-degree-of-freedom control system for active front-and-rear wheel steering, *SAE Technical Paper no. 901746*.
- [122] Zhang, Z., Kim, J., Xuan, D. and Kim, Y. (2011) Design of active front steering (AFS) system with QFT control, *International Journal of Computer Applications in Technology*, 41(3-4), 236-245.
- [123] Zheng, B. and Anwar, S. (2008) Fault-tolerant control of the road wheel subsystem in a steer-by-wire system, *International Journal of Vehicular Technology*, 2008(2008).
- [124] Hiraoka, T., Nishihara, O. and Kumamoto, H. (2008) Steering reactive torque presentation method for a steer-by-wire vehicle, *Review of Automotive Engineering*, 29(2008), 287-294.
- [125] Gillespie, T.D. (1983) Comparative study of vehicle roll stability, University of Michigan, Ann Arbor, Transportation Research Institute, UMTRI-83-25.
- [126] Farazandeh, A., Ahmed, A.K.W. and Rakheja, S. (2012) Performance enhancement of road vehicles using active independent front steering (AIFS), *SAE International Journal of Passenger Cars-Mechanical Systems*, 5(4), 273-1284.
- [127] Modaressi-Tehrani, K., Rakheja, S. and Sedaghati, R. (2006) Analysis of the overturning moment caused by transient liquid slosh inside a partly filled moving tank, *Proceedings of the Institution of Mechanical Engineers, Part D: Journal of Automobile Engineering*, 220(3), 289-301.

- [128] Ranganathan, R. and Yang, Y.S. (1996) Impact of liquid load shift on the braking characteristics of partially filled tank vehicles, *Vehicle system dynamics*, 26(3), 223-240.
- [129] Pape, D.B., et al. (2007) Cargo tank roll stability study, Final report, Contract no. GS23-F-0011L, Batelle, 30.
- [130] Kang, X., Rakheja, S. and Stiharu, I. (1999) Optimal tank geometry to enhance static roll stability of partially filled tank vehicles, *SAE Technical Paper no.* 1999-01-3730.
- [131] Ziarani, M.M., Richard, M.J. and Rakheja, S. (2004) Optimisation of liquid tank geometry for enhancement of static roll stability of partially-filled tank vehicles, *International Journal of Heavy Vehicle Systems*, 11(2), 155-173.
- [132] Yan, G., Siddiqui, K., Rakheja, S. and Modaressi, K. (2005) Transient fluid slosh and its effect on the rollover-threshold analysis of partially filled conical and circular tank trucks, *International Journal of Heavy Vehicle Systems*, 12(4), 323-343.
- [133] Rawat, V. (2007) Active independent front steering for yaw-rate control and tire work-load equalization in road vehicles, Master thesis, Concordia University, Canada.
- [134] Lin, R.C., Cebon, D. and Cole, D.J. (1996) Optimal roll control of a single-unit lorry, *Proceedings of the Institution of Mechanical Engineers, Part D: Journal of Automobile Engineering*, 210(1), 45-55.
- [135] Hudha, K., Zakaria, M.H. and Tamaldin, N. (2011) Hardware in the loop simulation of active front wheel steering control for yaw disturbance rejection, *International Journal of Vehicle Safety*, 5(6), 356-373.
- [136] Mammar, S. and Koenig, D. (2002) Vehicle handling improvement by active steering, *Vehicle System Dynamics*, 38(3), 211-242.
- [137] McCann, R. (2000) Variable effort steering for vehicle stability enhancement using an electric power steering system, *SAE Technical Paper no.* 2000-01-0817.
- [138] Cheng, C. and Cebon, D. (2008) Improving roll stability of articulated heavy vehicles using active semi-trailer steering, *Vehicle System Dynamics*, 46(S1), 373-388.
- [139] Mokhiamar, O. and Abe, M. (2006) How the four wheels should share forces in an optimum cooperative chassis control, *Control Engineering Practice*, 14(3), 295-304.

- [140] Farazandeh, A., Ahmed, A.K.W. and Rakheja, S. (2013) Performance analysis of active independent front steering (AIFS) for commercial vehicles with greater lateral load shift propensity, *SAE International Journal of Commercial Vehicles*, 6(2), 288-300.
- [141] Bin, S. and PengKai, J. (2011) The analysis and modeling of active front steering system, *Presented at 2011 IEEE 2nd International Conference on Computing, Control and Industrial Engineering (CCIE)*, Wuhan, China, 237-242.
- [142] Hancock, M.J., Williams, R.A., Gordon, T.J. and Best, M.C. (2005) A comparison of braking and differential control of road vehicle yaw-sideslip dynamics, *Proceedings of the Institution of Mechanical Engineers, Part D: Journal of Automobile Engineering*, 219(3), 309-327.
- [143] Tai, M., Hingwe, P. and Tomizuka, M. (2004) Modeling and control of steering system of heavy vehicles for automated highway systems, *Mechatronics, IEEE/ASME Transactions on*, 9(4), 609-618.
- [144] Dorf, R.C. (1995) *Modern control systems*, Addison-Wesley Longman Publishing Co., Inc, Boston, MA, USA.
- [145] ISO 14794, (2001) Heavy commercial vehicles and buses-braking in a turn-open-loop test methods.
- [146] Iguchi, M. (1959) A study of manual control, *Mechanic Society of Japan*, 62(481).
- [147] Farazandeh, A., Ahmed, A.K.W. and Rakheja, S. (2014) Effectiveness of active steering systems under different handling maneuvers, *Presented at FISITA World Automotive Congress*, Maastricht, The Netherlands.
- [148] Nuessle, M., Rutz, R., Leucht, M., Nonnenmacher, M. and Volk, H. (2007) Objective test methods to assess active safety benefits of ESP, *Presented at 20th Int. Technical Conf on the Enhanced Safety of Vehicles (ESV)*, Lyon, France.
- [149] Hisaoka, Y., Yamamoto, M. and Okada, A. (1999) Closed-loop analysis of vehicle behavior during braking in a turn, *JSAE Review*, 20(4), 537-542.
- [150] El-Gindy, M. (1992) The use of heavy vehicle performance measures for design and regulation, *Presented at ASME WAM*, California, USA.

- [151] Xia, X. and Law, E.H. (1990) Nonlinear dynamic response of four wheel steering automobiles to combined braking and steering commands in collision avoidance maneuvers, *SAE Technical Paper no. 901731*.
- [152] Pandit, C.M. (2013) A model-free approach to vehicle stability control, Master thesis, Clemson University, USA.
- [153] Anstrom, J.R. (2003) Model development for integrated hybrid electric vehicle dynamic stability systems, *Presented at ASME 2003 International Mechanical Engineering Congress and Exposition, American Society of Mechanical Engineers, Washington, DC, USA, 167-175*.
- [154] Xiang, D., Yuan, J. and Xu, W. (2012) Study on fuzzy PID algorithm for a new active front steering system, *Journal of Control Engineering and Technology (JCET)*, 2(1), 24-29.
- [155] Gao, Z., Wang, J. and Wang, D. (2011) Dynamic modeling and steering performance analysis of active front steering system, *Procedia Engineering*, 15(2011), 1030-1035.
- [156] Zhang, Q., Wu, X. and Liu, F. (2011) The overview of active front steering system and the principle of changeable transmission ratio, *Presented at 3d International Conference on Measuring Technology and Mechatronics Automation (ICMTMA)*, Shangshai, China, 894-897.
- [157] Team#12. (2012) Tubular racing car with independent active front steering system, Capstone Final Report, Concordia University, Canada.

Appendix A

AFS MECHANISMS WITH PLANETARY GEAR SYSTEMS

In this section, the kinematic of active steering mechanisms consisting of planetary gear systems are investigated for implementation of the concept for the proposed AIFS system.

The steering ratio, ($i_s = \frac{\delta_d}{\delta_{FW}}$), is defined as the ratio between the driver steering angle (δ_d) and the average angle of the front road wheels (δ_{FW}). In comparison with the conventional steering system (Fig. A.1(a)), the pinion angle (δ_p) could be obtained through the linear superposition of the driver angle with the electric motor angle in an active steering system, (Fig. A.1(b)), such as:

$$\delta_p = q_1\delta_d + q_2\delta_m \quad (\text{A.1})$$

where δ_m is the angle of rotation of the electric motor, q_1 and q_2 are the gains which are formulated based on the gearing mechanism. It should be noted that there is a nonlinear relation between the pinion and the front wheels originated from the steering and suspension mechanism and is expressed by function, f_w . Using equation (A.1), the average angle of the front wheels, δ_{FW} , can be expressed as [13]:

$$\delta_{FW} = f_w(\delta_p) = f_w(q_1\delta_d + q_2\delta_m) \quad (\text{A.2})$$

The steering ratio thus could be rewritten such as:

$$i_s = \frac{\delta_d}{f_w(q_1\delta_d + q_2\delta_m)} \quad (\text{A.3})$$

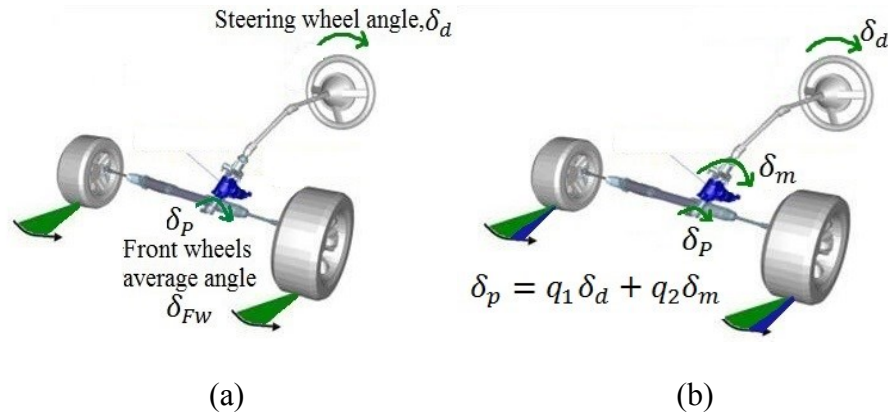


Figure A.1: Relation between the steering wheel angle and the front wheels angle in: (a) conventional; and (b) active steering system [154].

The kinematic analysis of planetary gear system must be thoroughly examined for its successful implementation in an active system. Reviewing the literature on the planetary gear arrangements used in active steering systems suggested different steering ratio which could affect the responsiveness, inertia and the size of the active steering system. As discussed earlier, three possible configurations in terms of gears used for input, output and integrating with motor are possible. The functions of three planetary gear configurations are examined in detail in the following and summarized in Table A.1.

Configuration 1:

Gao et al. [155] studied the mechanism of an AFS system using a dual planetary gear as shown in Fig. A.2. The kinematic relations between the parts are as follows: the sun gear (I) is fixed to the steering wheel, thus, it has the same rotation as the steering wheel. The stepped planet gears connect the sun gear (I) to the sun gear (II). This mechanism is capable of transmitting the hand wheel steering rotation to the road wheels in both conventional and active

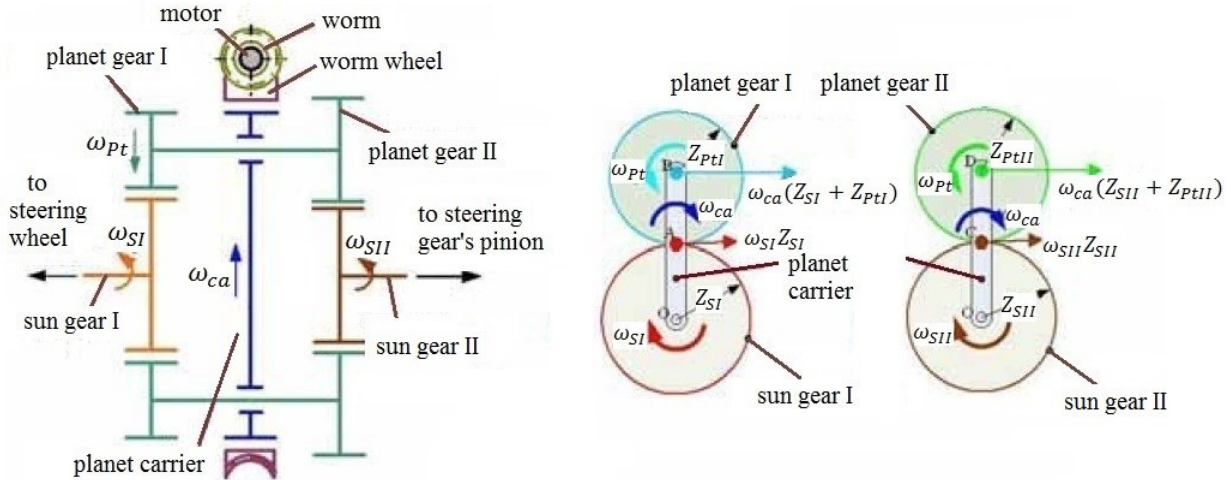


Figure A.2: Configuration I of planetary gear system [155].

steering modes. In the conventional mode, when the motor is fixed, the worm wheel does not rotate and holds the planet carrier stationary. The rotation of the sun gear (I) is transmitted to the sun gear (II) through the planet gears (I) and (II). This motion is subsequently transmitted to the rack via the pinion meshed into the sun gear (II).

In case where the motor is activated, based on the driving situation and ECU decision, the electric motor turns the worm and then the worm gear. As mentioned earlier, the worm gear and the carrier are integrated, so this motion is transferred to the planet gear (II) and the sun (II). Finally, a variable steering ratio and a required steering angle can be obtained by the simultaneous turn of the sun gear (I), through the steering wheel, and the worm gear, via the electric motor. The resultant wheel angle also depends on the turning direction of the sun gear (I) and the worm gear. When the worm gear and the sun gear (I) rotate in the same direction, the resultant wheel angle is smaller than the angle applied by the driver while it is increased when they rotate in the opposite direction. It should be noted that the safety of the system is guaranteed

by locking the worm gear with the electromagnetic locking unit and the system convert to the conventional steering system.

Configuration II:

Zhang et al. [156] analyzed the AFS mechanism applied in BMW steering system as depicted in Fig. A.3. This configuration consists of two planetary gear systems connected by carrier (H) while the first outer ring, gear (3) is fixed and the second one, (gear 7), can be driven by the electric motor. In conventional mode, when the motor is fixed, the rotating input from the first sun, gear (1), transmitted to the planet gear (2). This gear walks inside the fixed outer ring and turns the carrier H. The planetary gear (8) then will be rotated by the carrier and resulted in rotation of gear (9) which is meshed to the pinion gear meshed with the steering rack.

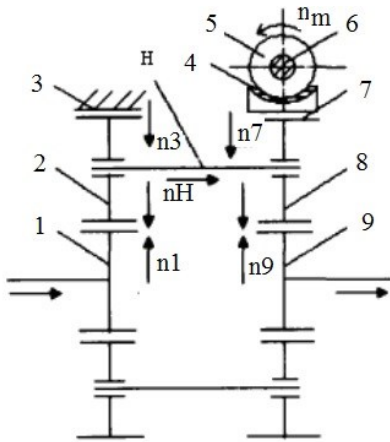


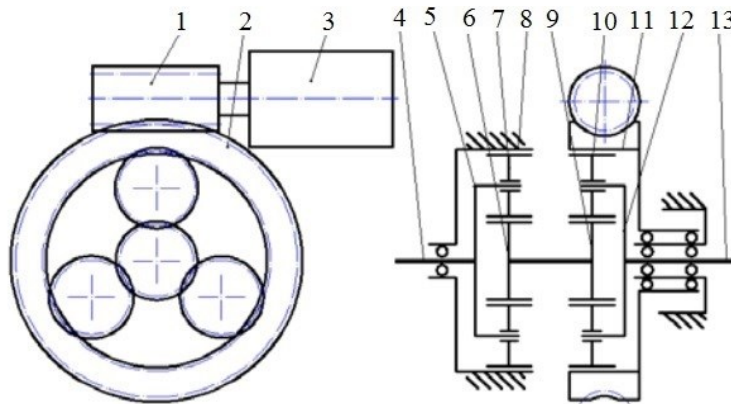
Figure A.3: Configuration II of planetary gear system [156].

In case when motor (4) is active, this motor drives the endless screw (5). This motion is then transmitted to the worm gear (6) which is coupled with the outer ring (7) in the second planetary gear set. The outer ring consequently turns the planetary gear (8) and it drives the sun gear (9) which is meshed to the pinion. As a result, the final output angle is the composition of the angle

comes from the first planetary set, which is originally imparted by the driver, and the angle generated by the electric motor as the compensated angle that ECU decided. Similar dual planetary gear system was also found in the reference [116] while in this study, the electric motor was positioned to rotate the ring of the first planetary set while the second ring was held fixed.

Configuration III:

Figure A.4 illustrates another planetary gear configuration proposed in a study performed by Xiang et al. [154]. In this design, the driver steering angle input rotates the carrier (5), instead of the sun gear compared to the configuration II. This motion is transmitted to the sun gear (9) through the planet gear (7) and the sun gear (6) while the outer gear (8) is fixed in the first planetary gear system. In case where the motor is braked, the rotation of the sun gear (9) coupled with the planet gear (10) is transmitted to the carrier (12) which is meshed to the pinion gear.



1. worm, 2. worm wheel, 3. motor, 4. input shaft, 5,12. planetary carrier, 6,9. sun wheel, 7,10. planet gear, 8,11. outer gear, 13. output shaft.

Figure A.4: Configuration III of planetary gear system [154].

In case where the motor is active, the superposition rotation of the sun gear (9) and the outer gear (11), which is attached to the electric motor, resulted in rotation of the second carrier (12) meshed with the pinion.

This design could provide more flexibility for positioning of the gears of the planetary system in engine compartment since the position of the input shaft could be changed with the output shaft by positioning the worm wheel on the outer gear (8). It was also claimed that this system could provide smaller volume, higher efficiency, accurate rotational positioning and less manufacturing cost compared to the configuration II. The study of the aforementioned active steering mechanisms thus revealed that each layout could provide different steering ratio and transmission efficiency based on how the driver, driven or fixed gear is selected as summarized in Table A.1.

Table A.1: Summary of the planetary gear configurations and resulting pinion angle.

Planetary gear configuration	Driver gear	Driven gear	Gear attached to the motor	Pinion angle (δ_p)
Configuration I	sun I	sun II	carrier	$\left(\frac{Z_{SI}Z_{PtII}}{Z_{SII}Z_{PtI}}\right)\delta_d - \left(1 - \frac{Z_{SI}Z_{PtII}}{Z_{SII}Z_{PtI}}\right)\frac{1}{G_m}\delta_m$
Configuration II	sun (1)	sun (9)	Outer gear (7)	$\left(\frac{Z_1(Z_7+Z_9)}{Z_9(Z_1+Z_3)}\right)\delta_d - \left(\frac{1}{G_m}\frac{Z_7}{Z_9}\right)\delta_m$
Configuration III	carrier (5)	carrier (12)	Outer gear (11)	$\left(\frac{Z_9(Z_6+Z_8)}{Z_6(Z_9+Z_{11})}\right)\delta_d + \left(\frac{Z_6Z_{11}}{G_m(Z_9+Z_{11})}\right)\delta_m$

where $Z_{SI}, Z_{SII}, Z_{PtI}, Z_{PtII}$ refer to the size of the sun gear I, sun gear II, planet gear I and planet gear II, respectively, as depicted in Fig. A.2. Z_i refers to size of the related gear in configurations II and III as shown in Figs A.3 and A.4. G_m is the ratio between the motor and the coupled gear in all configurations. The mechanism presented in Chapter 2 (Paper 1) uses two of

the planetary gear systems where the motors for the left and right wheel remain fixed until correction is required by the AIFS system. When correction and the corresponding wheel is demanded by the CPU, the respective motor will be activated to alter the angle of that wheel alone. A first prototype of the design is manufactured to study its functionality in application to AIFS system and described in the following Appendix.

Appendix B

AIFS STEERING MECHANISM PROTOTYPE

As stated earlier, the successful implementation of AIFS concept is largely dependent on the mechanism that can provide the required independent control of the steer angles in a fail-safe manner. Following an extensive review of literature, a mechanical system based on tandem planetary gear systems that can be readily adapted for this application was identified as the one reported in [117] and presented in sections 2.5. Figure B.1 shows a 3D-schematic of the AIFS mechanism developed prior to manufacturing of the components. As demonstrated in this figure, the AIFS mechanism consists of two sets of planetary gear trains, each comprising a sun gear, four planet gears, a planet carrier and an outer ring gear coupled with a servo motor through a spur gear.

The first prototype manufactured in collaboration with an undergraduate capstone team [157] is shown in Fig B.2. The mechanism using two half racks and two planetary gear systems presented in this figure has been configured in order to realize the steering system that functions like a conventional active steering, except that the angle of a selected wheel can be altered to provide an AIFS control. The first prototype of the mechanism was built in order to examine: the functionality of the mechanism for independent control; effectiveness of the design in providing necessary motions at the wheels; effectiveness of the design and motor torques to provide necessary forces at the wheels; limit the correction feedback to the driver through the steering wheel; compactness of design; ideal sensors and their locations etc.

Figure B.3 shows a photograph of the AIFS system installed on a project vehicle structure

with the racks attached to the front wheels. In this setup, both the sun gears are attached to the steering wheel of the vehicle while the motors are coupled with the ring gears using spur gears.

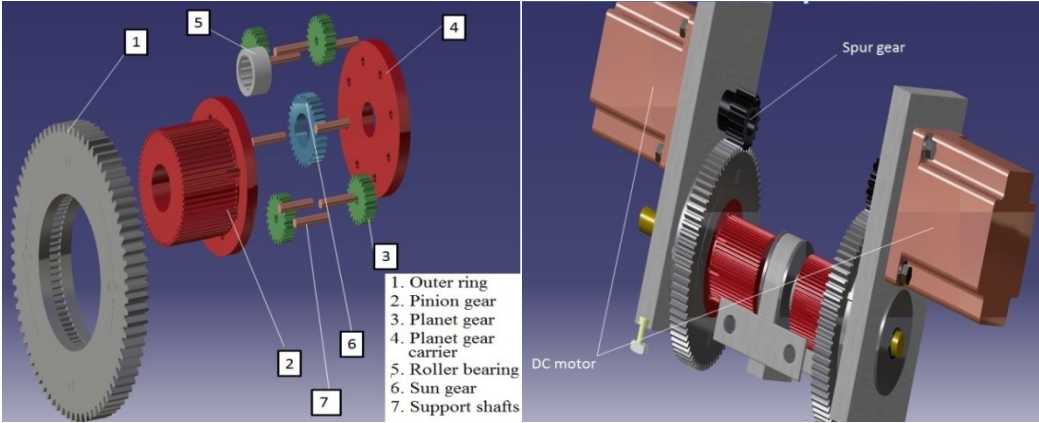


Figure B.1: 3D-layout of proposed AIFS mechanism.

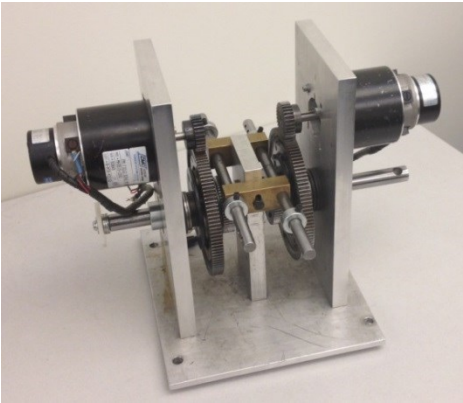


Figure B.2: First prototype of the AIFS mechanism.



Figure B.3: Designed AIFS prototype installed on a project vehicle structure.

Physically, the designed AIFS mechanism was found capable of providing active independent steering of the left and right wheels on demand. The same mechanism can also be used to generate variable steering ratio depending on the vehicle speed and the driving condition. A number of observations, however, were made in the implementation of the AIFS which must be addressed in the design of the next prototype. Some of these concerns are outlined in the following.

- The design having two racks for the front steering system must be reconfigures to accommodate the function like a single in-line rack in order to ensure preservation of the pro-Ackerman geometry. In the trial of the first prototype, therefore, the right- and the left-steering racks were bolted to threaded rods which were mated with the vehicle tie rods. As shown in Fig B.4, washers were used as spacers to correct the offset between the racks and tie rod. The pro-Ackerman geometry was thus validated as required at low speeds and in the absence of any correction.
- Available motors and sensors (potentiometers) in the laboratory were used to investigate the function of the prototype. The power of the motors, however, was found inadequate to generate corrections under load of tires. It is thus concluded that servo motors with higher power using worm gears, instead of spur gears, meshed with rings are desirable. Servo motors should thus be used which could be returned to their neutral positions and locked by use of an internal motor brake in case of any failure and convert the system into a conventional steering system.
- Using available motors and sensors for steering input and wheel angles, a preliminary hardware-in-the-loop-simulation (HILS) has been performed to study the effectiveness of the

designed mechanism with the synthesized PI controller. The test was only marginally successful due to inadequate motor torque and lack of preciseness of the sensors, as they were not appropriate for the applications.

- The prototype also exhibited certain feedback of the motor correction to the driver steering wheel. It was intended that the system do not generate any feed back to the driver and the correction could be performed without the knowledge of the driver. This issue can be addressed to a large extent by replacing the spur gear with a worm gear as discussed earlier.
- A compact design packaging of the mechanism is another very important element that is essential for successful implementation. Alternative configurations must thus be explored with compactness and efficiency in mind.
- Rapid prototyping of possible designs would be the best course of action, when testing different iterations of the gearing system and compactness of the designs. This process would minimize manufacturing time and cost. Based on the findings and experience, therefore, a second prototype should be redesigned and manufactured for tests using the hardware-in-the-loop (HIL) technique.

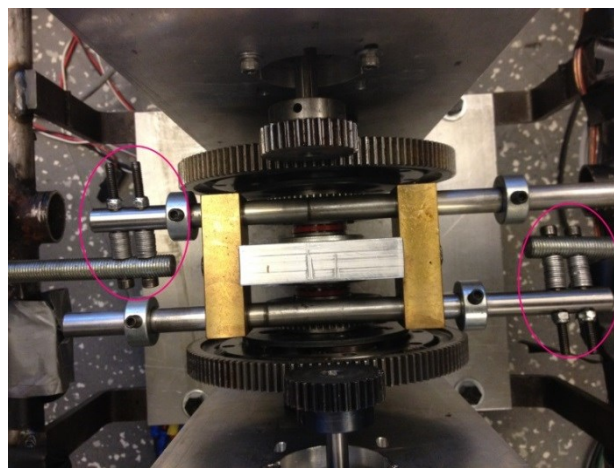


Figure B.4: Modified connection between the tie rods and racks using threaded rods

Appendix C

VEHICLE PARAMETERS

Table C.1: Simulation parameters for a step van vehicle.

Parameter	Value
Vehicle mass, m (kg)	4631
Mass moment of inertia about z-axis, I_{zz} (kgm ²)	15064
Wheelbase, L (m)	3.5
Distance of C.G from front axle, b (m)	1
Distance of C.G from rear axle, c (m)	2.5
Height of C.G from the ground, $h_{c.g}$ (m)	1.2
Half front track width, T_F (m)	0.85
Half rear track width, T_R (m)	0.85

Table C.2: Simulation parameters for fully loaded two-axle truck.

Parameter	Value
Vehicle total mass, m (kg)	13730
Load mass, m_c (kg)	9079.7
Chassis and tare tank, m'_s (kg)	3000
Front unsprung mass, m_{uF} (kg)	550
Rear unsprung mass, m_{uR} (kg)	1100
Sprung mass moment of inertia:	
I_{zs} (kgm ²)	32000
I_{xs} (kgm ²)	22200
I_{xzs} (kgm ²)	305
Unsprung mass moment of inertia, I_{zu} (kgm ²)	1028
Wheel moment of inertia, I_w (kgm ²)	12.5
Wheelbase, L (m)	3.49
Distance of CG from front axle, b (m)	1.98

Distance of CG from rear axle, c (m)	1.51
Half front track width, T_F (m)	1.00
Half rear track width, T_R (m)	0.93
Wheel radius, R_w (m)	0.548
Tank radius, R (m)	1.0
Tank base height from chassis CG, Z_b (m)	0.2
Tank Length, L_c (m)	3.5
Overall CG height from the ground, h_{cg} (m)	1.56
Sprung mass CG height from the roll center (rigid cargo), h_s (m)	1.02
Chassis CG height from roll center, h'_s (m)	0.12
Liquid cargo CG height from roll center, h_c (m)	1.32
Height of front unsprung mass CG, h_{uF} (m)	0.5
Height of rear unsprung mass CG, h_{uR} (m)	0.5
Roll center height- Front axle, h_{Froll} (m)	0.68
Roll center height- Rear axle, h_{Rroll} (m)	0.68
Front suspension roll stiffness, $K_{\phi F}$ ($\frac{Nm}{rad}$)	260000
Rear suspension roll stiffness, $K_{\phi R}$ ($\frac{Nm}{rad}$)	350000
Front suspension roll damping, $C_{\phi F}$ ($\frac{Nms}{rad}$)	11000
Rear suspension roll damping, $C_{\phi R}$ ($\frac{Nms}{rad}$)	11000
Distance between geometric center of side body and CG, e_w (m ²)	0.15
